LA-10069-PR

Progress Report

C.3

Los Alamos National Laboratory is operated by the University of California for the United States Department of Energy under contract W-7405-ENG-36.

Applied Nuclear Data Research and Development Semiannual Progress Report

April 1, 1983—September 30, 1983

Los Alamos
Los Alamos National Laboratory
Los Alamos, New Mexico 87545

The four most recent reports in this series, unclassified, are LA-9262-PR, LA-9468-PR, LA-9647-PR, and LA-9841-PR.

This work was performed under the auspices of the US Department of Energy's Division of Reactor Research and Technology, Office of Basic Energy Sciences and Office of Fusion Energy, and the Electric Power Research Institute.

Prepared by A. Mutschlecner, Group T-2

LA-10069-PR
Progress Report

UC-34c
Issued: June 1984

Applied Nuclear Data Research and Development Semiannual Progress Report

April 1, 1983—September 30, 1983

Compiled by
E. D. Arthur

Los Alamos
Los Alamos National Laboratory
Los Alamos, New Mexico 87545

CONTENTS

APPLIED NUCLEAR DATA RESEARCH AND DEVELOPMENT
SEMIANNUAL PROGRESS REPORT
April 1, 1983-September 30, 1983

Compiled by

E. D. Arthur

ABSTRACT

This progress report describes the activities of the Los Alamos Nuclear Data Group for April 1, 1983, through September 30, 1983. The topical content is summarized in the Contents.

I. THEORY AND EVALUATION OF NUCLEAR CROSS SECTIONS

A. Level Structure of ^{4}He from Four-Nucleon R-Matrix Analysis (G. Hale and D. Dodder)

Recent interest in the polarized d+d reactions has focused additional attention on the level structure of ^{4}He, particularly above the d+d threshold. We have obtained information about ^{4}He levels[1] from our present 4-nucleon R-matrix parameters by finding poles and residues of the reactance (K) matrix. While we believe the poles and residues of the scattering (S) matrix give more meaningful resonance parameters, the K-matrix prescription corresponds more closely to what others have used.

The resulting pole positions are shown in Fig. 1, compared to those from the compilation of Fiarman and Meyerhof (FM).[2] The structures are qualitatively similar, although our T=1 levels are systematically lower than those of FM. The widths of our T=1 levels are consistently larger than those for the T=0 levels, although both isospins have essentially the same (single-particle) reduced widths in the R-matrix.

It is interesting to note that we fit the recent $D(\vec{d},p)T$ analyzing-power measurements of Grüebler et al.[3] without requiring the 4^+ level they propose, and that we see a 2^+, ^5S(d-d) level that was first identified[4] in $^6Li(d,\alpha)^4He^*$

spectra, but was later withdrawn because presumably it was not evident in d-d elastic scattering measurements.[5] The tail of the 2^+ resonance accounts for the large second-rank analyzing tensors observed in the d+d reactions at low energies and results in only slight suppression of the d+d reactions when they are polarized spin-parallel.

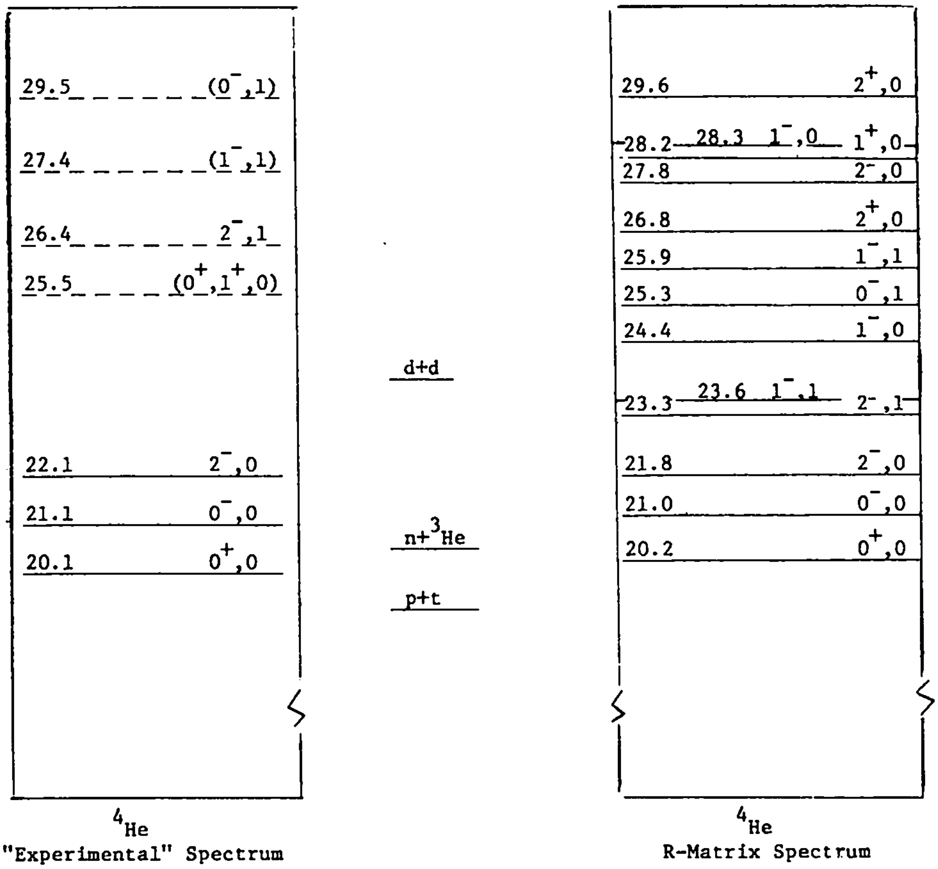

Fig. 1. R-matrix spectrum, obtained from K-matrix poles (right), compared with the compilation of Fiarman and Meyerhof[2] (left).

B. Angular Distributions for Polarized d+d Reactions [G. Hale and G. Doolen (X-5)]

Using the R-matrix parameters from the analysis described in the preceding contribution, one can predict polarized cross sections averaged over initial d-d relative velocity directions $\hat{v}$,

$$\bar{\sigma}_{m,n}(\hat{v}',v) = {}_{4\pi}\int d\Omega_{\underline{v}}\ \sigma_{m,n}(\underline{v}',\underline{v}),$$

as a function of final relative directions $\hat{v}'$. Here, $\sigma_{m,n}(\underline{v}',\underline{v})$ is the center-of-mass differential cross section for deuterons having spin projections m and n, respectively, on the axis of quantization to collide with relative velocity $\underline{v}$ to form reaction products with relative velocity $\underline{v}'$. Correspondingly, thermonuclear reaction rates can be defined,

$$<\sigma_{m,n}v>(\hat{v}') = \int dv\bar{\sigma}_{m,n}(\hat{v}',v)vf(v,kT) ,$$

by averaging over the normalized Maxwellian speed distribution f(v,kT) for temperature T.

Fig. 2 shows polar plots of the reaction rates $<\sigma_{m,n}v>(\hat{v}')$ for the four independent combinations of spin projections (m,n) = (1,1), (1,0), (1,-1), and (0,0) for the D(d,p) and D(d,n) reactions at kT = 10 keV. One sees that the angular distributions for the (1,1) and (0,0) cases are strongly directional, whereas the unpolarized angular distributions would be isotropic. These characteristic angular distributions could be useful indicators of how well polarization is maintained in an initially polarized deuterium plasma.

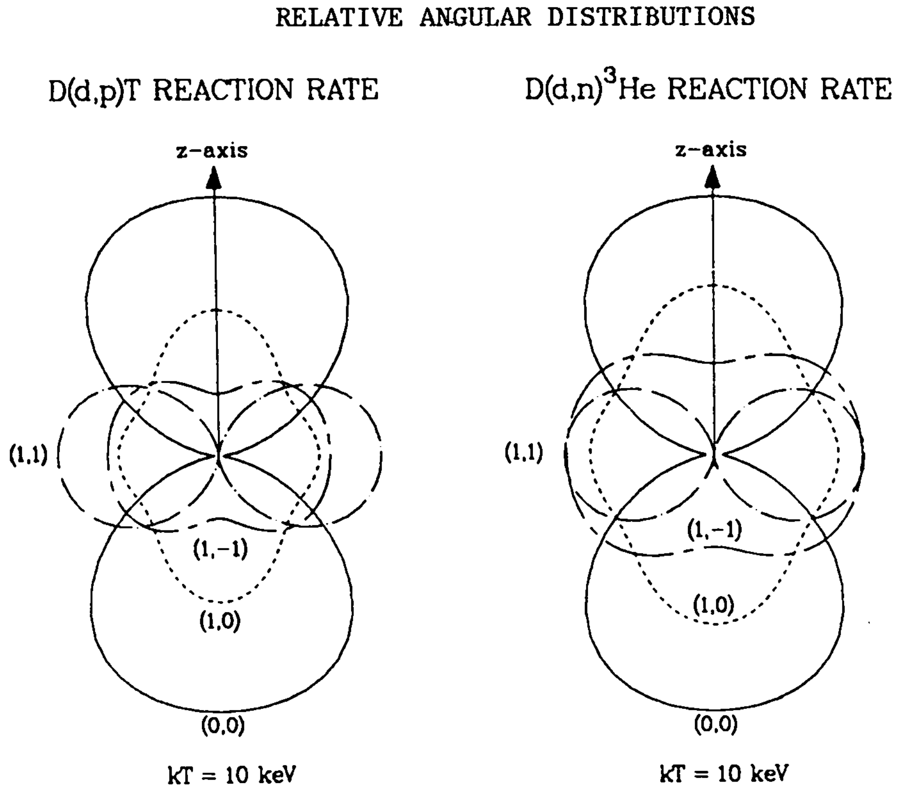

Fig. 2. Relative angular distributions of the reaction rate $<\sigma_{m,n}v>(\hat{v}')$ for D(d,p)T and D(d,n)^{3}He at kT = 10 keV.

C. Spectra for the $^6Li(t,n)2\alpha$ Reaction* (G. Hale)

The t-^{6}Li reaction could be an important process in the blanket of a fusion reactor if the cross section were in the few-hundred-mb range at low energies. Unfortunately, the available experimental information is too scattered and discrepant to give a clear indication of the magnitude of the integrated cross section.

We have done a preliminary calculation of t-^{6}Li spectra based on better determined information for the ^{3}He-^{6}Li reaction. A resonance-model fit of ^{6}Li(^{3}He,p)2α proton spectra, which includes contributions from the first five levels in ^{8}Be, plus the ground state of ^{5}Li, was charge-reflected to give predictions for neutron and α-particle spectra for the t-^{6}Li reaction. The predictions indicate that the contributions from the 16.7- and 16.9-MeV states in ^{8}Be could grow large enough to make the t-^{6}Li reaction cross section as large as several hundred mb at a few MeV, but this is based on quite uncertain extrapolations of low-energy cross-section measurements for the two excited levels.

Work continues to refine the parameters of the calculation by using more experimental input, particularly from new measurements of t-^{6}Li spectra in progress at Bruyères-le-Châtel and Los Alamos.

D. Preliminary Calculation of Gamma-Ray Emission Data from 14-MeV Neutrons on ^{11}B (P. G. Young)

As a prelude to new experimental gamma-ray production measurements in the Physics Division and a new evaluation of n+^{11}B data in the Theoretical Division, we have performed scoping calculations to estimate gamma-ray production cross sections for 14-MeV neutrons incident on ^{11}B.

The calculations were performed with the GNASH statistical-preequilibrium code,[6] using neutron, proton, and alpha-particle transmission coefficients from an earlier analysis of n+^{14,15}N data (see articles by Arthur and Young, pp. 6 and 9 of Ref. 7). Similarly, gamma-ray transmission coefficients were calculated from the ^{16}N gamma-ray strength function used in n+^{15}N calculations (page 9 of Ref. 7). Discrete-level data for the appropriate residual nuclei were taken from the compilations of Ajzenberg-Selove,[8,9] and level densities were chosen to match the discrete levels, as described in Ref. 7 (see p. 9).

---

*Most of this work was done at the Centre d'Études de Bruyères-le-Châtel, France.

The integrated gamma-ray production cross section for 14-MeV neutrons on ^{11}B was estimated to be 0.50 b. Of this, 0.44 b results from (n,n'γ) reactions, and the rest of the cross section mainly comes from (n,α) and (n,nα) reactions. A comparison of the calculated spectrum (histogram) is made with our ^{15}N calculations (open squares) in Fig. 3.

The present ENDF/B-V evalution[10] of n+^{11}B reactions is based primarily on a 1966 study by the United Kingdom Atomic Energy Agency and therefore does not incorporate many modern measurements (for example, see the article by Young and Stewart in Ref. 7). When the Physics Division $^{11}B(n,x\gamma)$ measurements are complete, we plan to perform a full evaluation of all n+^{11}B experimental data. At that time we will optimize our model parameters using the ^{11}B data and will use model calculations for interpolating and extrapolating the experimental data.

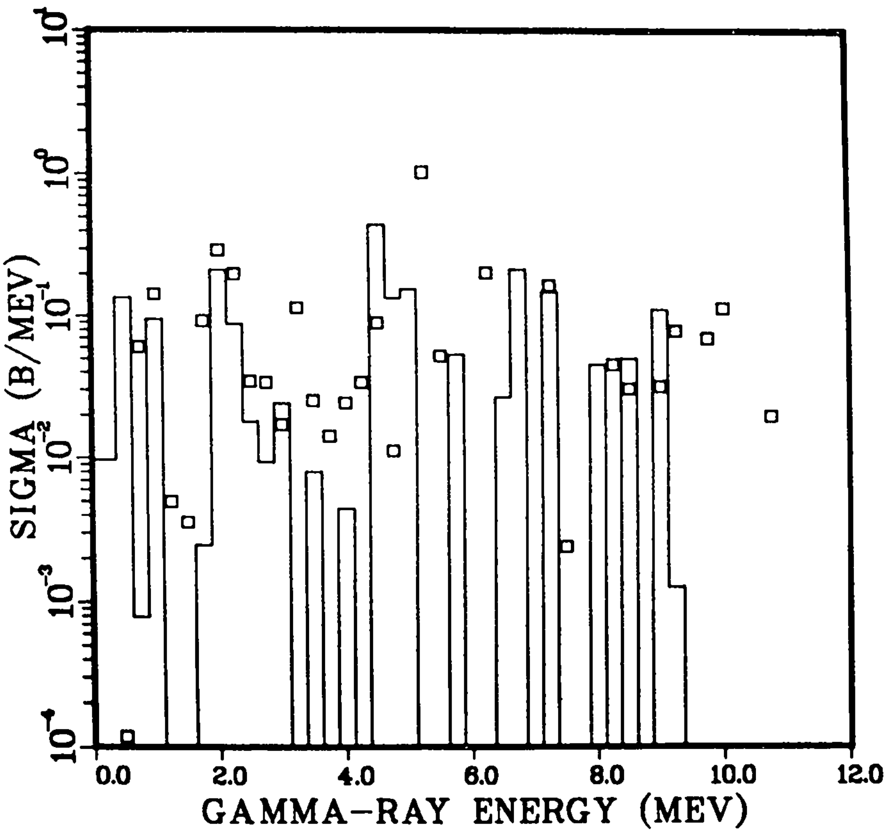

Fig. 3. Gamma-ray emission spectra calculated for 14-MeV neutrons incident on ^{11}B (histogram) and ^{15}N (open squares). See text for details.

E. Nuclear Model Code Calculations for n+^{93}Nb Reactions (P. G. Young)

We are participating in an international nuclear model code comparison study organized by the Nuclear Energy Agency Data Bank (NEADB) at Saclay.[11] The study is aimed primarily at comparing preequilibrium calculations but inevitably involves statistical-theory Hauser-Fesbach models, level densities, gamma-ray strength functions, and the optical model. The nucleus ^{93}Nb was chosen primarily because of the availability of measured neutron spectra at 14.6 and 25.7 MeV,[12,13] (n,2n) and (n,3n) cross section to 24 MeV,[14,15] and proton and alpha emission spectra at 15 MeV.[16]

The primary nuclear model code used for our calculations is the GNASH[6] statistical-preequilibrium program. Most of the model parameters were specified for the exercise. Optical model potentials similar to those of Perey[17] were used for neutrons and protons, whereas Igo and Huizenga's[18] potential was selected for alpha particles. Several possibilities were available for level-density representations. We chose to use the Gilbert and Cameron representation, including their original spin cutoff formula,[19] together with level-density parameters, pairing energies, continuum cutoff energies, and level-matching parameters specified for the exercise.[11] Information on discrete energy levels was largely prescribed by the NEADB, although it was necessary for us to provide gamma-ray branching ratios for all residual nuclei except ^{92}Nb and ^{93}Nb. Masses and Q-values were specified for the exercise, although we elected to use the GNASH default values as they were very similar. We used the spherical optical model code SCAT2[20] to calculate neutron total and shape elastic cross sections for ^{93}Nb.

Multipolarities of E1, M1, and E2 were permitted for gamma rays in the calculations. In each case the gamma-ray strength functions [$f_{x\ell}(E_\gamma)$] were normalized by the relationship

$$\frac{\langle \Gamma_\gamma^{x\ell} \rangle}{\langle D_0 \rangle} = \int_0^{B_n} f_{x\ell}(E_\gamma) E_\gamma^{2\ell+1} \rho(B_n - E_\gamma) dE_\gamma \quad ,$$

where B_n is the neutron binding energy and $\rho(B_n - E_\gamma)$ is the level density of ^{94}Nb. The quantities $\langle \Gamma_\gamma^{x\ell} \rangle$ and $\langle D_0 \rangle$ were provided for the calculations. A giant-dipole resonance expression was assumed for f_{E1}, whereas the Weisskopf form ($f_{x\ell}$ = constant) was used for M1 and E2. Gamma-ray transmission coefficients were computed from the expression

$$T_{\gamma}^{x\ell}(E_{\gamma}) = 2\pi f_{x\ell}(E_{\gamma})E_{\gamma}^{2\ell+1} \quad .$$

Because of the variety of forms commonly used to calculate preequilibrium effects, parameters for these calculations were not prescribed by the NEADB. Instead, the participants were asked to adjust their preequilibrium parameters to agree with Hermsdorf's neutron emission data at secondary neutron energies between 6 and 9 MeV. We used the GNASH default preequilibrium parameters in our calculations because they agreed with Hermsdorf's data to better than ± 4% at these secondary energies.

The reaction sequences we included in our GNASH calculations are depicted in Fig. 4. The solid circles in the figure indicate the compound nuclei that were populated and permitted to decay. The various radiation types are indicated, and the solid and dashed curves show the reaction chains followed. No other chains were found to contribute in any significant amount.

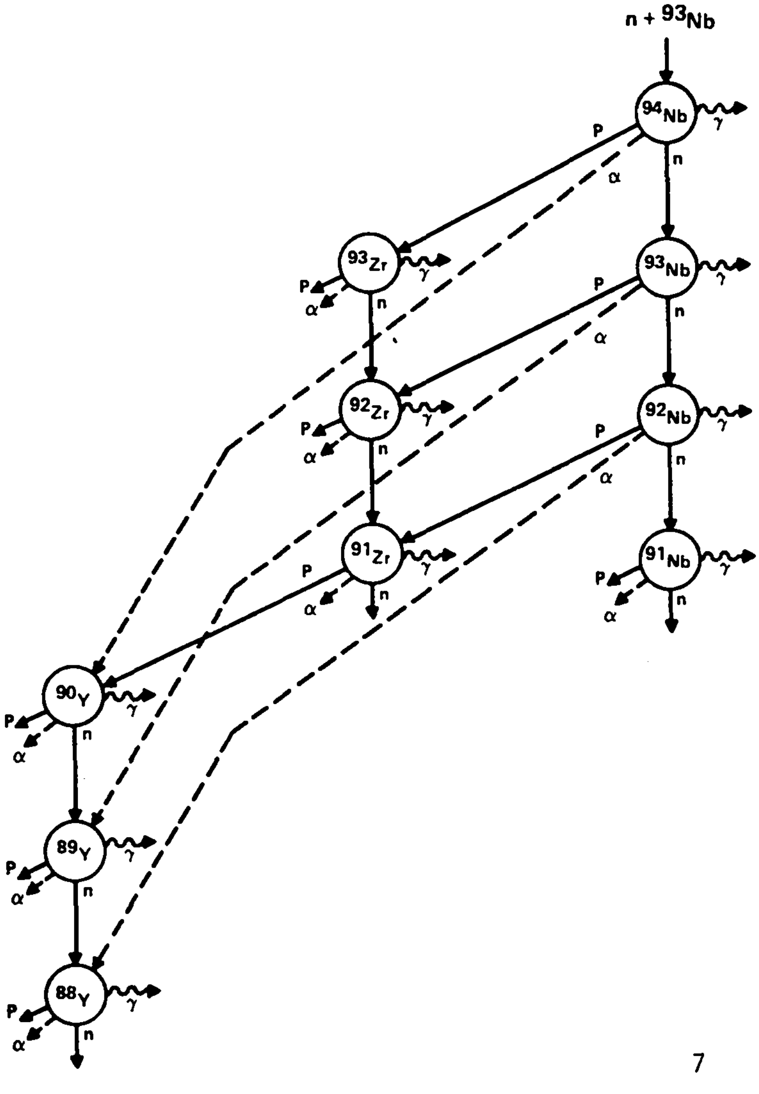

Fig. 4. Schematic diagram of the reaction sequences included in the $n+{}^{93}Nb$ calculations.

The integrated cross-section results from our calculations are included in Table I. The (n,2n) and (n,3n) cross-section calculations are compared with the measurements of Veeser et al.[15] and Frehaut et al.[14] in Fig. 5. The neutron emission spectra from our calculation are compared in Fig. 6 to the measurements at 14.6 MeV by Hermsdorf et al.[12] and in Fig. 7 with the measurements at 25.7 MeV by Marcincowski et al.[13] These and other results have been provided to the NEADB, who will compile results from all participants and provide systematic comparisons.

TABLE I

INTEGRATED CROSS SECTIONS

The numbers in parentheses were obtained with the preequilibrium correction set to zero. All cross sections are in mb units.

Reaction	E_n=10 MeV	14.6 MeV	20 MeV	25.7 MeV	Footnote
σ_t	4294.7	4020.4	3372.2	2919.8	
σ_{el}	2473.2	2265.4	1695.5	1309.6	a
σ_r	1821.6	1755.3	1677.1	1610.3	
$\sigma_{n,nx}$	1802. (1817.)	1708. (1749.)	1599. (1667.)	1509. (1598.)	b
$\sigma_{n,px}$	12.85 (2.40)	35.74 (5.23)	66.03 (8.55)	90.57 (11.29)	b
$\sigma_{n,\alpha x}$	6.21 (1.19)	10.80 (1.16)	11.72 (0.89)	10.28 (0.61)	b
$\sigma_{n,n'}$	1298. (1202)	332.8 (97.34)	180.2 (7.83)	111.2 (1.09)	
$\sigma_{n,2n}$	503.0 (613.8)	1369. (1644.)	1123. (1189.)	454.9 (183.1)	
$\sigma_{n,3n}$	—	—	271.9 (435.9)	874.3 (1310.)	

---

[a] Includes small compound elastic component.

[b] First emission by ^{94}Nb of neutrons, protons, and alphas in binary reactions only.

TABLE I (Cont.)

Reaction	E_n=10 MeV	14.6 MeV	20 MeV	25.7 MeV	Footnote
$\sigma_{n,np}$	0.53 (0.63)	3.34 (4.32)	16.30 (23.35)	23.61 (30.84)	c
$\sigma_{n,p}$	12.81 (2.36)	28.21 (1.88)	28.55 (0.20)	21.34 (0.005)	
$\sigma_{n,pn}$	0.04 (0.042)	7.53 (3.35)	37.35 (8.22)	57.43 (5.35)	c
$\sigma_{n,n\alpha}$	0.57 (0.66)	2.61 (3.34)	6.50 (8.78)	9.22 (12.11)	c
$\sigma_{n,\alpha}$	6.21 (1.18)	9.07 (0.59)	4.99 (0.034)	2.14 (0.001)	
$\sigma_{n,\alpha n}$	(0.01) (0.006)	1.73 (0.57)	6.73 (0.85)	8.07 (0.56)	c
$\sigma_{n,2np}$	——	——	1.17 (1.85)	46.26 (64.71)	d
$\sigma_{n,2n\alpha}$	——	——	<0.001 (<0.001)	1.13 (1.98)	d
$\sigma_{n,3np}$	——	——	——	0.021 (0.041)	d
$\sigma_{n,np\alpha}$	——	——	0.003 (0.001)	0.106 (0.140)	d
$\sigma_{n,p\alpha}$	——	<0.001 (<0.001)	0.001 (0.001)	<0.001 (<0.001)	d
$\sigma_{n,2p}$	——	——	<0.001 (<0.001)	<0.001 (<0.001)	d
$\sigma_{n,2\alpha}$	——	——	<0.001 (<0.001)	0.001 (<0.001)	d
$\sigma_{n,n2p}$	——	——	——	0.021 (0.011)	d
$\sigma_{n,nem}$	2305. (2431.)	3086. (3396.)	3311. (3739.)	3837. (4480.)	

---

[c] The ordering of the reaction subscripts indicates the sequence of these reactions.

[d] The ordering of the reaction subscripts has no significance--all possible reaction paths are considered.

TABLE I (Cont.)

Reaction	E_n=10 MeV	14.6 MeV	20 MeV	25.7 MeV	Footnote
$\sigma_{n,pem}$	13.39 (3.03)	39.09 (9.55)	83.38 (33.61)	148.8 (101.1)	
$\sigma_{n,\alpha em}$	6.78 (1.85)	13.41 (4.50)	18.22 (9.67)	20.66 (14.80)	
$\sigma_{n,\gamma em}$	4520. (4442.)	3675. (3523.)	3928. (3800.)	4184. (4326.)	
$\sigma_{n,n'}$(13.6y)	480.8 (455.4)	144.8 (60.38)	74.45 (6.01)	46.3 (0.90)	e
$\sigma_{n,2n}$(10.1d)	148.9 (182.3)	559.5 (674.0)	385.9 (382.0)	143.7 (40.12)	f

---

e ^{93}Nb(n,n')^{93m}Nb; $T_{1/2}$ = 13.6y; E_x = 0.0304 MeV.

f ^{93}Nb(n,2n)^{92m}Nb; $T_{1/2}$ = 10.1d; E_x = 0.1355 MeV.

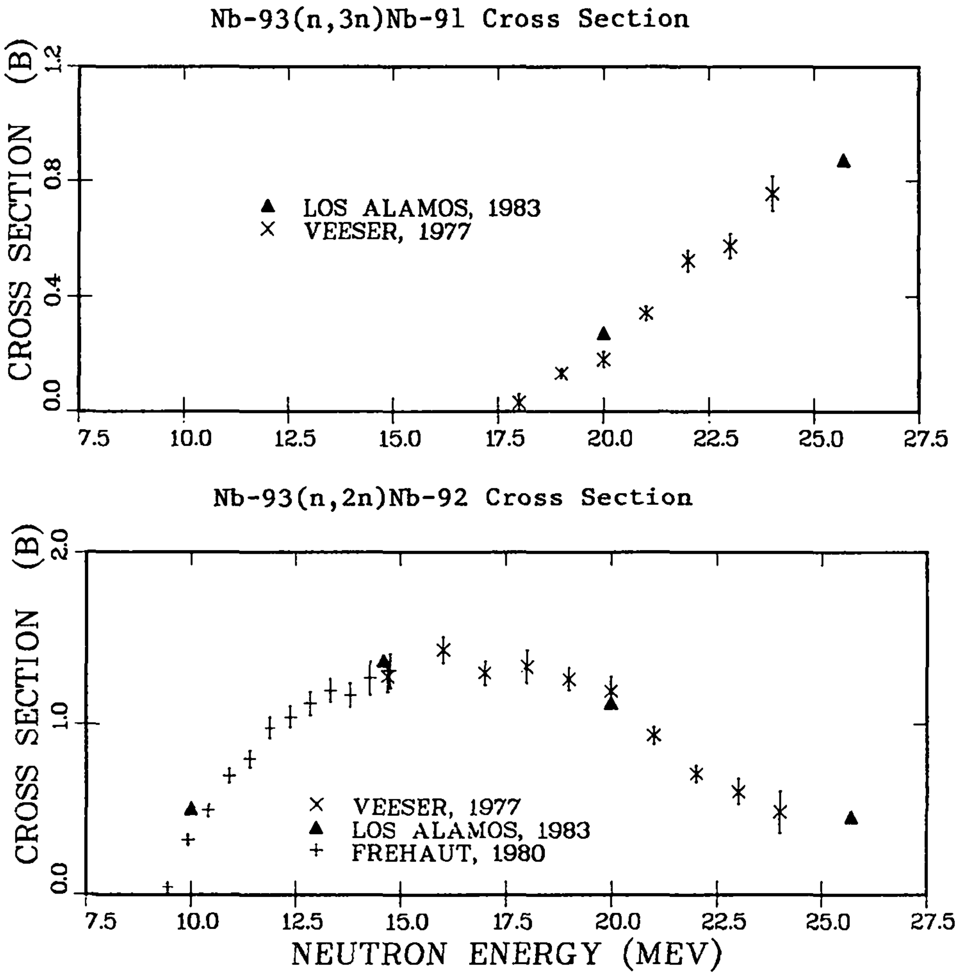

Fig. 5. Comparison of calculated ^{93}Nb (n,2n) and ^{93}Nb(n,3n) cross sections (solid triangles) with the experimental data of Frehaut et al.[14] and Veeser et al.[15]

Fig. 6. Comparison of neutron emission spectra from 14.6-MeV neutrons on ^{93}Nb calculated with (solid curve) and without (dashed curve) preequilibrium effects with experimental data by Hermsdorf et al.[12]

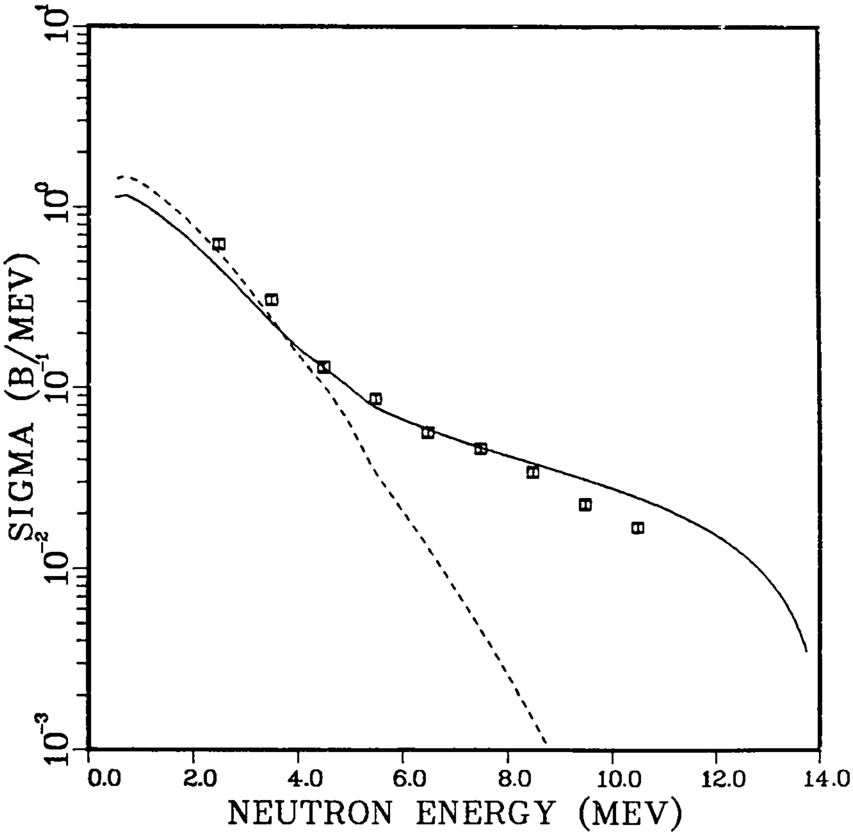

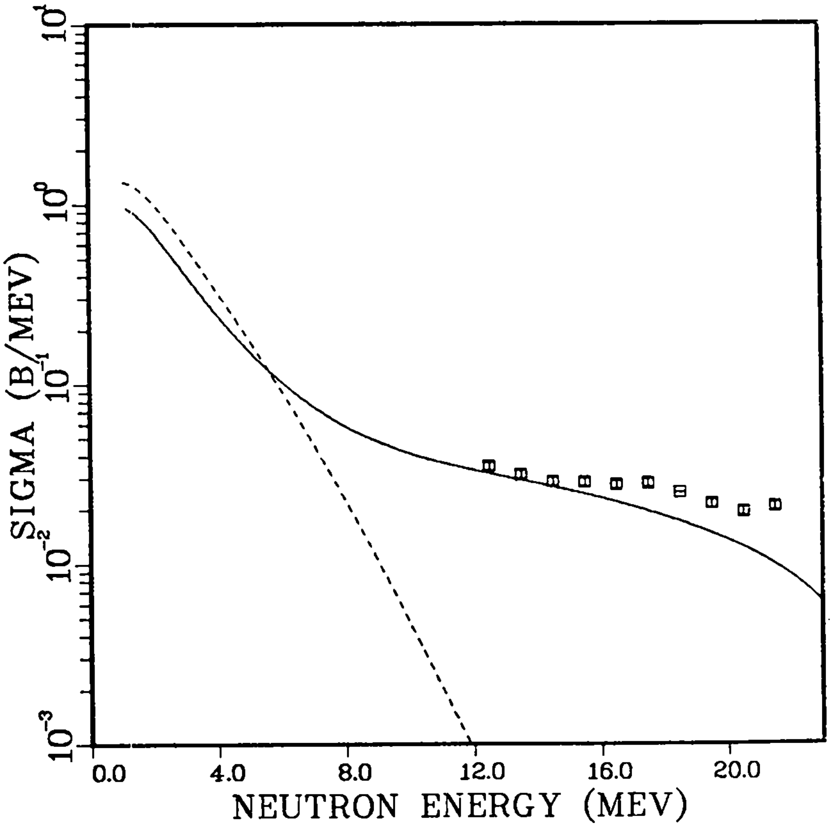

Fig. 7. Comparison of neutron emission spectrum from 25.7-MeV neutrons on ^{93}Nb calculated with (solid curve) and without (dashed curve) pre-equilibirum effects with experimental data by Marcincowski et al.[13]

F. Analysis of n+^{197}Au Cross Sections from E_n = 0.01 to 30 MeV (P. G. Young and E. D. Arthur

An analysis of nuclear data for n+^{197}Au reactions between E_n = 0.01 and 30 MeV is nearing completion. Particular emphasis has been given in the analysis to obtaining gamma-ray strength functions that permit calculation of extensive gamma-ray emission measurements by Morgan and Newman.[21]

The deformed optical model parameterization derived by Delaroche[22] was adopted in our analysis. This parameterization gives good agreement with neutron total cross-section measurements on ^{197}Au between 80 keV and 27 MeV, elastic (n,n) angular distributions near 5 MeV, and, making use of isospin relationships, ^{197}Au(p,p) elastic-scattering angular distributions at 13.8 and 55 MeV. The neutron optical model parameters are listed in Table II.

TABLE II

DEFORMED OPTICAL MODEL PARAMETERS FOR n+^{197}Au[a]

			r	a
V	$= 46.34 - 0.25E$		1.26	0.64
W_{VOL}	$= -8.54 + 2.7\sqrt{E}$	$E > 10$ MeV	1.26	0.64
V_{SO}	$= 6.2$		1.12	0.47
W_{SD}	$= 2.42 + 0.5\ E$	$E < 10$ MeV	1.26	0.47
	$= 7.42 - 0.18\ (E-10)$	$E \geqq 10$ MeV	1.26	0.47
β_2	$= -0.13$	$\beta_4 = -0.05$ MeV		

---

[a] All well depths are in MeV and geometrical parameters in fm.

The coupled-channel code ECIS[23] was used for our deformed optical model calculations. The lowest three states of the ^{197}Au ground-state rotational band were coupled in the calculation ($J^\pi = 3/2^+, 5/2^+, 7/2^+$ at E_x = 0, 279, 548 keV, respectively). Neutron transmission coefficients were calculated to 30 MeV with ECIS and were collapsed to a form depending only on incident neutron energy and orbital angular momentum ℓ for use in Hauser-Feshbach calculations.

The Hauser-Feshbach statistical-theory calculations were performed with the COMNUC[24] and GNASH[6] reaction theory codes. The COMNUC cross-section calculations include width-fluctuation corrections, important at lower energies, and the GNASH calculations incorporate preequilibrium effects, which become significant at higher energies. In our analysis, COMNUC was used to calculate cross sections below 3 MeV, whereas GNASH was used for cross sections above 3 MeV and for spectra calculations at all energies. Both codes use the Gilbert and Cameron[19] level-density formulation and the Cook[25] tabulation of level-density parameters, although these values were adjusted slightly as described below. A maximum amount of experimental information on discrete energy levels was incorporated into the calculations, and the constant temperature part of the Gilbert and Cameron level densities was matched to the discrete-level data for each residual nucleus in the calculations.

Gamma-ray transmission coefficients were calculated from E1 and M1 strength functions. A giant-dipole resonance shape[26,27] was used for the M1 strength function with the parameters $E_R^{M1} = 8$ MeV and $\Gamma_R^{M1} = 5$ MeV.[28] The shape of the E1 strength function was determined for $E_\gamma < 8$ MeV by trial-and-error calculation of the ^{197}Au(n,γ) spectrum measurements of Morgan and Newman.[21] Above $E_\gamma = 8$ MeV, the empirically determined E1 strength function was joined to a giant-dipole resonance shape.[26,27]

The normalizations of the strength functions were determined with the relationship

$$\frac{\langle\Gamma_\gamma\rangle}{\langle D_0\rangle} = \int_0^{B_n} [f_{E1}(E_\gamma) + f_{M1}(E_\gamma)]\, E_\gamma^3 \rho(B_n - E_\gamma) dE_\gamma$$

where $f_{x\ell}(E_\gamma)$ are the gamma-ray strength functions, B_n is the neutron binding energy of ^{198}Au, $\langle\Gamma_\gamma\rangle$ is the average gamma-ray width (= 0.122 eV),[29] and $\langle D_0\rangle$ is the mean s-wave resonance spacing (= 16.2 eV).[29] The ratio $\Gamma_{M1}/(\Gamma_{M1} + \Gamma_{E1}) = 0.12$ was assumed in the calculations.[28]

The E1 gamma-ray strength function that resulted from this analysis is compared in Fig. 8 with values inferred from experiments by Joly et al.,[30] Loper et al.,[31] and Veyssiere et al.[32] The present curve is quite similar to one obtained from Morgan's data[21] by Kitazawa[33] using different neutron transmission coefficients and level-density parameters.

The ^{197}Au(n,γ) spectrum that results from our analysis is compared in Fig. 9 with Morgan's data[21] over the incident neutron energy bin 0.2 to 0.6 MeV. Note that the calculated curve has not been broadened for detector resolution or for the 0.4-MeV-wide incident neutron energy bin.

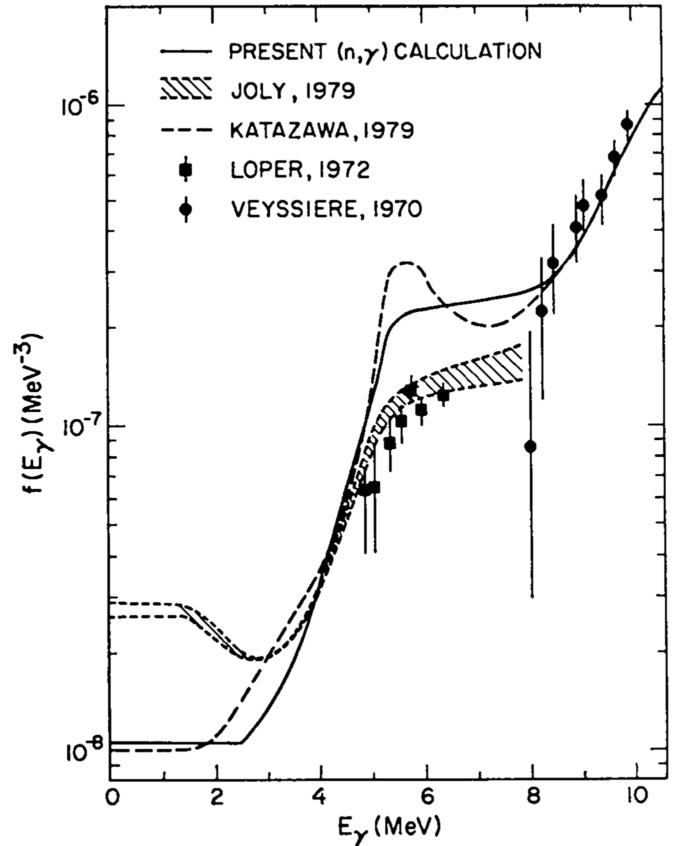

Fig. 8. E1 gamma-ray strength functions inferred from ^{197}Au(n,γ) ^{198}Au measurements. The solid curve (present results) and the dashed curve[33] were both obtained from the experiment of Morgan and Newman.[21] The other results[31,32] are from independent measurements.

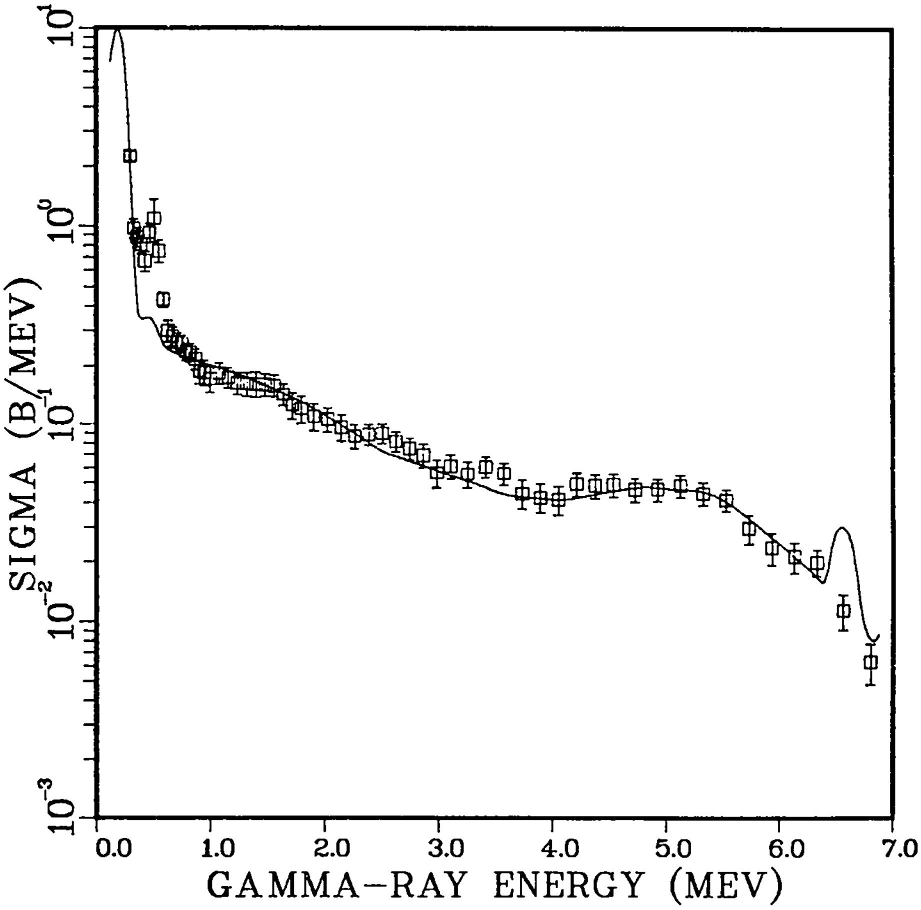

Fig. 9. Comparison of the present calculations with the measured gamma-ray emission spectrum at E_n = 0.2 - 0.6 MeV by Morgan and Newman.[21] Above E_γ ~ 0.6 MeV, the spectrum results exclusively from the ^{197}Au(n,γ) reaction.

The calculated $^{197}Au(n,\gamma)^{198}Au$ cross section from 0.01 to 1 MeV (multiplied by $\sqrt{E_n}$ to remove the 1/v dependence) is compared with a selection of experimental data* and with ENDF/B-V[34] (dashed curve) in Fig. 10. For this comparison, the ENDF/B-V curve, which contains pronounced structure at lower energies, was averaged below E_n = 200 keV. The calculated results above 1 MeV are shown with ENDF/B-V and a different sampling of experimental data in Fig. 11. The pronounced peak in the theoretical cross section near E_n = 12 MeV results from inclusion of a semidirect component[35] in the calculation, which is clearly necessary to reproduce the measurements near 14 MeV.

The strength function found for the $^{197}Au(n,\gamma)$ spectra was not satisfactory for calculating spectra at higher neutron energies, where $(n,n'\gamma)$, $(n,2n\gamma)$, and $(n,3n\gamma)$ reactions dominate. A modified form of $f_{E1}(E_\gamma)$ was inferred from Morgan's data at E_n = 6-7 MeV, however, and was found to give reasonable agreement with his data out to E_n = 20 MeV.

The preequilibrium parameters and the level-density parameter 'a' were adjusted slightly from the default values used by GNASH to concurrently optimize agreement with 14-MeV neutron emission spectra,[12,36] a precise value of the (n,2n) cross section at 14.7 MeV determined in a covariance analysis of all data,[37] and the energy dependence of the (n,2n), (n,3n), and (n,4n) cross sections[14,15,38] over the energy range E_n=8-28 MeV. In no case was the level-density parameter adjusted by more than 10% from the Cook values.[25] The preequilibrium fraction that results at 14 MeV in our analysis is 33%.

The $^{197}Au(n,2n)$ cross section that resulted from this analysis is compared to a selection of experimental data[14,15,38] and to ENDF/B-V[34] in Fig. 12. Similarly, the (n,3n) and (n,4n) results are compared to measurements and to ENDF/B-V in Fig. 13. The calculated (n,2n) results agree well with the data to about 22 MeV but are somewhat high at higher energies. Excellent agreement between the calculation and the measurement of Bayhurst et al.[38] is found at all energies for the (n,3n) cross section. Reasonable agreement is also found in the case of (n,4n), although the calculation is again somewhat high at the highest energy.

After more thorough comparisons with experimental data are completed, the results of this calculation will be cast in ENDF/B-V format and merged with the existing ENDF/B-V evaluation at energies below E_n=0.1 MeV.

---

*Experimental data were obtained on magnetic tape from the National Nuclear Data Center, Brookhaven National Laboratory, Upton, NY.

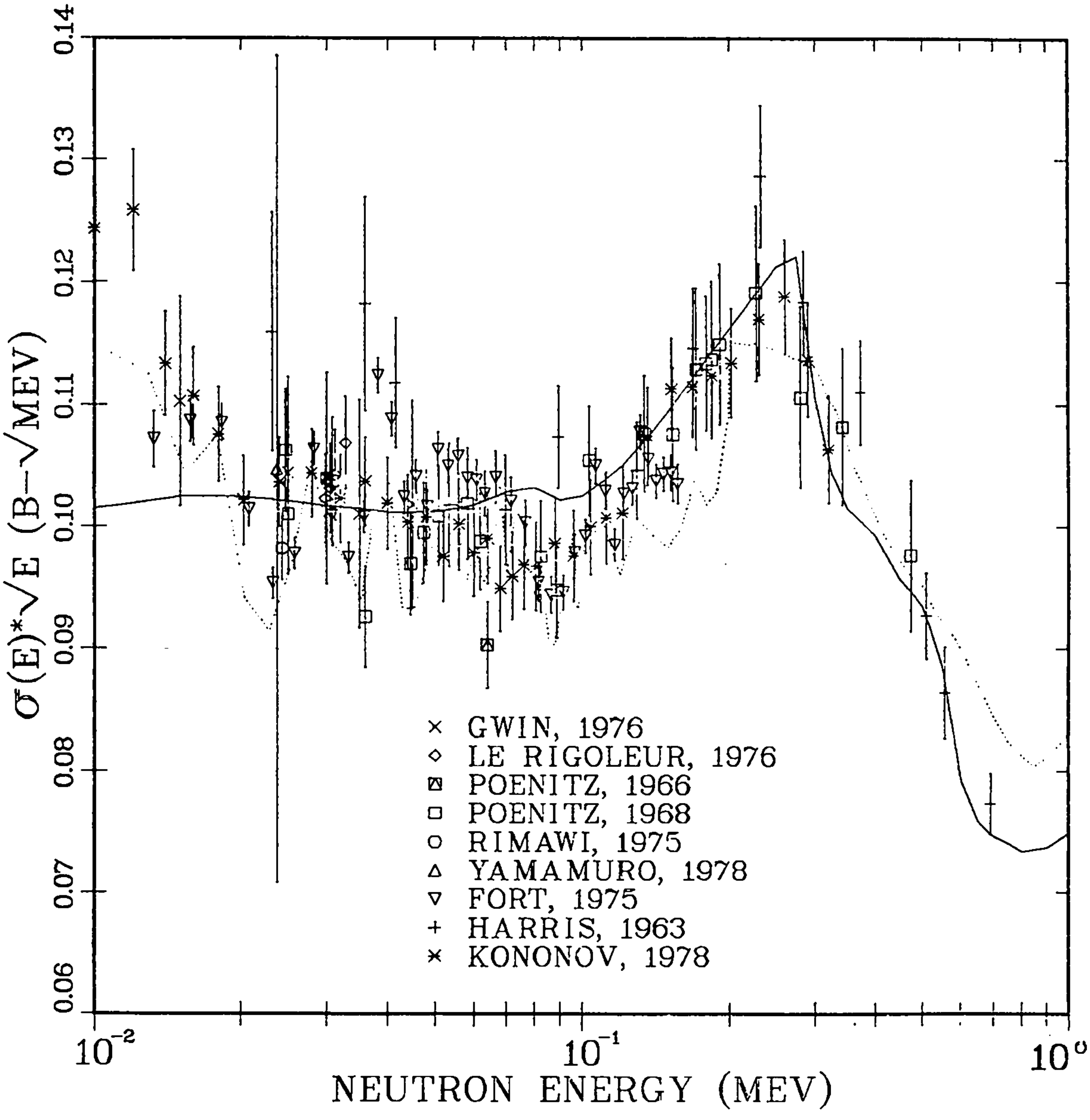

Fig. 10. Measured and calculated $^{197}Au(n,\gamma)^{198}Au$ cross sections from 0.01 to 1.0 MeV. The solid curve represents the present calculation and the dashed curve is ENDF/B-V after averaging.

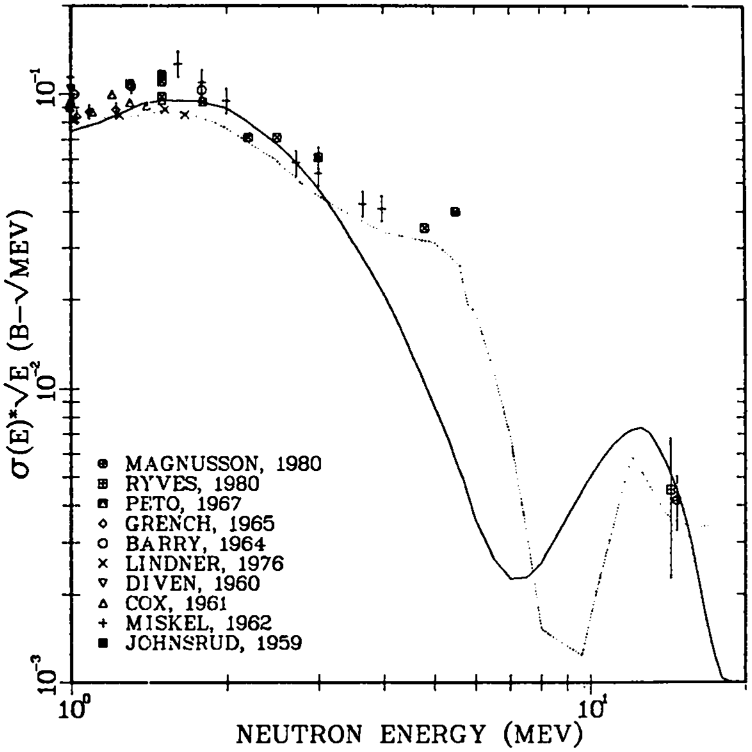

Fig. 11. Measured and calculated $^{197}Au(n,\gamma)^{198}Au$ cross sections from 1.0 to 20.0 MeV. The solid curve is the present calculation and the dashed curve is ENDF/B-V.

Fig. 12. Comparison of the present calculation of the ^{197}Au (n,2n) cross section from threshold to 30 MeV with ENDF/B-V[34] and experimental data.[14,38] The solid curve is the present calculation and the dashed curve is ENDF/B-V.

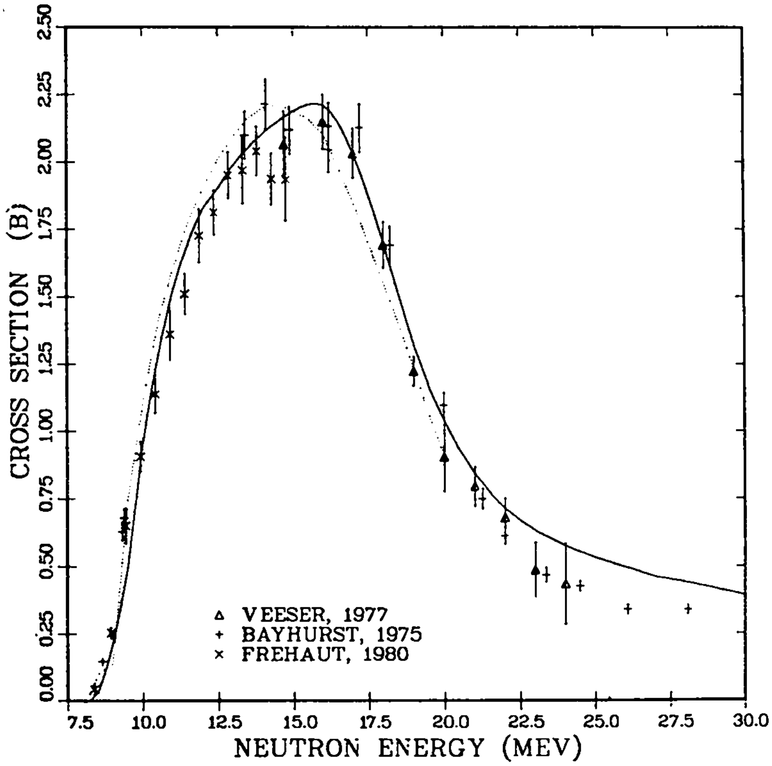

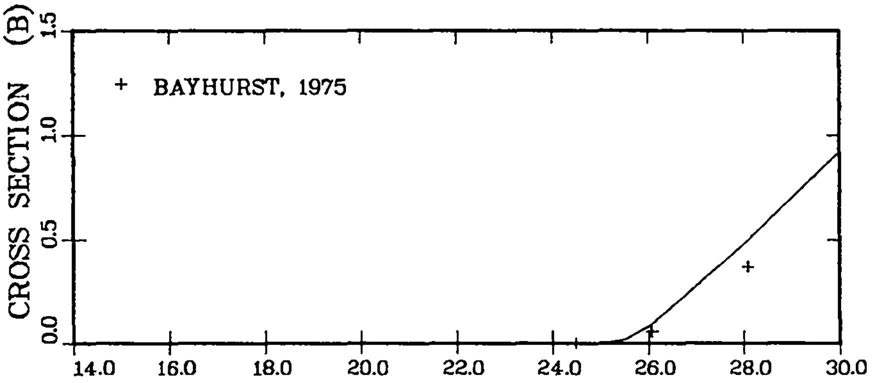

AU-197(N,3N)AU-195 CROSS SECTION

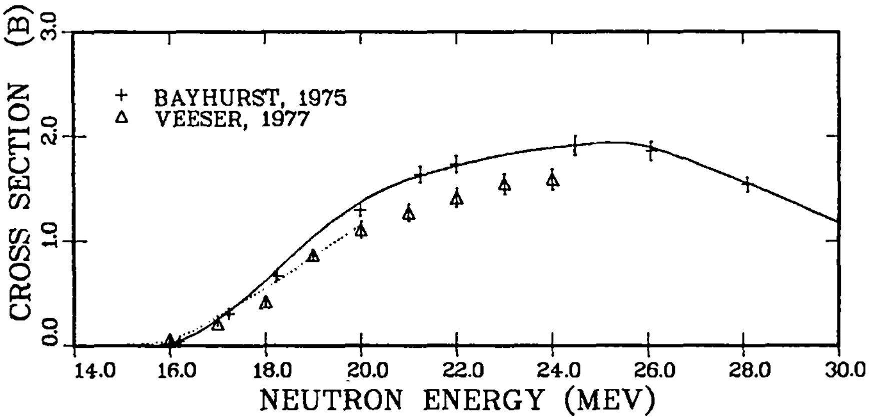

Fig. 13. Calculated and measured values ^{15,38} of the ^{197}Au(n,3n) and ^{197}Au(n,4n) cross sections from threshold to 30 MeV. The solid curve is the present calculation and the dashed curve is ENDF/B-V.^{34}

G. Theoretical Analyses of Recent Simulation Experiments Involving Proton Reactions on Strontium Isotopes (E. D. Arthur)

Experimental measurements have been made recently that provide data pertinent to the determination of model parameters for neutron reaction calculations in the A = 90 mass region. Two general classes of experiments were performed, the first being $^{86-88}$Sr(p,xn) and ^{86}Sr(p,γ) activation measurements made by INC-11,^{39} while the second involved proton emission spectra measured^{40} for (p,pn + p,np) reactions on ^{87}Sr and ^{91}Zr. (Analysis of the ^{91}Zr data will be discussed in the following contribution to this progress report.) Both of these data types were shown previously^{41} to be sensitive to the choice of model parameters, particularly those associated with proton emission from the ^{87}Y compound system.

To compare with these data, calculations were made with the GNASH^{6} multistep Hauser-Feshbach statistical model code that includes preequilibrium corrections. In these statistical calculations, isospin effects[42] were not included that could possibly enhance proton emission probabilities through population of upper isospin states in a given compound system. These states can only decay by proton emission, and their influence can in some instances lead to increased proton emission cross sections. Such effects would be most important for proton cross sections involving minor reaction paths and should be apparent in such instances. However, examination of the proton spectrum data from these experimental measurements showed no strong isospin effects, which provided the principal justification for their neglect in the calculations. Additionally, the presence of isospin mixing further clouds the theoretical analysis of such data. Finally, as we shall illustrate, we were able to achieve consistent analyses of several diverse proton reaction types using realistic parameter values.

Our first set of calculations employed the nuclear model parameters obtained from our 1978 study,[35] which have subsequently been used for the majority of our mass 90 calculations.[43,44] As a reminder, the parameters determined in Ref. 35 were based upon analysis of a large amount of experimental data relevant to the calculations of interest. Neutron optical parameters were adjusted to reproduce resonance data as well as total and elastic cross sections, systematics were derived for gamma-ray strength functions, and low energy (p,n) data were analyzed to determine the sub-Coulomb barrier behavior of the proton optical parameters.

Figure 14 compares ^{87}Sr(p,pn + p,np) cross sections using this parameter set with data measured by P-3 for proton energies between 15 and 17.6 MeV. These measurements detected protons in coincidence with neutrons, so that in the calculations the neutron detector threshold must be accounted for. The solid curve in the figure illustrates the calculated results when the experimentally determined detector threshold of 0.6 MeV is included, while the dashed curve ignores such detector effects. Figure 15 compares our calculations made for the ^{87}Sr(p,n) cross section (solid curve) and (p,2n) cross section (dashed curve) to the recently measured activation data of Ref. 39.

Reasonable agreement with the data exists for the (p,np + p,pn) comparison shown in Fig. 14, but the calculated (p,n) values (Fig. 15) significantly underpredict the measured ones. The principal reason is the overprediction of the cross section for the competing (p,n'p) reaction, which consequently lowers the calculated (p,n) values.

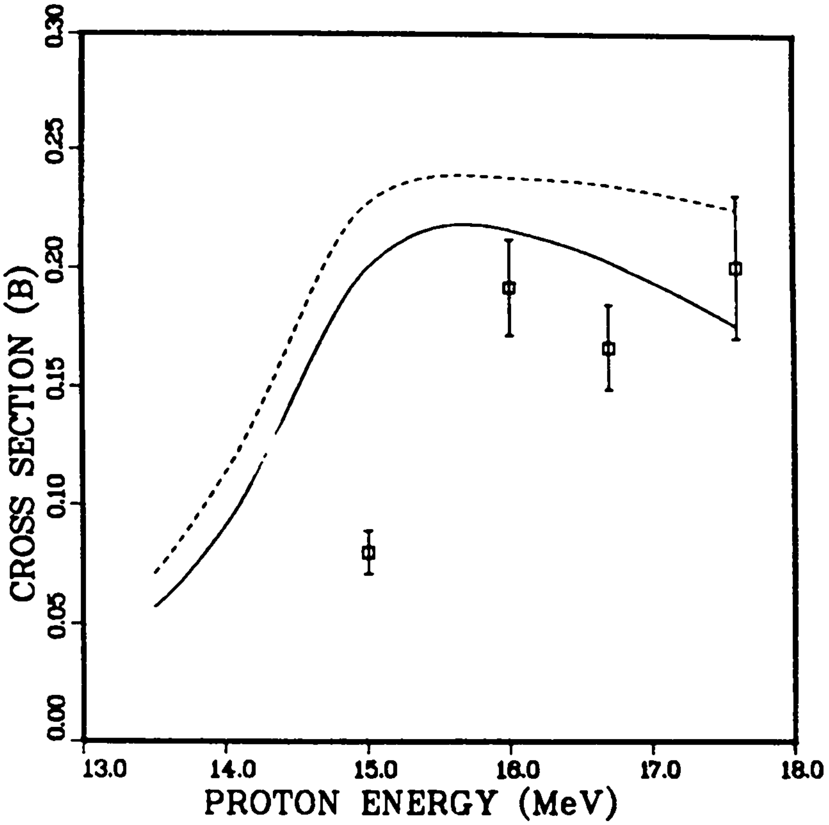

Fig. 14. Cross sections for the ^{87}Sr(p,pn+p,np) reactions calculated using the parameters of Ref. 35 are compared with recent measurements.[40] The solid curve results when a neutron detector threshold of 0.6 MeV is included in the calculations, while the dashed curve is obtained when the detector threshold is ignored.

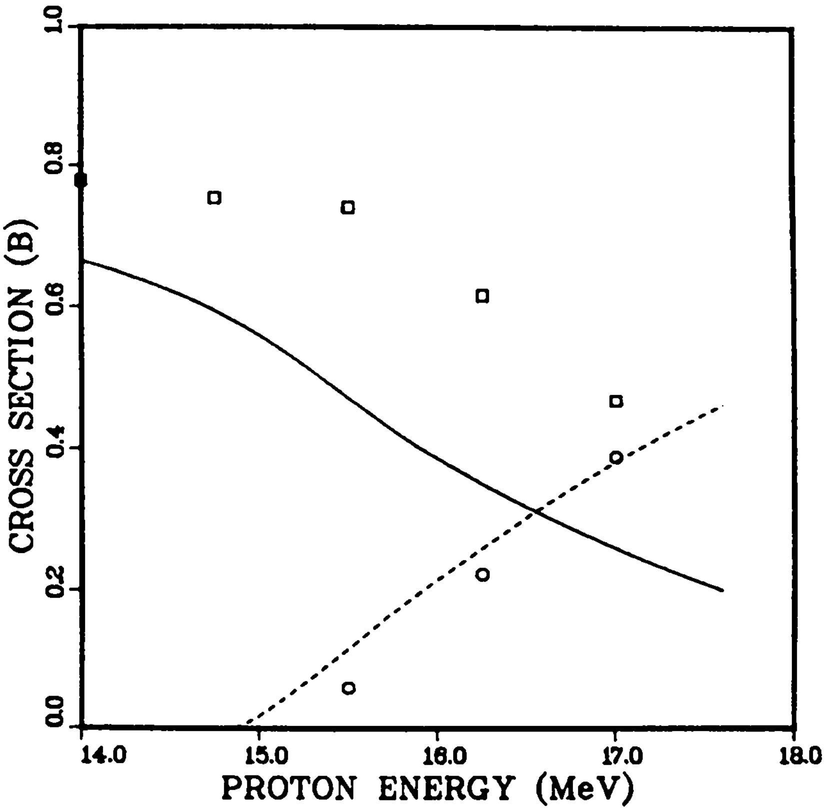

Fig. 15. Cross sections for ^{87}Sr(p,n) (solid curve) reactions calculated using the parameters of Ref. 35 (p,2n) (dashed curve) are compared with the data of Ref. 39.

To improve the agreement between our calculations and such measurements, we examined other data relevant to parameter determinations needed for this problem. We concentrated on recent data that would guide such efforts, particularly those that impact the determination of gamma-ray and proton emission probabilities. Such parameters are important in this problem because of the 6.1-MeV-wide proton window that exists for the ^{87}Y compound nucleus. In this excitation energy region, proton emission occurs unencumbered by neutron competition. Neutron parameters are still important because of the role they play in populating ^{87}Y compound nucleus states that subsequently decay by proton emission. To improve upon the low-energy behavior of the neutron optical potential, we employed new resonance information[45] available since our 1978 calculations. Table III compares these new experimental data with values calculated previously and with those now obtained after suitable parameter adjustment.

TABLE III

NEUTRON RESONANCE DATA FOR n+^{89}Y CALCULATED USING THE
1978 OPTICAL PARAMETERS AND CURRENT ONES DESCRIBED IN THE TEXT

	Expt. (Ref. 45)	1978 OM	1983 OM
S_0 (x 10^{-4})	0.27 ± 0.05	0.496	0.338
S_1 (x 10^{-4})	2.65 ± 0.3	4.8	3.75
R'(fm)	6.7 ± 0.1	6.5	6.55

Likewise, the proton optical parameters from the 1978 parameter set were adjusted to improve agreement to the recently measured low-energy ^{87}Sr(p,n) data of Ref. 39. In doing so the resultant parameters are more consistent with proton optical parameters extracted from the 1978 analysis of more reliable ^{89}Y(p,n) data.[46] Updated and improved discrete-level information was incorporated into the second group of calculations to be discussed below. Particularly for ^{87}Y, new information available since 1978 dramatically changed the discrete-level spectrum as well as the nuclear level densities for excitation energies between 3 and 6 MeV. Finally, the normalization of the gamma-ray strength function was adjusted to reproduce newly available ^{86}Sr(p,γ) cross sections.[39] Comparison with these data appears in Fig. 16. Calculations were not attempted at higher energies (above 6 MeV) since gamma-ray cascades were not included. This leads to a theoretical overprediction of the (p,γ) cross section because (p,γx) contributions were not removed from the calculated values.

Again, the existence of such data allows one to realistically determine the gamma-ray competition to proton emission occurring in the ^{87}Y compound nucleus.

These parameter changes were incorporated into the theoretical models and the calculations were repeated. In addition, the Fermi-gas level-density parameter for ^{87}Y was increased by 6%. No firm corroborating evidence was available for this ad hoc change, but the agreement to the higher energy (p,pn + p,np) data appeared to be improved. The revised calculations are compared with data in Figs. 17 and 18. The result of the parameter adjustments discussed above is a significant improvement in the overall agreement, particularly for the case of the ^{87}Sr(p,n) reaction.

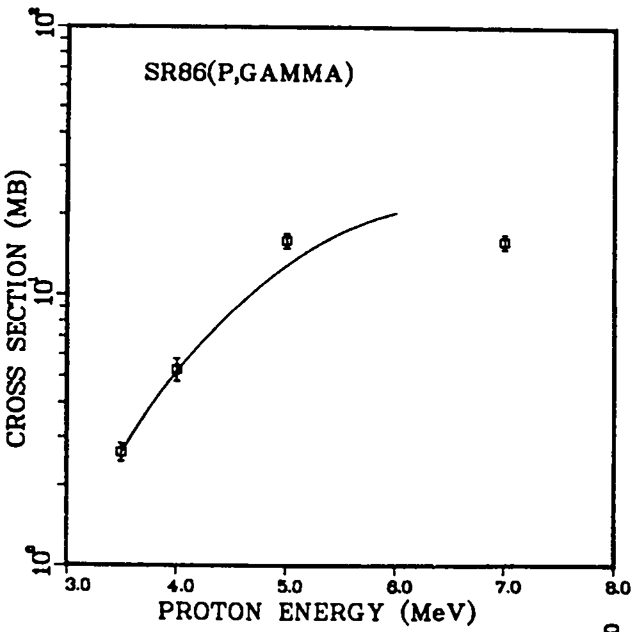

Fig. 16. Calculation of the ^{86}Sr(p,γ) cross section used to optimize the theoretical normalization for the ^{87}Y gamma-ray strength function. The data are from Ref. 39.

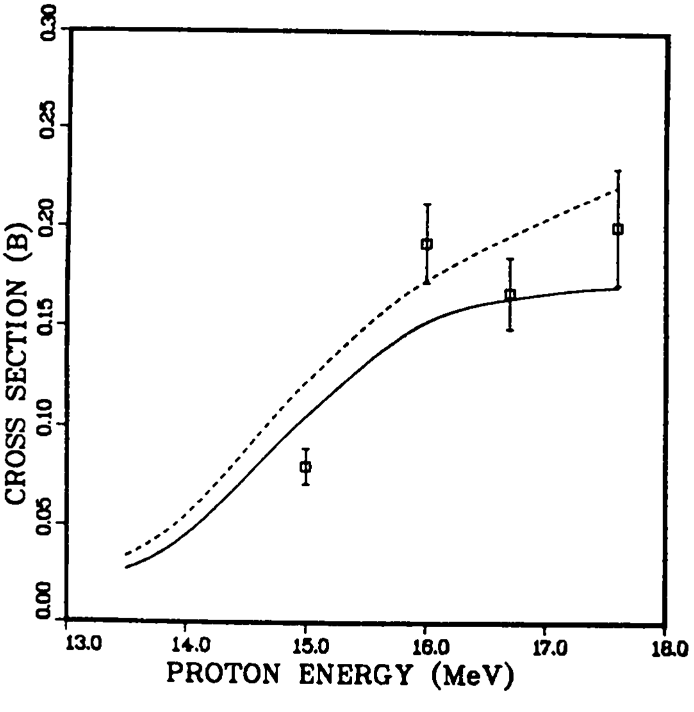

Ref. 17. Cross sections for the ^{87}Sr(p,pn+p,np) reactions calculated, using the revised parameters described in the text, are compared with recent measurements.[40] The solid curve results with a neutron detector threshold of 0.6 MeV, while the dashed curve is obtained when the detector threshold is ignored.

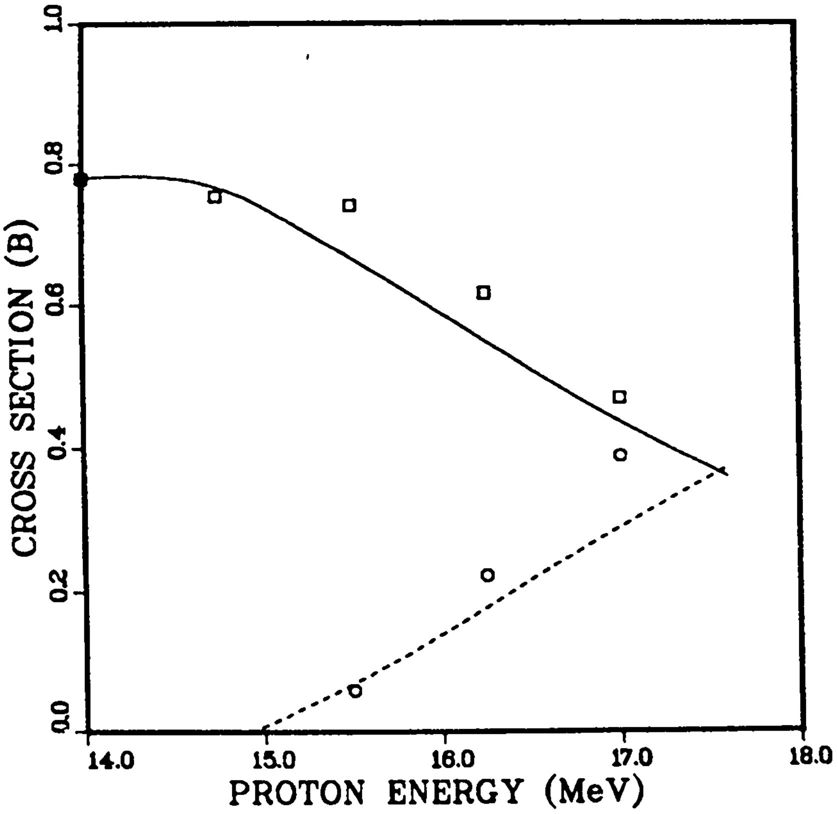

Fig. 18. Cross sections for ^{87}Sr(p,n) (solid curve) and (p,2n) (dashed curve) reactions calculated with the updated parameters described in the text.

Additional data for population of discrete levels of the ^{86}Sr residual nucleus produced in ^{87}Sr(p,pn + p,np) reactions were measured by P-3 at proton energies of 15, 16, and 16.7 MeV. Specifically, cross sections were measured for production of the 0^+ ground state, the 2^+ state at 1.077 MeV, the 2^+ state at 1.855 MeV, and the sum of the 4^+ and 3^- levels at 2.23 and 2.48 MeV, respectively. Populations of higher lying levels were small and were therefore lumped together. Comparison with these data appears in Figs. 19 and 20, where the datum occurring around E_x = 3 MeV actually refers to the sum over higher lying levels. Comparison with the data places very stringent constraints on the model parameters since final states of well-characterized energy, spin, and parity are populated.

In summary, parameters are available for the ^{87}Y and ^{88}Y compound systems, which when used in preequilibrium-statistical model calculations, can reproduce in a consistent and concurrent manner these newly measured data available for proton reactions on strontium isotopes.

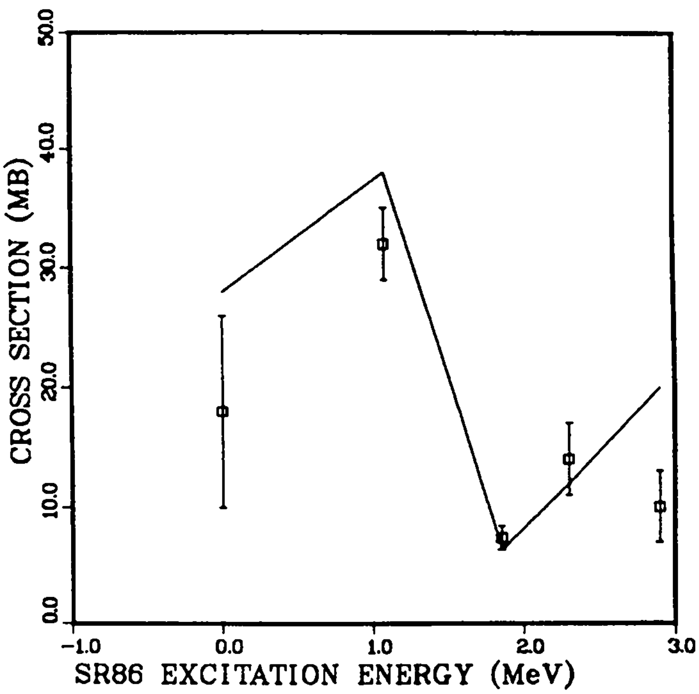

Fig. 19. Calculated values for population of discrete levels in ^{86}Sr through ^{87}Sr(p,pn + p,np) reactions are compared with data[40] measured at E_p = 15 MeV.

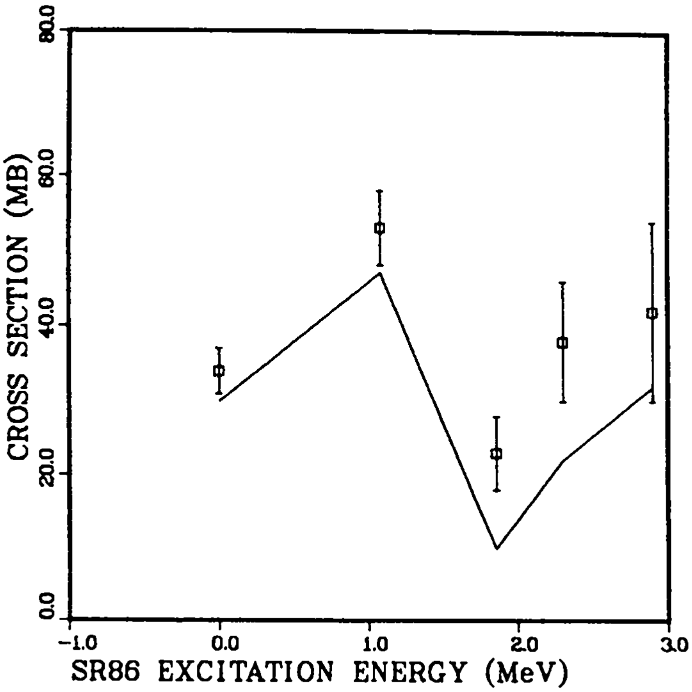

Fig. 20. Calculated values for population of discrete levels in ^{86}Sr through ^{87}Sr(p,pn + p,np) reactions are compared with data[40] measured at E_p = 16 MeV.

H. Theoretical Calculations of ^{91}Zr(p,pn+p,np) Cross Sections (E. D. Arthur)

Section I-G of this progress report describes the comparison of theoretical calculations with newly measured proton reaction data[39,40] available for strontium isotopes. The experiment[40] performed by the physics group P-3 also measured the proton emission spectrum originating from ^{91}Zr(p,pn+p,np) reactions by detecting emitted protons in coincidence with neutrons. In this section we report preliminary results of our analysis of this data.

The theoretical models and parameters used are similar to those described in the previous section. A principal difference, however, is reliance on parameters determined from our earlier calculations described in Ref. 35. We chose to retain such parameters because relevant data are lacking for p+^{91}Zr reactions from which parameters can be further determined or adjusted. Secondly, with the exception of a datum at 14 MeV, these parameters reproduce the majority of the data measured in this experiment.

Figure 21 compares our calculation with data[40] measured for ^{91}Zr(p,pn+p,np) reactions between energies of 14 and 17.6 MeV. In this comparison, all calculations have included a 0.6-MeV threshold for neutron detection. This reproduces the experimental situation in which a proton and neutron were measured in coincidence. The solid curve is based on the parameters of Ref. 35 and reproduces the shape of the data at the higher energies. It does overpredict, substantially, the value measured for for E_p = 14 MeV. In an attempt to improve the low-energy agreement, the gamma-ray competition in the ^{90}Zr compound system was increased by a factor of two. The calculations that include this modification are shown by the dashed curve. Again, an overprediction occurs. Currently we have not found a combination of parameters that allow us to reproduce the cross-section shape of Fig. 21. The absence of relevant data for other reaction channels hinders this effort.

Despite these problems, other comparisons show good agreement between theory and experiment. Figures 22 and 23 compare the calculated and measured cross sections for residual levels of ^{90}Zr produced by these reactions at proton energies of 16 and 17 MeV. In particular, data were measured for the 0^+ state at 1.261 MeV, the sum of 2^+ and 5^- states at 2.186 and 2.139 MeV, and the sum of of 4^- and 3^- states at 2.739 and 2.748 MeV. Cross sections for higher lying levels were summed together and represented in the figures by the datum occurring at 4-MeV excitation energy. For both incident energies, the theoretical calculations reproduce well the magnitude of the cross sections for production of these discrete levels. Again, this comparison produces rather stringent tests on the model and its parameters because the characteristics of the final states (energy, spin, and parity) are well known. This is in contrast to the ambiguous conditions often occurring in such calculations where a continuum of states are populated in a given reaction sequence.

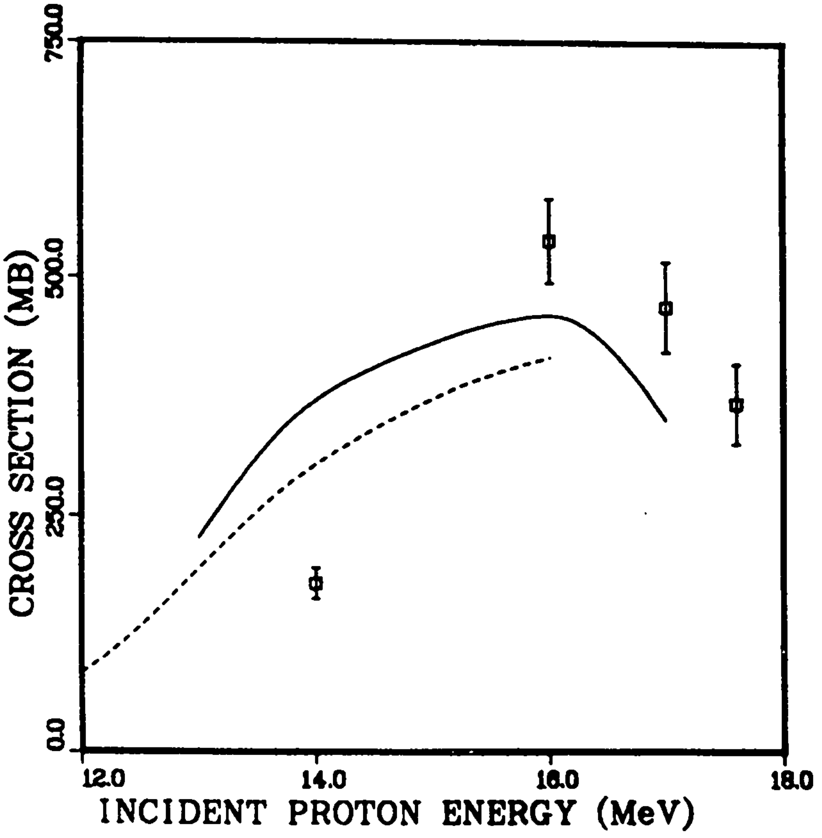

Fig. 21. The calculated ^{91}Zr(p,pn+p,np) cross sections are compared with the data of Ref. 40. The solid curve represents threshold-corrected results obtained using the model parameters described in Ref. 35, while the dashed curve was obtained with a factor-of-two increase in gamma-ray emission from the ^{90}Zr compound nucleus.

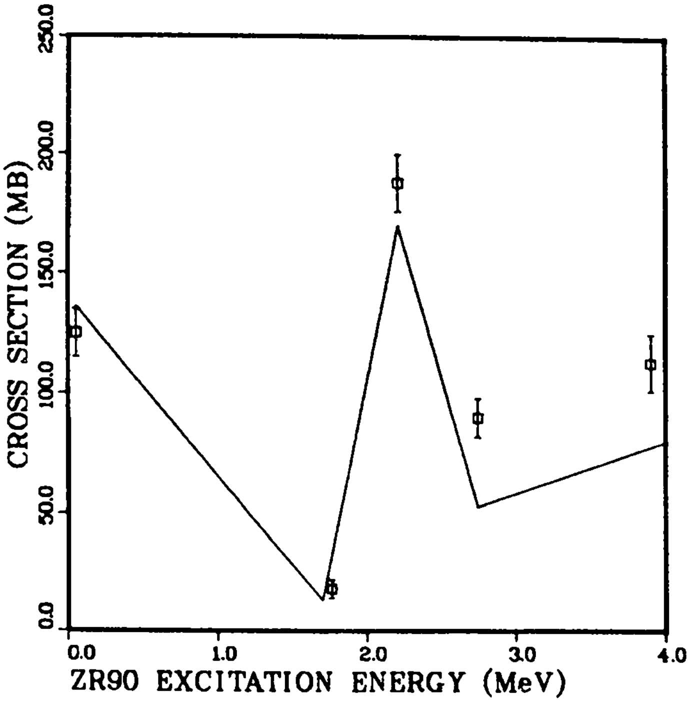

Fig. 22. Calculated values for the population of discrete levels in ^{90}Zr are compared with data for E_p = 16 MeV.

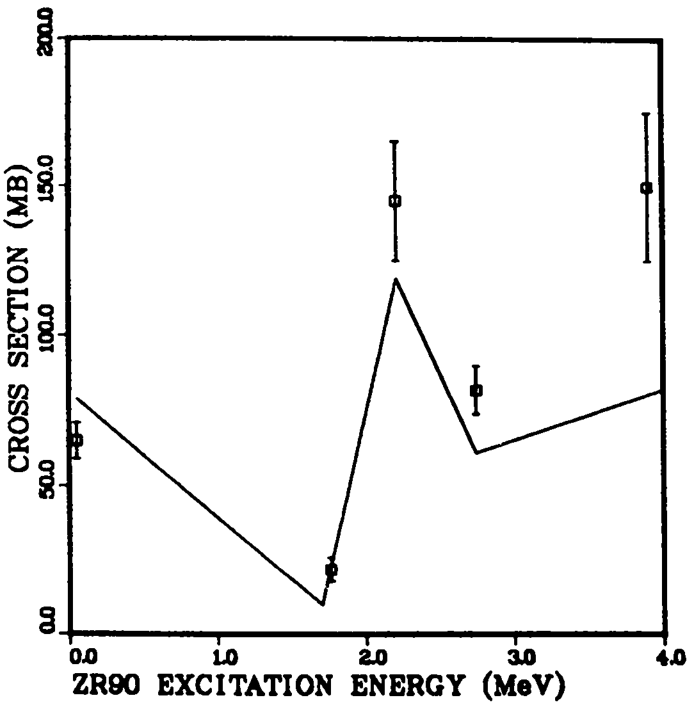

Fig. 23. Calculated values for the population of discrete levels in ^{90}Zr are compared with data for E_p = 17 MeV.

Because the overprediction at 14 MeV was disturbing, we performed an additional calculation of the total proton emission spectrum from p+^{91}Zr reactions at 12.8 MeV. Figure 24 illustrates the comparison to data [47] consisting of contributions from (p,pn), (p,np), and (p,p') reactions. For this figure, our calculations were normalized to these data using two methods. The first involved use of the measured isobaric analogue cross sections, which could be correlated with a distinct $\bar{p}$ peak occurring in the spectrum. Under this peak was a background consisting of contributions from (p,pn) and (p,np) processes. In the comparison of Fig. 24, the $\bar{p}$ peak was removed, as were contributions from contaminant reaction peaks. The other technique involved normalization to data in the secondary proton energy region around 7-8 MeV where the spectrum is composed mainly of inelastically scattered protons. We chose the latter method because of possible difficulties associated with subtraction of a large background from the $\bar{p}$ peak. However, both normalizations agree with each other to within 25-30%. As shown, our calculated spectrum reproduces reasonably well the shape and magnitude of the experimental results, particularly the portion below 5.5 MeV that is dominated by protons from (p,np) and (p,pn) processes. This comparison increases our confidence in our lower energy calculation but does not still explain the discrepancy with the lower energy cross section measured by P-3.

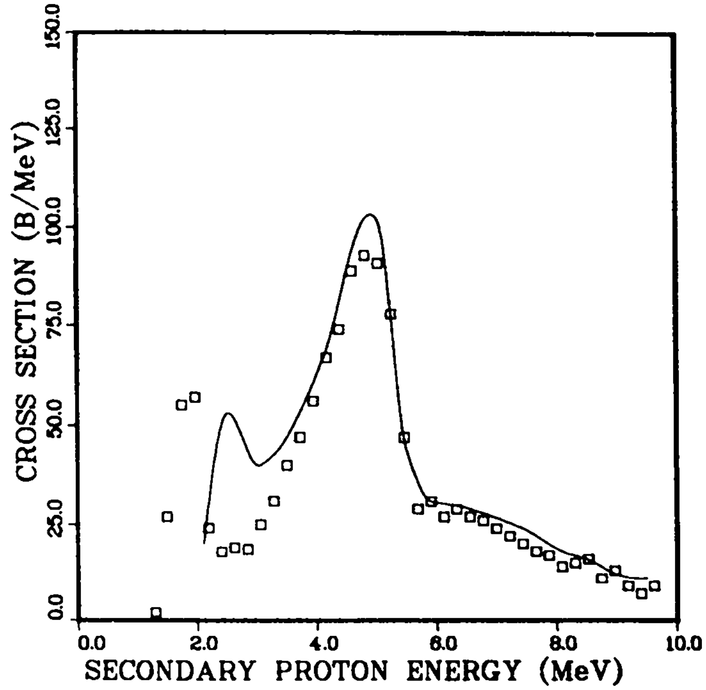

Fig. 24. Comparison of the calculated total proton emission spectra induced by 12.8-MeV protons on ^{91}Zr with the data of Ref. 47. The theoretical and experimental results were normalized to each other at secondary energies around 8 MeV.

I. Calculated (t,n) Cross Sections (E. D. Arthur)

We recently completed preliminary calculations for the interactions of low-energy tritons with medium-mass nuclei. Such calculations are difficult because of strong Coulomb barrier effects that produce low-interaction cross sections and because triton optical parameters are generally not derived to describe sub-Coulomb barrier energy regions. Additionally, there is a paucity of measured low-energy (t,n) cross sections with which theoretical models and parameters can be verified.

Spherical, optical, and Hauser-Feshbach statistical model calculations were made for triton energies up to 5 MeV. The optical model calculations employed the SCAT2 code[20] and examined several optical parameter sets. Particularly useful were parameters deduced by Goldfarb et al.[48] from 2.-to 3.5-MeV triton elastic scattering on ^{40}Ca. Analysis of such data shows strong sub-Coulomb barrier effects, and calculated reaction cross sections differ substantially from similar quantities obtained using global parameters.[49] Such differences appear in Fig. 25, which compares reaction cross sections calculated using the parameters of Ref. 48 (solid curve) with values produced using the Becchetti-Greenlees parameters.[49] In this comparison, calculations were made for 2.7-MeV incident tritons, and the reaction cross section is presented as a function of the mass of the target nucleus. Approximately a factor-of-two difference exists in calculated values. Also evident is the strong Coulomb barrier suppression of the reaction cross section occurring over a restricted region in mass.

The triton optical parameters used appear in Table IV. They were coupled with neutron and proton optical parameters employed by us in previous structural materials calculations[50] to produce particle transmission coefficients. Discrete-level information was obtained using recent compilations,[51] and other parameters such as gamma-ray strength functions and level-density data were taken from other related calculations.[50] The (t,n) calculations were performed using the GNASH Hauser-Feshbach code,[6] and neither width fluctuations nor isospin effects were included. These corrections are probably less than the uncertainty associated with the magnitude of the reaction cross section for sub-Coulomb barrier energies (~ 30-40%).

To test these parameters, ^{58}Ni(t,n) cross sections were calculated and compared with the one available datum[52] occurring in the literature. Figure 26 shows this comparison. No errors were provided with this experimental measurement, so we have arbitrarily assigned a ± 25% error. There exists reasonable agreement with this datum, but this situation may be fortuitous. With this step complete, we extended our calculations to include ^{46}Ti(t,n) and ^{54}Fe(t,n) reactions. These results appear in Figs. 27 and 28. Finally, Fig. 29 presents calculated 2.7-MeV (t,n) cross sections as a function of target mass. Again, substantial Coulomb barrier effects are present for these low-energy reactions.

TABLE IV

TRITON OPTICAL PARAMETERS[a] USED FOR THE PRESENT CALCULATIONS

	r	a
$V = 150 - 0.17E$	1.3	0.65
$W_{vol} = 10. - 0.2E$	1.3	0.65
$r_c = 1.2$		

---

[a] Well depths in MeV; geometrical parameters in fermis.

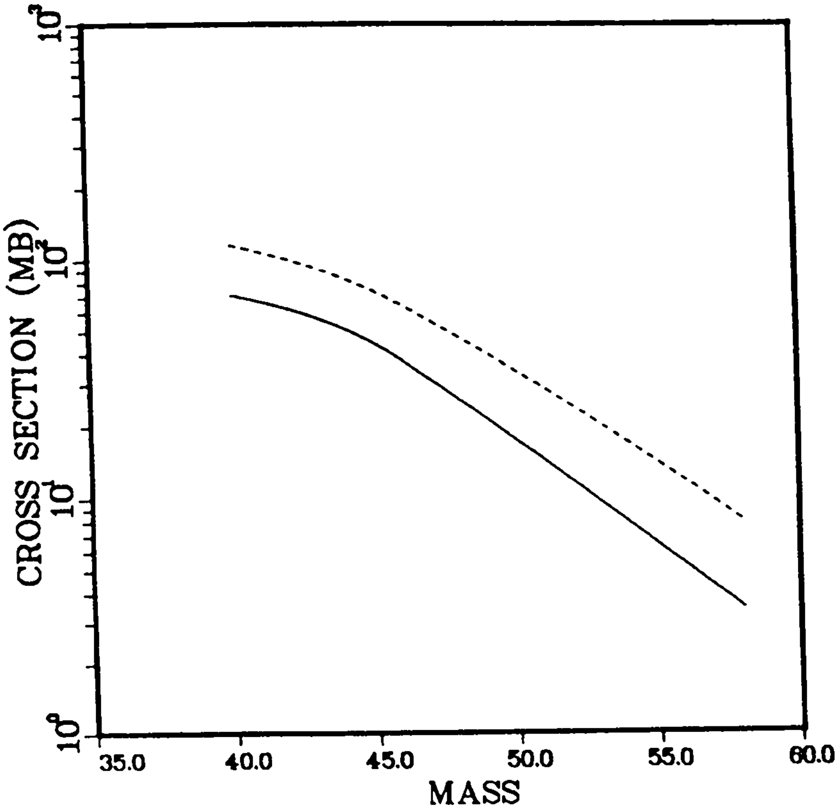

Fig. 25. Reaction cross sections calculated for 2.7-MeV triton interactions with medium-mass nuclei. The solid curve was calculated using the parameters of Ref. 48, while the dashed curve results from use of the Becchetti-Greenlees optical parameters.[49]

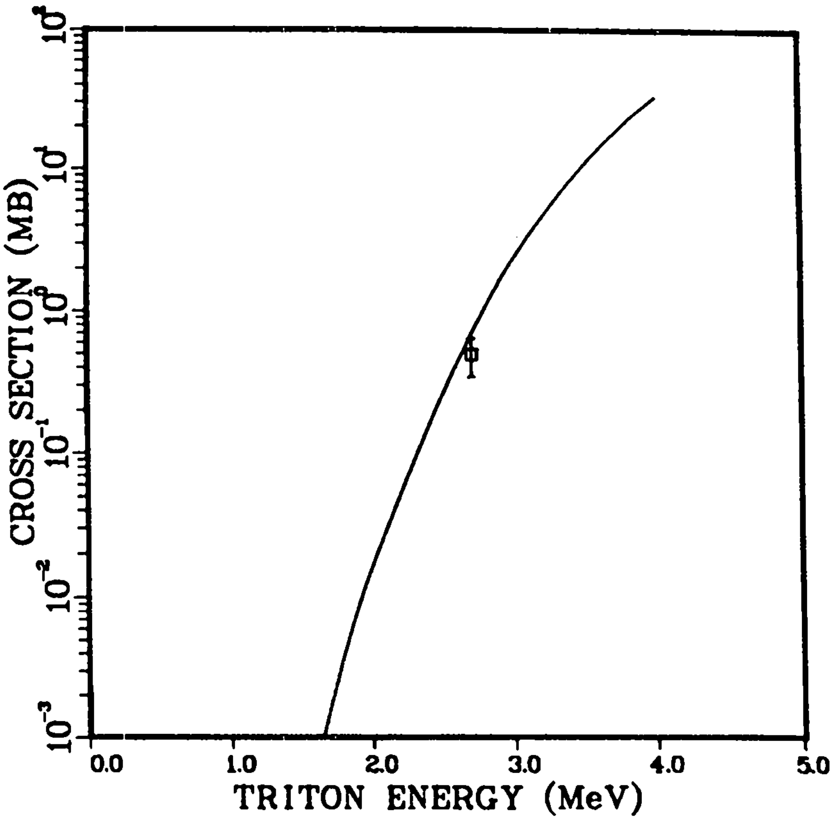

Fig. 26. Comparison of present ^{58}N(t,n) calculations with the datum of Ref. 6.

Fig. 27. Calculated ^{46}Ti(t,n) cross sections.

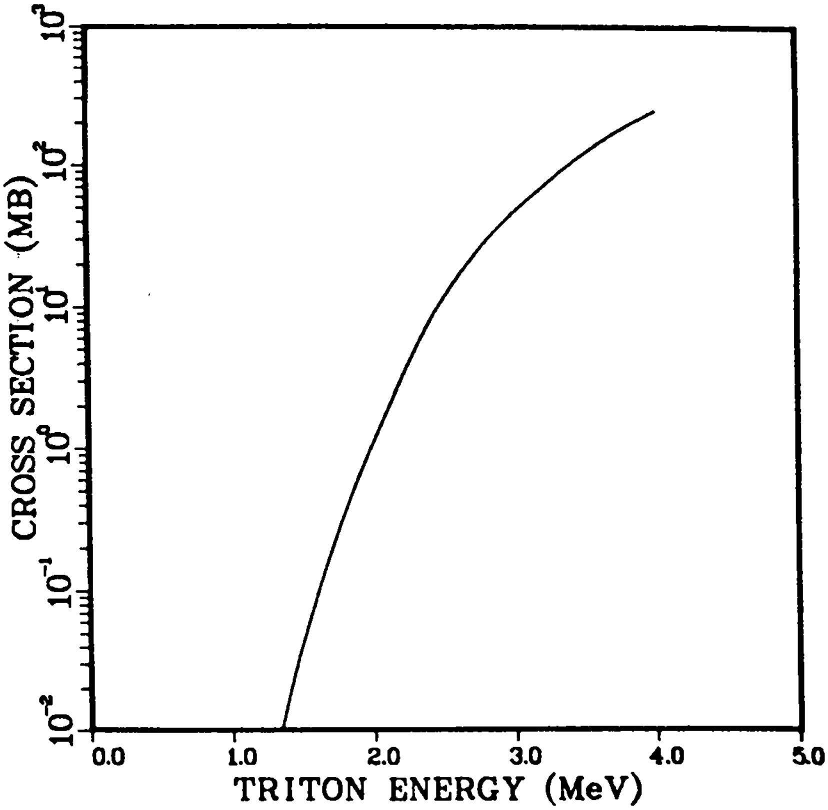

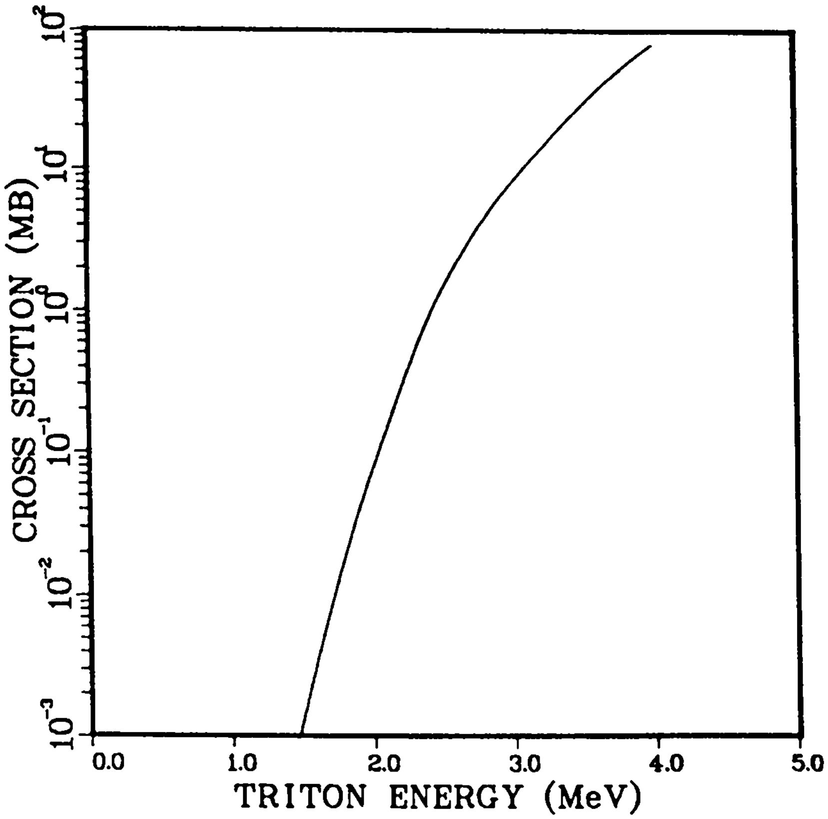

Fig. 28. Calculated ^{54}Fe(t,n) cross sections.

Fig. 29. Calculated cross sections for 2.7-MeV (t,n) reactions on medium-weight nuclei.

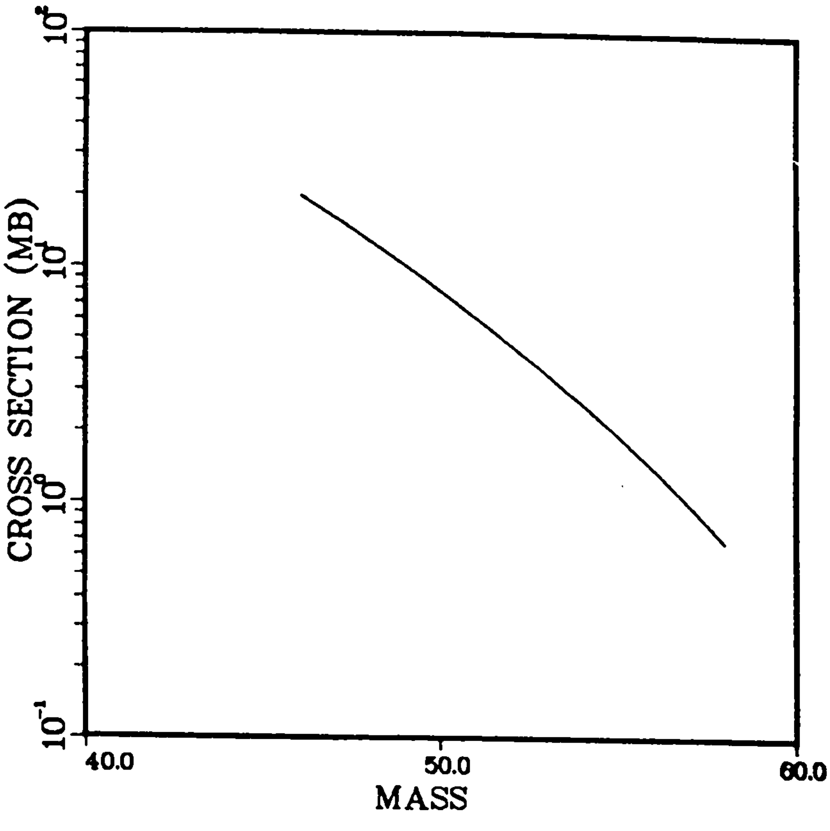

J. Calculation of Activation Cross Sections for Titanium and Vanadium Isotopes

(E. D. Arthur)

The use of titanium-vanadium alloys is of interest in certain low-activation designs for fusion reactors. (See Ref. 53 and the contribution by D. W. Muir in Sec. II-A of this progress report.) Several minor reaction paths and isotopes for Ti and V are important because of their effect on long-term activation properties of such alloys. To provide reliable activation cross sections for such cases, we have employed the GNASH[6] multistep Hauser-Feshbach nuclear model code. To utilize the code effectively for the cross-section problems mentioned above, we must determine input parameters using a wide variety of data sources, not just those related to the calculational problem of interest.

For example, the theoretical description of neutron emission requires knowledge of neutron transmission coefficients over an extended energy range (~ 0.1-20.0 MeV). These we calculate using optical model parameters obtained by simultaneous fits to resonance data (s- and p-wave strengths, scattering radii[45]) as well as total and elastic cross sections. We followed such a procedure to fit data pertinent to the titanium and vanadium isotopes of interest here, and the resulting neutron optical parameters appear in Table V.

TABLE V

NEUTRON OPTICAL PARAMETERS OBTAINED FOR TITANIUM AND VANADIUM ISOTOPES[a]

		r	a
Ti	$V = 49.46 - 0.192E$	1.261	0.6
	$W_{VOL} = -0.544 + 0.39E$	1.261	0.6
	$V_{SO} = 6.2$	1.12	0.47
	$W_{SD} = 3.975 + 0.74E$	1.364	0.42
	for $E_n > 6$ MeV		
	$W_{SD} = 4.419 - 0.1(E-6)$	1.364	0.42
V	$V = 48.86 - 0.43E +$ $0.0003E^2$	1.292	0.6076
	$W_{VOL} = -0.207 + 0.253E$	1.292	0.6076
	$V_{SO} = 6.2$	1.12	0.47
	$W_{SD} = 4.91 + 0.074E$	1.3685	0.429
	for $E_n > 6$ MeV		
	$W_{SD} = 5.354 - 0.17(E-6)$	1.3685	0.429

---

[a] All well depths in MeV; geometrical parameters in fermis.

We likewise followed a similar procedure for charged-particle transmission coefficients. We began with global parameters sets[54,55] and adjusted them to optimize agreement with experimental data, principally elastic-scattering angular distributions and nonelastic cross sections. The resulting parameters were further validated through (p,n) and (α,n) cross-section calculations for nearby nuclei. Since several of the nuclei of interest to this study exhibit significant amounts of neutron-induced charged-particle emission, the proper behavior of these transmission coefficients is essential to the correct theoretical description of such processes, particularly (n,np) reactions.

Independent data were likewise used in the determination of the remaining input parameters, in particular, the gamma-ray strength function and the nuclear level density. For the strength function, we assumed a giant-dipole resonance shape[26] and normalized it to reproduce (n,γ) cross sections for several nuclei in this mass region. The form of the nuclear level density was taken to be that given by the Gilbert-Cameron model.[19] This model was utilized in conjunction with the maximum amount of discrete nuclear level information[51] available for each residual nucleus occurring in the reaction sequence. To determine the pertinent model parameters, we simultaneously fitted data for the cumulative number of levels occurring at a given excitation energy as well as available s-wave resonance-spacing information.[45]

As a final preparatory step in our calculational effort, we computed direct-reaction contributions to neutron inelastic-scattering cross sections from collective levels using the Distorted Wave Born Approximation (DWBA). Such contributions are important over the energy range of interest and cannot be described using Hauser-Feshbach or preequilibrium models. To determine the deformation parameters necessary for normalization of the DWBA results, we used values[56,57] obtained from proton inelastic scattering measurements.

With these preparations complete, we proceeded to cross-section calculations on ^{45,46}Ti and ^{50,51}V, some results of which appear in Fig. 30. Calculated ^{46}Ti(n,2n) cross sections (solid curve) are compared with data[58] in the energy range from threshold to 16 MeV. The agreement is good, especially considering that no attempt has been made to optimize the calculations to this particular reaction. Within this energy range the theoretical cross section for the (n,2n) reaction involves only population of discrete levels in ^{45}Ti so that the proper energy behavior of neutron transmission coefficients is essential for realistic results. Equally important is the proper description of competing reactions, particularly those involving charged-particle emission, because they dominate for this target nucleus. The calculations simultaneously reproduce such data well, as illustrated in Fig. 31 where a comparison is made to the ^{46}Ti proton spectrum[59] induced by 15-MeV neutrons. The agreement is particularly significant in the low-energy portion of the spectrum, because this region encompasses protons from the (n,np) process that compete directly with the (n,2n) reaction. In Fig. 30, the dashed curve shows the predicted behavior of the (n,2n) reaction on the unstable ($t_{1/2}$ = 3.08 h) ^{45}Ti target nucleus. Although the ^{45}Ti(n,2n) threshold lies significantly lower than for ^{46}Ti(n,2n), the 14-MeV cross section is still fairly small (less than 100 mb), because of sizable competition from charged-particle emission.

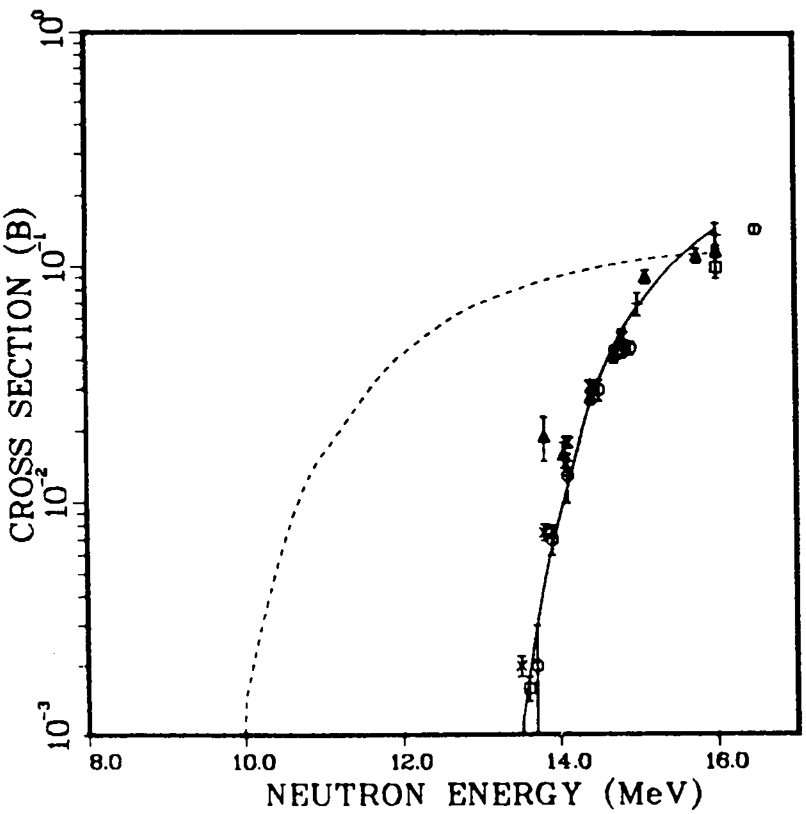

Fig. 30. Calculated ^{45,46}Ti(n,2n) values are compared to experimental data.[58] The dashed curve represents ^{45}Ti results, while the solid curve indicates similar cross sections for ^{46}Ti(n,2n).

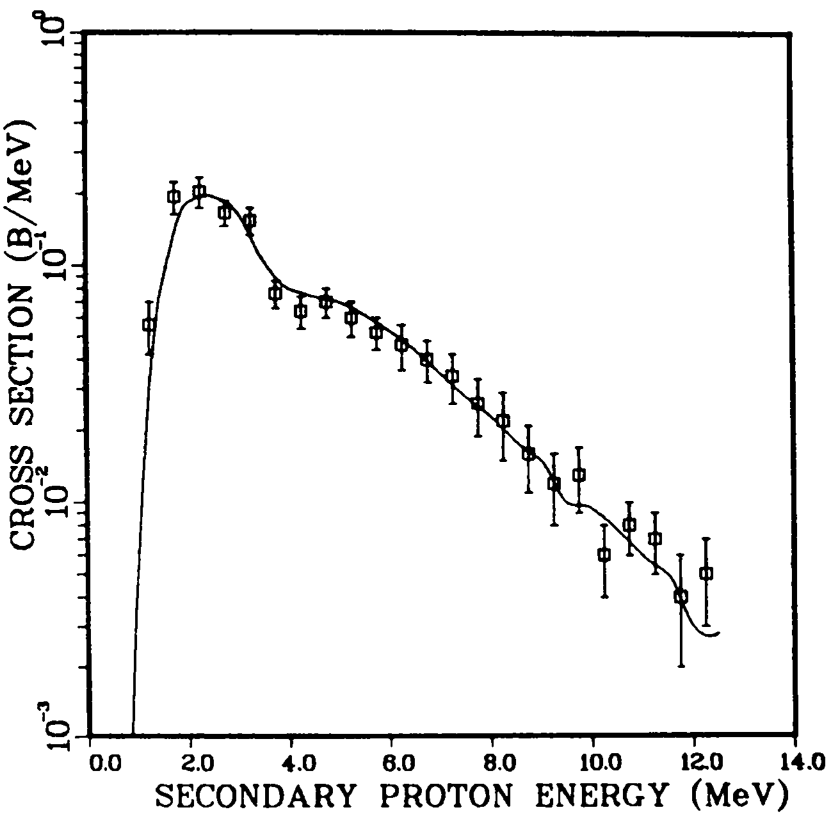

Fig. 31. The calculated proton emission spectrum induced by 15-MeV neutrons on ^{46}Ti is compared with experimental data.[59]

Figure 32 compares calculated (n,2n) cross sections with data[58] available for naturally occurring vanadium isotopes. In this instance, neutron emission is the dominant reaction mechanism rather than charged-particle emission, as was the case previously for ^{45,46}Ti. [We did, however, compare our calculations with measured values of ^{51}V(n,p) and (n,α) reactions where we found agreement on the order of 10%, even though cross-section magnitudes were small compared with (n,2n) values.] For such (n,2n) reactions, the calculations are dominated by transitions to discrete levels in the ^{49,50}V residual nuclei, so again a realistic low-energy description of the neutron transmission coefficients is important. The dashed curve illustrates the calculated ^{50}V(n,2n) cross section for which no experimental data exist. Its threshold lies about 2 MeV lower than for ^{51}V(n,2n), but around 14 MeV, the cross sections are comparable. The cross sections appearing in these figures as well as cross sections calculated for other reactions appear in Tables VI and VII.

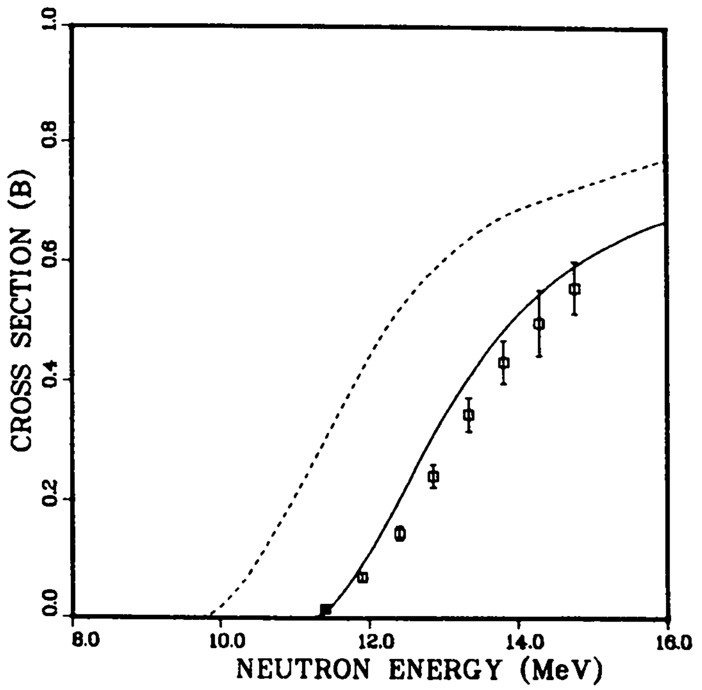

Fig. 32. Calculated ^{51}V(n,2n) (solid curve) and ^{50}V(n,2n) (dashed curve) cross sections are compared with available experimental results[58] for ^{nat}V.

TABLE VI

CALCULATED ACTIVATION CROSS SECTIONS FOR SELECTED TITANIUM ISOTOPES

^{45}Ti	Cross Section (millibarns)	
E_n (MeV)	(n,2n)	(n,np+n,pn)
10	1.4	3.6
11	15.5	61.0
12	42.0	178.0
13	70.0	330.0
14	91.0	462.0
15	107.0	555.0

^{46}Ti	Cross Section (millibarns)	
E_n	(n,p)	(n,2n)
13.5	324.0	1.1
14.0	302.0	9.0
14.5	273.0	33.0
15.0	241.0	68.0
15.5	208.0	107.0
16.0	179.0	145.0

TABLE VII

CALCULATED ACTIVATION CROSS SECTIONS FOR SELECTED VANADIUM ISOTOPES

^{50}V	Cross Section (millibarns)		
E_n (MeV)	(n,α)	($n,2n$)	($n,n\alpha$)
8	16.0	—	—
9	19.0	—	—
10	20.0	19.0	—
11	21.0	209.0	—
12	22.0	442.0	—
13	23.0	603.0	—
14	25.0	688.0	—
15	27.0	733.0	0.36
16	26.0	744.0	2.7

^{51}V	Cross Section (millibarns)		
E_n (MeV)	(n,p)	(n,α)	($n,2n$)
6	4.2	—	—
7	6.6	0.0	—
8	14.0	1.4	—
9	18.0	3.7	—
10	24.0	5.2	—
11	30.0	5.5	0.0
12	36.0	7.0	110.0
13	40.0	10.0	342.0
14	40.0	13.5	514.0
15	37.0	18.0	613.0
16	34.0	22.0	670.0

These examples illustrate the use of a modern nuclear reaction code such as GNASH to calculate activation cross sections important for fusion reaction applications. These results also illustrate that, with proper care in parameter determination, realistic theoretical cross sections can be obtained even in the case of minor reaction paths. Such calculations can thereby be used with confidence to provide nuclear data in instances where experimental measurements are difficult (such as on a rare isotope) or totally impractical, as in cases involving unstable targets.

K. Review Paper for Structural Materials Nuclear Data (E. D. Arthur)

A review paper entitled "Calculational Methods for Structural Materials Nuclear Data," was prepared for presentation at the International Atomic Energy Agency (IAEA) Consultants' Meeting on Nuclear Data for Structural Materials, held in Vienna, Austria, in early November 1983. The abstract of this paper appears below.

"The nuclear models applicable to the evaluation of neutron cross sections for structural materials are briefly reviewed. Recent efforts to improve data models are discussed, particularly regarding techniques used to produce realistic input parameters. Examples of current calculations using such models for provision of structural materials nuclear data are given. In this context, emphasis is placed on the use of nuclear model calculations to correct certain fundamental problems occurring in evaluated data files. Finally, new areas of effort involving more basic nuclear models are described that may impact future applied theoretical calculations."

L. Calculation of n + ^{169}Tm Cross Sections as a Function of Temperature (D. G. Madland)

Spectrum-averaged neutron capture and total inelastic-scattering cross sections for the n + ^{169}Tm system have been calculated as a function of the temperature of the target nucleus environment and for a specified incident neutron energy spectrum. The mechanism for the temperature dependence of the cross sections is the contribution from neutron scattering by the target nucleus existing in low-lying excited states in competition with scattering from the standard or default target ground state. The calculation has been performed assuming thermodynamic equilibrium between populations of all participating target states for each value of the temperature considered. Accordingly, the results summarized here represent the maximum possible temperature effect due to occupation of excited states of the ^{169}Tm target nucleus. In the calculations to date, the values of the temperatures have been confined to the 0-to 50-keV region so that only the ground-state and first-excited-state populations are significant.

Given the pointwise capture and total inelastic cross sections for ^{169}Tm in its ground- and first-excited states from coupled-channel and Hauser-Feshbach statistical model calculations,[7] the spectrum-averaged temperature-dependent capture and total inelastic cross sections for ^{169}Tm are obtained in two steps.

The first step is to calculate the spectrum-averaged cross sections $\bar{\sigma}$ at room temperature (~ 0 keV) for both ground and excited state uses. These are obtained using the relation

$$\bar{\sigma} = \frac{\int \sigma(E)\phi(E)dE}{\int \phi(E)dE} , \tag{1}$$

where E is the incident energy of neutrons from the spectrum $\phi(E)$ and $\sigma(E)$ is the pointwise cross section. The values of $\bar{\sigma}$ obtained using the Standard TD Weight Function for $\phi(E)$ and using the pointwise cross sections of Ref. 7 are*

$\bar{\sigma}_{capture}$ (ground state) = 1.561 barns,
$\bar{\sigma}_{capture}$ (first-excited state) = 2.029 barns,
$\bar{\sigma}_{inelastic}$ (ground state) = 1.529 barns, and
$\bar{\sigma}_{inelastic}$ (first-excited state) = 1.964 barns.

The second step is to combine the spectrum-averaged ground and first-excited-state cross sections in proportion to the respective occupation probabilities of these states and to do so as a function of temperature. The occupation probabilities have been calculated as a function of temperature assuming Boltzmann statistics.** With these Boltzmann factors, the temperature-dependent spectrum-averaged cross sections $\langle\sigma\rangle$ have been obtained for the neutron capture and neutron total inelastic reactions. These are illustrated in Figs. 33 and 34 together with the constant or default cross sections that are obtained if excited-state effects are ignored. The figures show that the neutron capture and neutron total inelastic-scattering cross sections experience rapid rises at low temperatures followed by slower rises at higher temperatures due to the inclusion of excited-state capture and excited-state inelastic scattering. At a temperature of 10 keV, the magnitude of the effect is 14% in the capture reaction and 13% in the total inelastic scattering. At a temperature of 30 keV, these enhancements are 18% and 17%, respectively.

---

* R. E. Seamon, Los Alamos National Laboratory, assisted in this calculation, August 1983.

**G. D. Doolen, Los Alamos National Laboratory, provided the Boltzmann factors, August 1983.

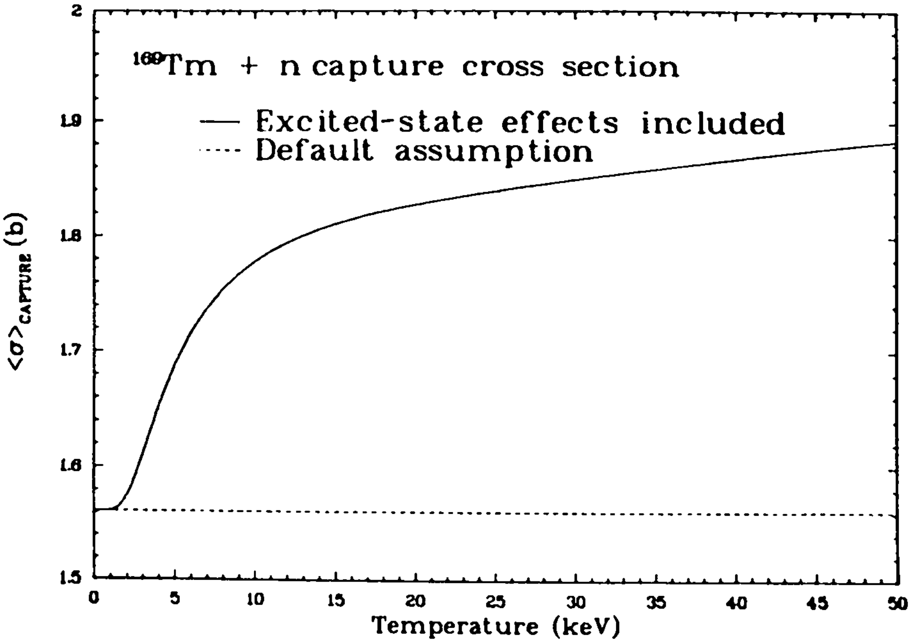

Fig. 33. Spectrum-averaged total capture cross section for the scattering of neutrons by ^{169}Tm as a function of temperature. The dashed line corresponds to the value obtained by ignoring excited-state effects, whereas the solid curve corresponds to the values obtained by including the capture reaction from the first-excited state. The neutron spectrum is represented by the Standard TD Weight Function. Note the suppressed zero of the vertical scale.

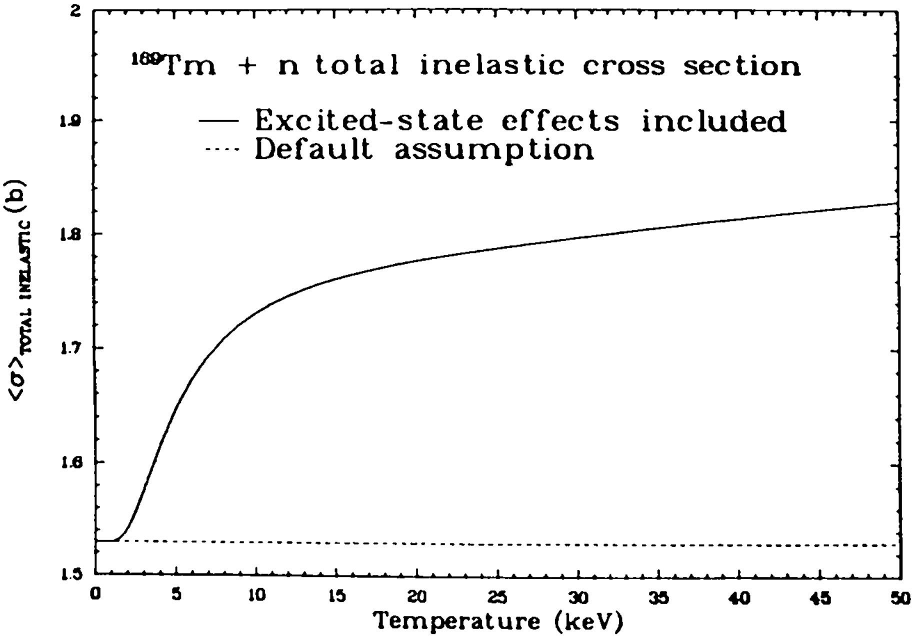

Fig. 34. Spectrum-averaged total inelastic cross section for the scattering of neutrons by ^{169}Tm as a function of temperature. The dashed line corresponds to the value obtained by ignoring excited-state effects, whereas the solid curve corresponds to the values obtained by including the inelastic scattering from the first-excited state. The neutron spectrum is represented by the Standard TD Weight Function. Note the suppressed zero of the vertical scale.

M. Calculation of Prompt Fission Neutron Spectra and $\bar{\nu}_p$ for the Neutron-Induced Fission of ^{237}Np (D. G. Madland)

New calculations of the prompt fission neutron spectrum matrix $N(E,E_n)$ and the average prompt neutron multiplicity $\bar{\nu}_p(E_n)$ have been completed for the ^{237}Np + n(E_n) system. These differ from our preliminary calculations[7] using default parameter values in that direct account is taken of the experimental $\bar{\nu}_p(E_n)$ data. Recall from Ref. 7 that the goal is to calculate accurately both $N(E,E_n)$ and $\bar{\nu}_p(E_n)$ by making use of their strong coupling and by reproducing the experimental data for these quantities. Since very few experimental data exist for $N(E,E_n)$, reliance must be placed on the constraints imposed by the experimental $\bar{\nu}_p(E_n)$ data. In this particular case, the method is complicated by the fact that the experimental $\bar{\nu}_p(E_n)$ data are discrepant for some ranges of the incident neutron energy E_n.

Accordingly, the approach here is to grid over the physically allowed ranges of those input parameters with the greatest uncertainties that are common to the calculation of $N(E,E_n)$ and $\bar{\nu}_p(E_n)$ in order to obtain the best possible compromise fit to the experimental data.[59-62] These parameters are the average energy release in fission $\langle E_r \rangle$, the total average fission fragment kinetic energy $\langle E_f^{tot} \rangle$, and the average effective nuclear level-density parameter a_{eff} used in the constant cross-section approximation. Thus, calculations on a three-dimensional grid are necessary to explore the chosen parameter space.

The grid in the $\langle E_r \rangle$ direction is performed by calculation, using a seven-point approximation, for six likely candidate pairs for the peaks of the fission fragment mass and charge distributions. The choices of the six pairs are based on systematics.[63] The grid in the $\langle E_f^{tot} \rangle$ direction is performed by incrementing the experimental value[64] of 174 ± 2 MeV in 0.25-MeV steps. Finally, the grid in the a_{eff} direction is performed by incrementing the denominator K in the expression $a_{eff} = A/K$ in 0.5-MeV steps.

Our results using this method of parameter optimization are shown in Figs. 35-38, where the calculations are compared with experiment and with ENDF/B-V. The best fit input parameters from the three-dimensional grid are listed in the "Second Pass" row of Table VIII, where they are compared with the values used in the "First Pass" calculations of Ref. 7.

Inspection of Fig. 35 shows that the calculation agrees well with the data of Vorobeva et al.[61] at all incident neutron energies ($E_n \leq 5.90$ MeV) of that experiment, agrees well with all but one point of the data of Veeser,[60] but agrees only with the high-energy portion ($E_n \geqq 6.03$ MeV) of the data of Frehaut et al.[62]

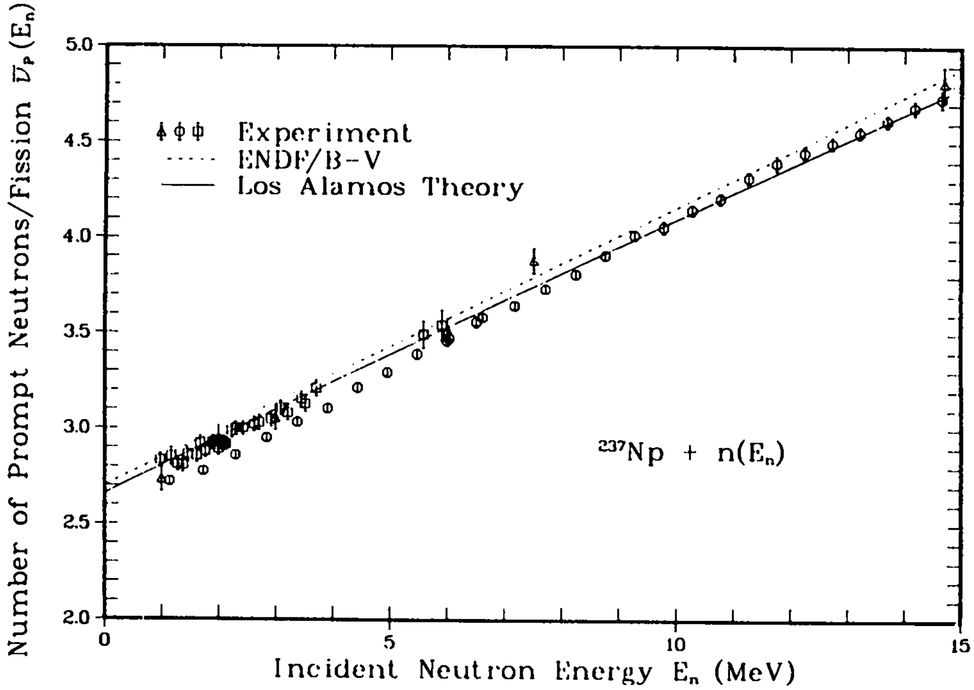

Fig. 35. Averaged prompt neutron multiplicity as a function of the incident neutron energy for the neutron-induced fission of ^{237}Np. The solid curve gives the second-pass calculation and the dashed curve gives the ENDF/B-V evaluation. The experimental data are those of Veeser[60], Δ; Frehaut et al.[62], 0; and Vorobeva et al.[61], □. Note the suppressed zero of the vertical scale.

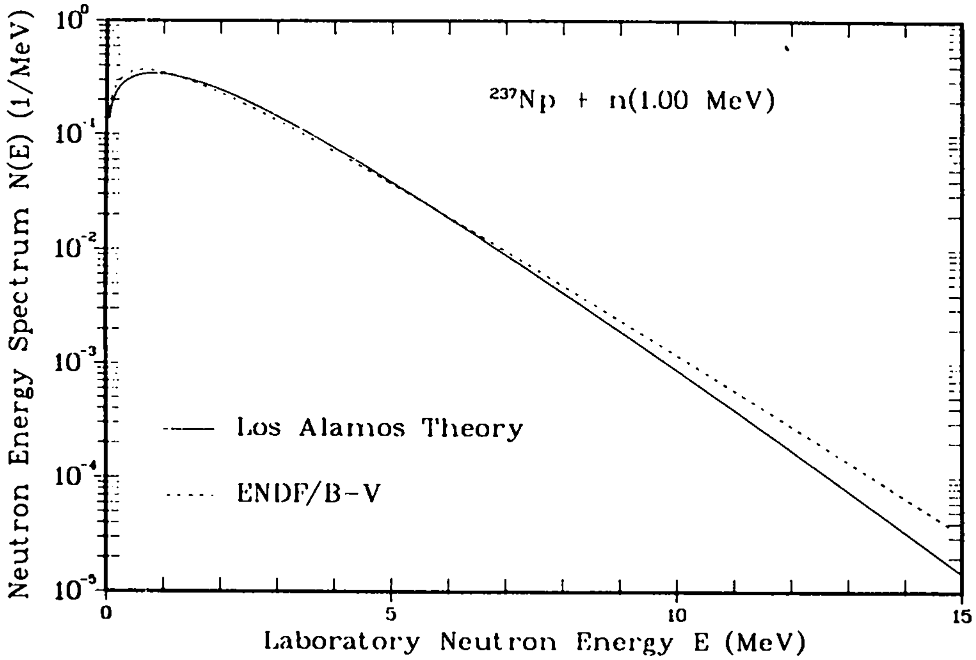

Fig. 36. Prompt fission neutron spectrum for the fission of ^{237}Np induced by 1-MeV neutrons. The solid curve gives the second-pass calculation and the dashed curve gives the ENDF/B-V Maxwellian spectrum.

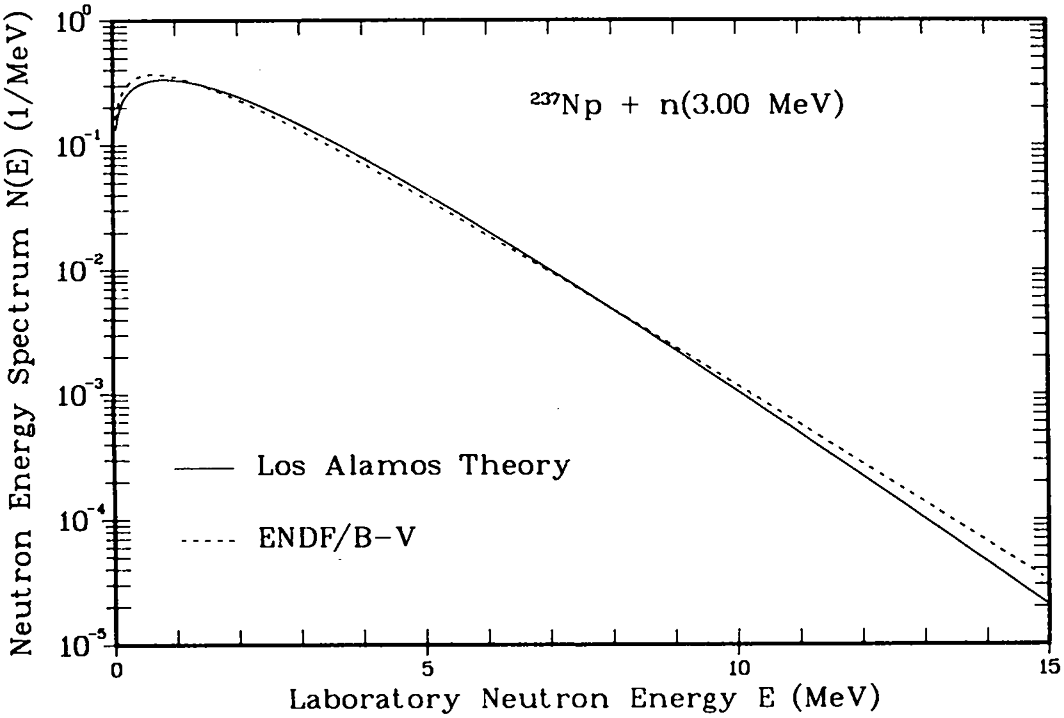

Fig. 37. Prompt fission neutron spectrum for the fission of ^{237}Np induced by 3-MeV neutrons, corresponding to the calculations shown in Fig. 36.

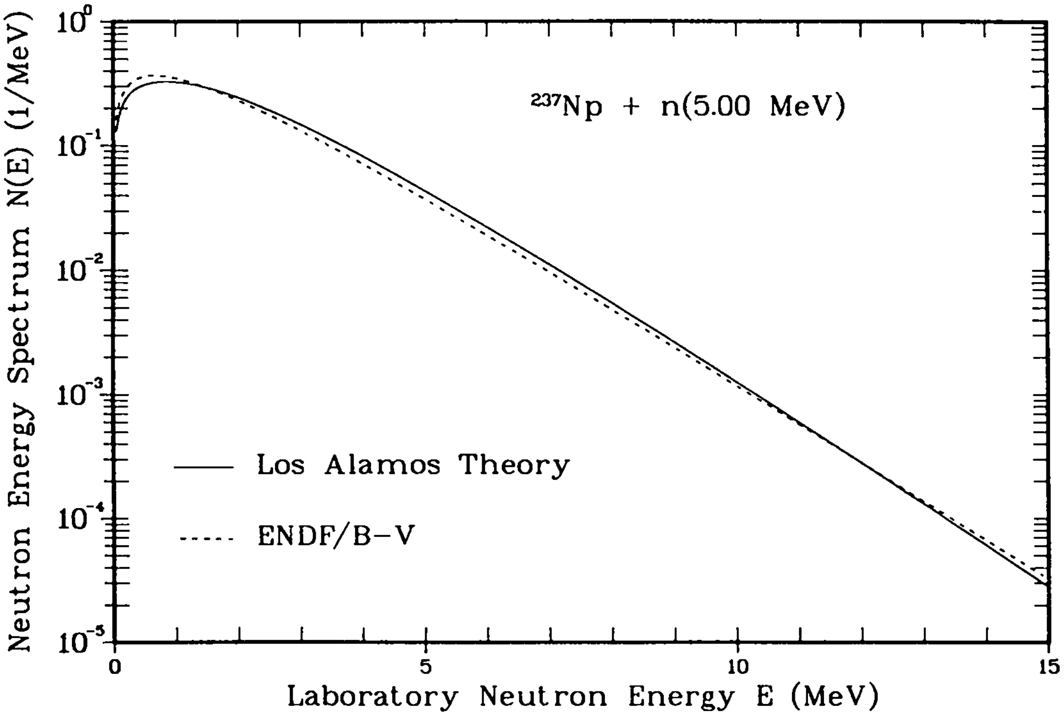

Fig. 38. Prompt fission neutron spectrum for the fission of ^{237}Np induced by 5-MeV neutrons, corresponding to the calculations shown in Fig. 36.

TABLE VIII

PARAMETER OPTIMIZATION FOR THE CALCULATION OF $N(E,E_n)$ AND $\bar{\nu}_p(E_n)$ FOR THE $^{237}N_p$ + n SYSTEM

Calculation	Fragment Mass Peaks	$\langle E_r \rangle$ (MeV)	$\langle E_f^{tot} \rangle$ (MeV)	a_{eff} (MeV^{-1})
First Pass	$^{100}_{39}Y + ^{138}_{54}Xe$	194.490	174.301[a]	A/(10.0)
Second Pass	$^{99}_{39}Y + ^{139}_{54}Xe$	193.937	176.00	A/(8.50)
Experiment	—	—	174 ± 2[b]	—

---

[a] Computed from the empirical relation of Ref. 63.
[b] See Ref. 64.

As a consequence, more accurate work on the calculation of $\bar{\nu}_p(E_n)$ for this system must await resolution of the discrepant measurements in the low-energy region. In addition, information on $\langle E_r(E_n) \rangle$, $\langle E_f^{tot}(E_n) \rangle$, and multiple-chance fission probabilities is needed for high-accuracy calculations of $\bar{\nu}_p(E_n)$.

Figures 36-38 illustrate the second-pass calculations of three elements of the fission-spectrum matrix $N(E,E_n)$. These spectra are softer than those of the first-pass calculation. The parameters for constructing the fission-spectrum matrix $N(E,E_n)$ from the second-pass calculation are given in Table IX.

TABLE IX

PARAMETERS FOR CONSTRUCTING THE ENDF LF = 12 FISSION-SPECTRUM MATRIX $N(E,E_n)$ FOR THE NEUTRON-INDUCED FISSION OF ^{237}Np

E_n (MeV)	EFL (MeV)	EFH (MeV)	TM (MeV)
0.0	1.038282	0.526691	0.914662
0.5	"	"	0.924372
1.0	"	"	0.933982
1.5	"	"	0.943493
2.0	"	"	0.952909
2.5	"	"	0.962233
3.0	"	"	0.971468
3.5	"	"	0.980616
4.0	"	"	0.989679
4.5	"	"	0.998660
5.0	"	"	1.007561
5.5	"	"	1.016384
6.0	"	"	1.025131

N. Calculation of the Prompt Fission Neutron Spectrum and Average Prompt Neutron Multiplicity for the ^{252}Cf(sf) Standard Reaction [D. G. Madland and J. R. Nix (T-9)]

We have already reported our preliminary studies on ^{252}Cf at the 1982 Antwerp meeting in Ref. 65, and here we summarize our progress since that meeting.

As in Ref. 65, we take two important new steps to calculate N(E) and $\bar{\nu}_p$ for the ^{252}Cf(sf) reaction. The first of these is that we perform a complete integration for the average energy release in fission $\langle E_r \rangle$ without approximation instead of using our normal seven-point approximation. In so doing, we obtain mass values from the new 1981 Wapstra-Bos mass evaluation[66] when they exist and otherwise from the new macroscopic-microscopic mass formula of Möller and Nix.[67] The second step is that we perform a least squares adjustment of our calculated spectrum to a well-measured experimental spectrum in order to determine the value of the nuclear level-density parameter a that enters our calculations of N(E) and $\bar{\nu}_p$. A least squares adjustment is performed because we wish to obtain the most accurate representations of the physical spectrum and physical neutron multiplicity as is possible. We do so with respect to the nuclear level-density parameter because it is the least well-known parameter that enters our formalism. The average neutron multiplicity is not included in the least squares adjustment because it depends only weakly on the nuclear level density.

We perform the least squares adjustments with respect to two recent measurements of the spectrum. The first of these is the measurement of Boldeman et al.,[68] Experiment no. 7, final data analysis;* and the second is the measurement of Poenitz and Tamura.[69]** Our results are given in Figs. 39-42 and in Tables X and XI, where they are compared with the two experimental measurements as well as with the results of least squares adjustments that we have performed with respect to the temperature T_M of a Maxwellian spectrum.

Considering first our results for the measurement of Boldeman et al.,[68]* shown in Figs. 39 and 40 and tabulated in Col. 1 of Tables X and XI, we find that a Maxwellian spectrum with temperature T_M = 1.426 MeV gives a better value of χ^2_{min} than does our energy-dependent cross-section calculation with tempera-

---

* This information was provided by J. W. Boldeman, Australian Atomic Energy Commission, Lucas Heights, N.S.W., Australia, in May 1983.

**This information was provided by W. P. Poenitz, Argonne National Laboratory, Argonne, Illinois, April 1983.

ture T_m = 1.124 MeV. The values of χ^2_{min} are 1.175 and 3.529, respectively. Inspection of Fig. 40 indicates that the difference between the two χ^2_{min} values is due largely to contributions to χ^2_{min} from the region 800 keV to about 1.1 MeV, where the Maxwellian spectrum is everywhere in better agreement with experiment than our calculated spectrum.

Considering second our results for the measurement of Poenitz and Tamura,[69]* shown in Figs. 41 and 42 and tabulated in Col. 2 of Tables X and XI, we find that our energy-dependent cross-section calculation with temperature T_m = 1.094 MeV gives a better value of χ^2_{min} than does a Maxwellian spectrum with temperature T_M = 1.429 MeV. In this case, the values of χ^2_{min} are 0.552 and 1.201, respectively. Inspection of Fig. 42 indicates that the difference between the two χ^2_{min} values is not due to the preference of our calculated spectrum in a specific energy region, as is the case for the Maxwellian spectrum preference with the Boldeman et al. experiment, but is instead due to uniformly better agreement with the experiment over most of the experimental range.

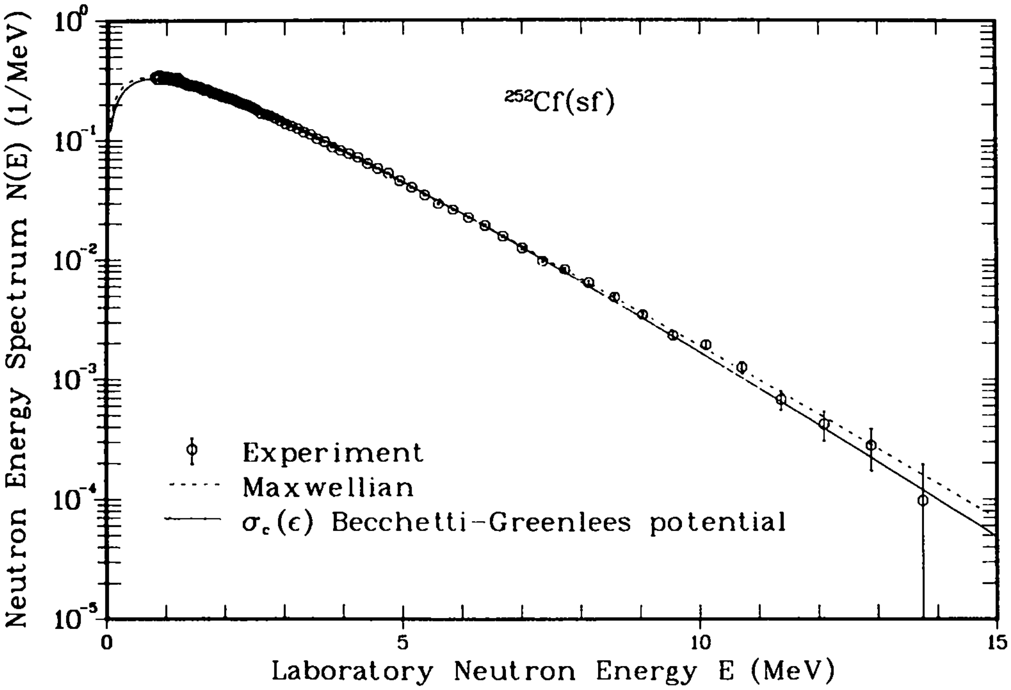

Fig. 39. Prompt fission neutron spectrum in the laboratory system for the spontaneous fission of ^{252}Cf. The dashed curve gives the least squares adjusted Maxwellian spectrum and the solid curve gives the least squares adjusted energy-dependent cross-section spectrum. The experimental data are those of Boldeman et al.[68] and Boldeman,** Experiment 7, final data.

---

* This information was provided by W. P. Poenitz, Argonne National Laboratory, Argonne, Illinois, April 1983.

**This information was provided by J. W. Boldeman, Australian Atomic Energy Commission, Lucas Heights, N.S.W., Australia, in May 1983.

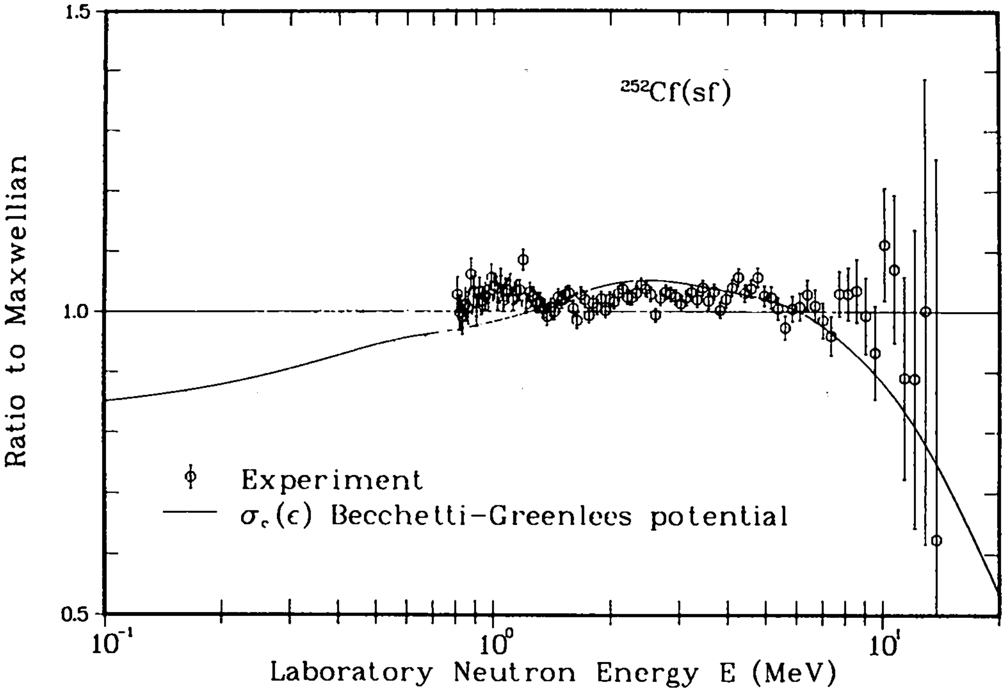

Fig. 40. Ratio of the energy-dependent cross-section spectrum and the experimental spectrum to the Maxwellian spectrum, corresponding to the curves shown in Fig. 39.

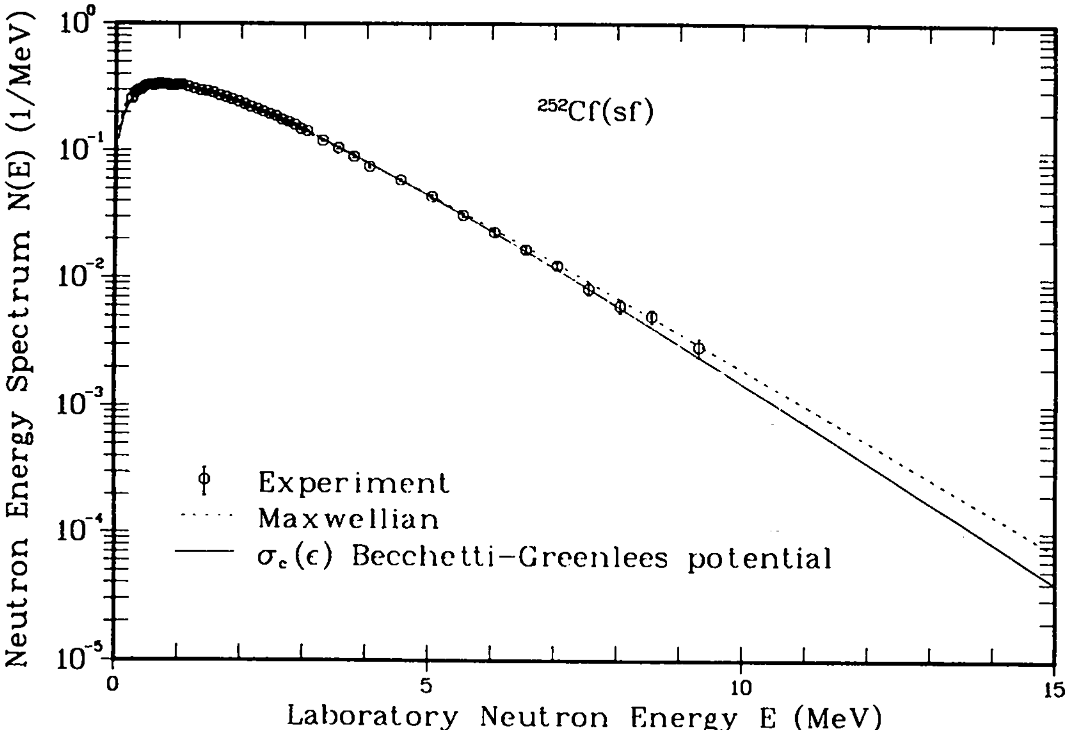

Fig. 41. Prompt fission neutron spectrum in the laboratory system for the spontaneous fission of ^{252}Cf. The dashed curve gives the least squares adjusted Maxwellian spectrum and the solid curve gives the least squares adjusted energy-dependent cross-section spectrum. The experimental data are those of Poenitz and Tamura[69] and Poenitz.*

---

*This information was provided by W. P. Poenitz, Argonne National Laboratory, Argonne, Illinois, April 1983.

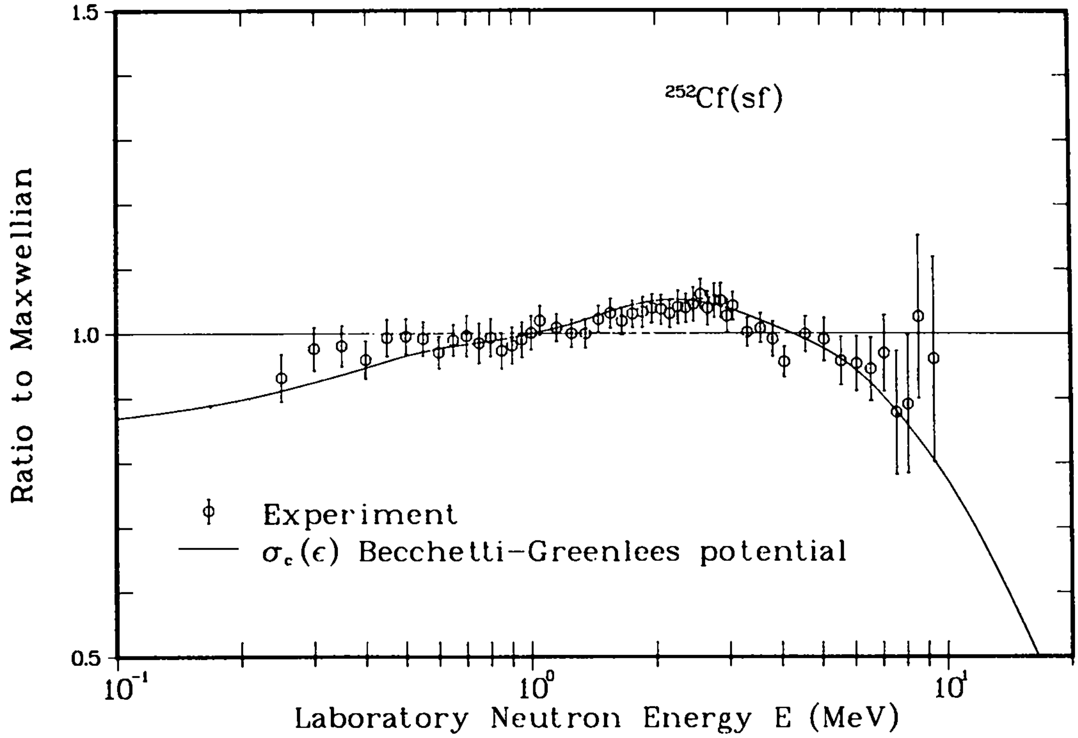

Fig. 42. Ratio of the energy-dependent cross-section spectrum and the experimental spectrum to the Maxwellian spectrum, corresponding to the curves shown in Fig. 41.

TABLE X

LEAST SQUARES ADJUSTMENTS OF MAXWELLIAN SPECTRA FOR THE SPONTANEOUS FISSION OF ^{252}Cf

	Experimental Spectrum	
Quantity	Boldeman et al.[a]	Poenitz and Tamura[b]
Number of data points	95	51
Energy range of experiment (MeV)	0.801-14.239	0.225-9.800
Fraction of theoretical spectrum (%)	77.13	95.39
T_M (MeV)	1.426	1.429
$\langle E \rangle$ (MeV)	2.139	2.144
$\langle E^2 \rangle$ (MeV^2)	7.626	7.658
χ^2_{min}	1.175	1.201

---

[a] See Ref. 68.

[b] See Ref. 69.

TABLE XI

LEAST SQUARES ADJUSTMENTS OF PRESENT ENERGY-DEPENDENT CROSS-SECTION SPECTRA FOR THE SPONTANEOUS FISSION OF ^{252}Cf

Quantity	Boldeman et al.[a]	Poenitz and Tamura[b]
Number of data points	95	51
Energy range of experiment (MeV)	0.801-14.239	0.225-9.800
Fraction of theoretical spectrum (%)	78.80	95.99
a (1/MeV)	A/9.65	A/9.15
T_m (MeV)	1.124	1.094
$\langle E\rangle$ (MeV)	2.171	2.134
$\langle E^2\rangle$ (MeV)	7.637	7.364
$\bar{\nu}_p$	3.789	3.810
χ^2_{min}	3.529	0.552

---

[a] See Ref. 68.

[b] See Ref. 69.

Thus, we see that the two spectrum measurements are inconsistent with each other and that these inconsistencies, although slight, are significant because they lead to different conclusions as to what the shape and energy moments of the real physical spectrum are. Therefore, additional existing or new experimental measurements of this spectrum are required to determine exactly the prompt fission neutron spectrum for the ^{252}Cf(sf) standard reaction.

In closing, we note that our calculated values of $\bar{\nu}_p$ appearing in Table XI are quite close to the experimental values of 3.757 ± 0.009 obtained from the measurements of Amiel[70] and Smith,[71] and 3.773 ± 0.007 obtained by Spencer et al.[72]

II. NUCLEAR CROSS-SECTION PROCESSING AND TESTING

A. Release of NJOY (6/83) and Preparations for Note (6/83-1) (R. E. MacFarlane and D. W. Muir)

In June 1983 a new, resequenced version of the NJOY[73,74] nuclear data processing system was released to the US code centers. This version is now undergoing a round of testing on a variety of computer systems as a collaborative effort involving Los Alamos, the National Energy Software Center at Argonne, the Radiation Shielding Information Center at Oak Ridge, the Atomic Energy Establishment at Winfrith, the NEA Data Bank at Saclay, and the IAEA Nuclear Data Section in Vienna, Austria. In early 1984 a Note will be distributed to all NJOY users informing them of the corrections required to overcome the minor problems uncovered in this testing. Below, we summarize the known problems with the version originally sent to the code centers. A corresponding set of code corrections is available from the code authors.

In the NJOY module, an incorrect code version number was printed in the "banner" of the output. In RECONR, the input instructions were slightly obsolete. In addition, a few isolated cases of "false convergence" were detected, so additional nodes have been added at the resonance inflection points. Also in RECONR, a problem that prevented the correct processing of unresolved-resonance data in multi-isotope materials was found and corrected. In several modules (RECONR, BROADR, HEATR, and THERMR), changes were made to allow CDC-7600 processing of isotopes that generate very large numbers of energy points (that is, over 131 000 points). Most other computer systems do not require this change. Finally, the estimation of the net error in resonance integrals was improved.

In HEATR, the energy-balance test for (n,γ) reactions was improved, and a printout of the total photon energy production cross section (eV-barns) was added for reactions with multiple subsections. Also, a kinematic check was added for the total photon energy production. (See Section II-E below.)

In GROUPR, a typographical error affecting IBM operation was found. In addition, logic was added to detect the input of "illegal" MFD values, and some input prompts were improved.

In ERRORR, the CLAW weight function was added as a built-in option in the group-averaging mode, and some prompts were repaired. An error was found and corrected that affected the IREAD=1 option (user-specified list of covariance reactions), as was an error in the lumped-partial treatment (MT=851-870). A problem was also found and corrected in the processing of "implicit" cross-material covariances arising from use of the same measurement standard in two different evaluations (LTY=4).

In COVR, some minor problems affecting IBM use were corrected. Also, a problem affecting the card-image library output option was corrected. In MATXS and NMATXS, some typographical errors affecting the IBM version were found and repaired.

In the ACER module, extensive corrections and improvements have been made. Persons interested in this particular module should contact the code authors for further information.

B. New NJOY Version at National Magnetic Fusion Energy Computing Center (D. W. Muir and R. E. MacFarlane)

A new executable version of NJOY (6/83), which performs a variety of functions of particular interest to the fusion neutronics community has been implemented and tested on the CDC-7600 (Machine A) at the National Magnetic Fusion Energy Computing Center at Livermore. This executable version, stored in the FILEM mass-storage system as .5044 .NJOY683 NJOYPFX, incorporates the modules RECONR, HEATR, GROUPR, ERRORR, COVR, MODER, and DTFR and thus is capable of resonance reconstruction, kerma and damage-energy calculations, multigroup averaging, covariance processing, and simple card-image output (DTF format). A test problem that illustrates the calculation of neutron-interaction and photon production transfer matrices as well as kerma, damage-energy, and helium production cross sections for ^{12}C, starting from an original ENDF/B "tape," was executed in both the interactive-input and batch-input modes on Machine A. The test problem input is stored as .5044 .NJOY683 DTFRIN and the corresponding "printout" as .5044 .NJOY683 DTFROUT. A copy of the ENDF/B-V standards tape, which contains the ^{12}C evaluation used in the test, is stored as .5044 .NJOY683 STAN5. This data set is referenced as TAPE20 in the test problem.

C. New Treatment of Particle Emission in NJOY Radiation Damage Calculations

[R. E. MacFarlane, D. W. Muir, and F. M. Mann (Hanford Engineering Development Laboratory)]

Damage to materials caused by neutron irradiation is an important design consideration in both fission and fusion energy systems. There are many radiation effects that may cause damage, including direct heating, gas production (for example, helium embrittlement), transmutation, and the production of lattice defects (DPA). All of these quantities can be calculated using modules of the NJOY nuclear data-processing system[73,74] together with evaluated nuclear data from ENDF/B-V.[75] Using a comprehensive system that combines the damage calculation with the other cross-section processing tasks is convenient; more importantly, it helps to assure consistency between the damage and heating cross sections and those used for neutron and photon transport.

The mathematical basis for the calculation of pointwise cross sections for the production of lattice defects, as implemented in the HEATR module of NJOY, is described in Chapter XII, Section E, of Ref. 74. One possible objection to the treatment described there is the use of a "delta-function" approximation for the spectrum of charged particles emitted in reactions such as (n,p) and (n,α). Specifically, the nuclear recoil energy for these reactions has been calculated up to now using the relation

$$E_R = \frac{1}{A+1} \left(E^* - 2\sqrt{mE^*E'}\,\mu + mE'\right) \quad , \tag{1}$$

where μ is the particle emission cosine in the laboratory system, m is the mass ratio of the emitted particle to the neutron, and E* is given by

$$E^* = \frac{(A+1-m)}{(A+1)} E \quad , \tag{2}$$

where E is the incident neutron energy. The particle energy E' is approximated as being equal to the smaller of the available energy,

$$E_{av} = Q + \frac{AE}{A+1} \quad , \tag{3}$$

or the Coulomb energy,

$$E_c = \frac{(1.029 \times 10^6) zZ}{m^{1/3} + A^{1/3}} \text{ (in eV)} \quad , \tag{4}$$

where z is the charge number of the emitted particle and Z is the charge number of the target atom. This delta-function approximation for E' has the advantage of avoiding the integration over final energy while still representing the most important feature of the charged-particle spectrum. The angular distribution for the emitted particle is assumed to be isotropic in the lab.

We have examined possible improvements in the treatment of charged-particle spectra in HEATR. Some earlier codes[76,77] have used a simple evaporation spectrum for emitted charged particles. The DISCS code[78] follows the method of Kikuchi and Kawaii,[79] who employ an energy-shifted evaporation model for the particle energy E':

$$g(E \rightarrow E') = C[E' - K(Z)E_{cb}] \exp[-(E' - K(Z)E_{cb})/\theta(E,Z,A)] \quad , \qquad (5)$$

where C is a normalization constant, K(Z) is a function fitted to data, and E_{cb} is the Coulomb barrier energy. The numerical value of E_{cb} used in DISCS is 1.4 times E_c as given in Eq. (4). Here θ is another fitted function which takes the place of a nuclear temperature. Specifically,

$$\theta(E,Z,A) = \sqrt{\frac{\mu E + A - E_{cb}}{a(Z,A)}} \quad , \qquad (6)$$

where μ is the reduced mass of the system, Q is the Q-value for the reaction, and a is the nuclear level-density parameter.

In order to evaluate the relative merits of the various models of particle emission, the Hauser-Feshbach computer code HAUSER*5[80] was used to calculate the outgoing proton and alpha spectra from n+^{27}Al, n+^{56}Fe, n+^{58}Ni, n+^{64}Ni, n+^{92}Mo, and n+^{100}Mo. Very good agreement has been obtained between such calculations and the sparse available experimental data. Using the results for aluminum and iron, a new fitting function was found:

$$g(E \rightarrow E') = C[E' - f(Z)] \sqrt{E + Q - E'} \exp[-g(A)E'] \quad , \qquad (7)$$

where

$$f(Z) = \begin{cases} 0.1\ Z & \text{for protons} \ , \\ 0.254\ Z & \text{for alphas} \ , \end{cases} \qquad (8)$$

and

$$g(A) = -0.072 \sqrt{A} \quad . \qquad (9)$$

Figure 43 shows a comparison for n+^{58}Ni for 14-MeV incident neutrons. For all the cases studied, the new formula gives good agreement with the calculated values. The new formula also works better than the formula and parameters of Kikuchi and Kawaii, especially for the cases where E+Q is small compared to the Coulomb barrier energy.

A typical total damage-energy production cross section (eV-barns) is shown in Fig. 44. The 1/v behavior at low energies is due to the photon recoil effect.[74] The sharp onset of the elastic contribution is due to the threshold implied by the Lindhard electronic-screening theory. Fig. 45 shows more detail for the high-energy range important, for example, for fusion. In Figs. 44 and 45 the smooth curves are from NJOY and the (n,particle) absorption reactions were computed with the old treatment. The points plotted with symbols are multigroup values from the DISCS code[78] and were kindly supplied by L. R. Greenwood of the Argonne National Laboratory.

The damage energy due to the (n,p) reactions in iron, as calculated at high energies by four different methods, is shown in Fig. 46. The solid line is the result obtained with the delta-function approximation in NJOY, the dashed line is that obtained with the new spectrum (Eq. 7), and the squares are results from the DISCS code. The NJOY results are based on ENDF/B-V (Rev. 2), and the DISCS results are based on ENDF/B-V (Rev. 1). The crosses are obtained by a direct integration of nuclear-model-generated proton spectra for ^{56}Fe, as described in Section II-D of this report. A slight systematic undercalculation is seen to appear in the NJOY results at very high neutron energies (≧ 16 MeV), but overall the agreement between NJOY (both "old" and "new") with the more exact nuclear model results is quite good.

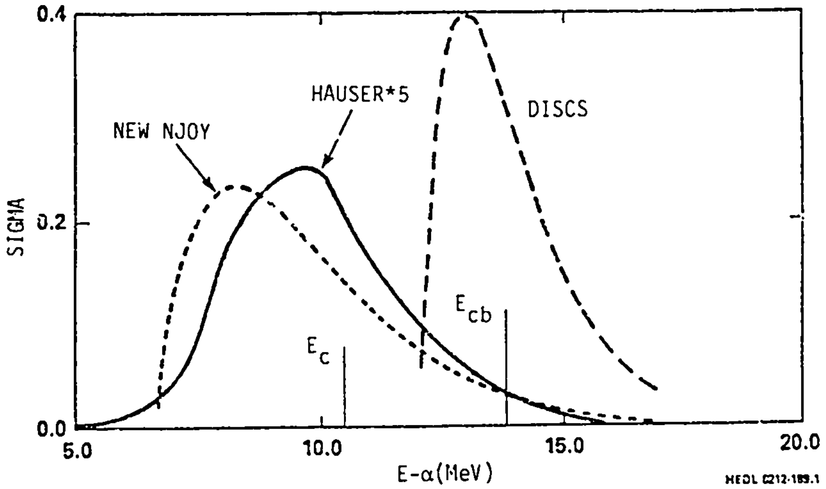

Fig. 43. Comparison of different models of the α-spectrum for the ^{58}Ni(n,α) reaction.

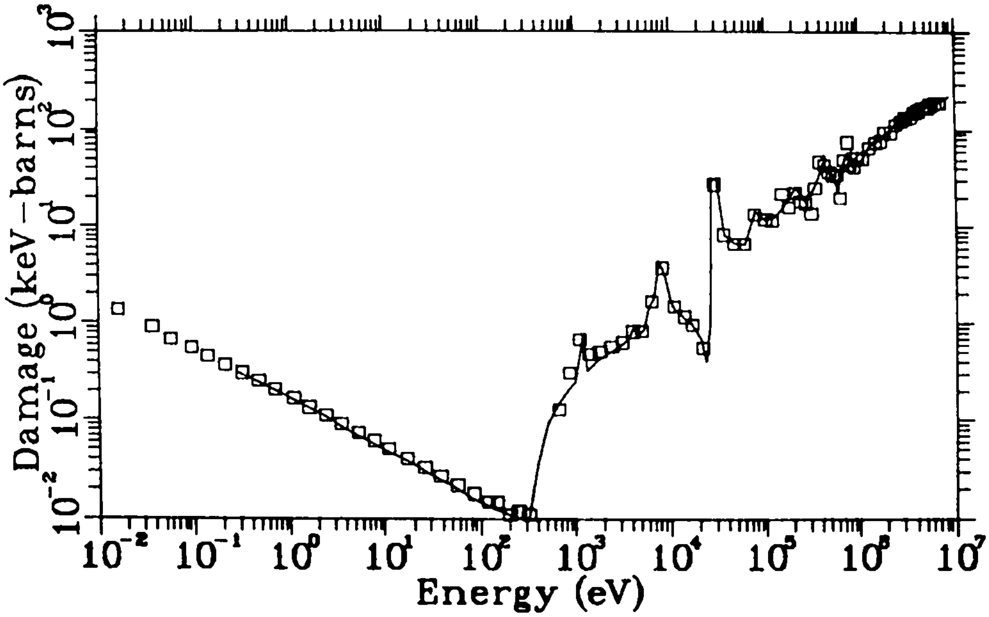

Fig. 44. Comparison of total damage-energy production for iron from "old" NJOY (solid) and DISCS (symbol). Both are multigroup sets plotted at the center of each group.

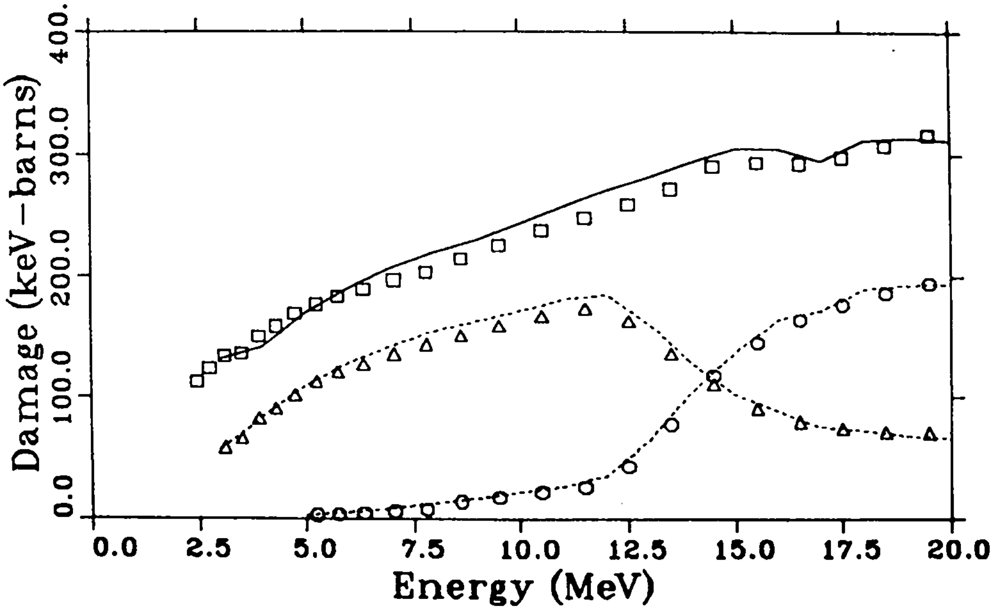

Fig. 45. Components of damage-energy production for iron at high energies. Curves are results from "old" NJOY and symbols are values from DISCS (squares are total, triangles are inelastic, and circles are everything but elastic and inelastic).

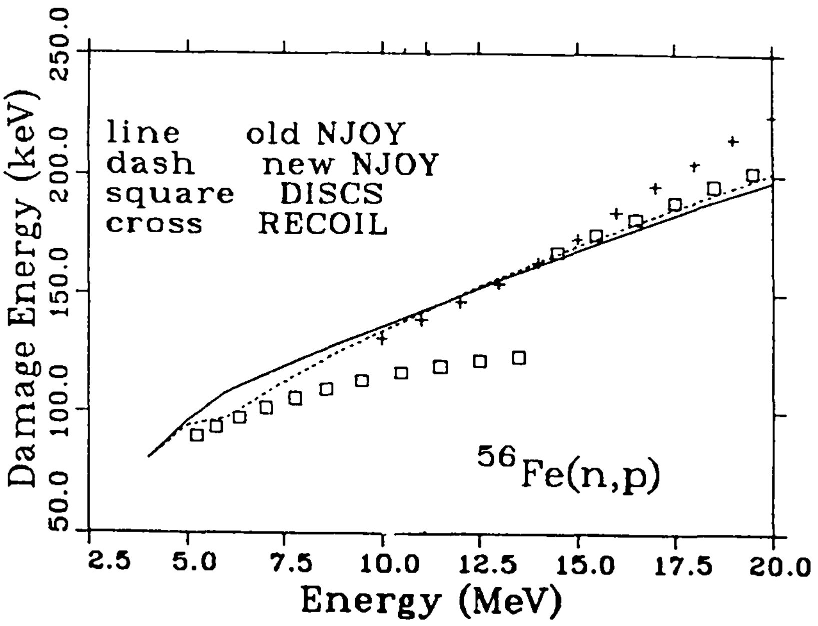

Fig. 46. Various calculations of damage energy due to (n,p) reactions in iron.

The effects of the new treatment of particle emission can also be seen in Tables XII and XIII. All three methods are again in reasonable agreement for (n,p) reactions, but the new model gives lower results for (n,α) reactions due to the improved treatment of Coulomb barrier penetration. The large difference for "other" in Table XIII comes from the large (n,n'p) reactions for nickel. Contrary to the assumption used in current versions of NJOY, the charged particle here is actually more important than the neutron. Better results can be obtained by using the (n,p) treatment for the (n,n'p) reaction.

TABLE XII

DAMAGE-ENERGY PRODUCTION (keV·barns)
FOR 14- TO 15-MeV NEUTRONS ON IRON

Reaction	DISCS	Old NJOY	New NJOY
(n,p)+(n,d)+(n,t)	23.3	23.3	23.3
(n,α)	12.3	11.6	11.2
elastic	62.3	63.5	63.5
inelastic	110.0	114.6	114.6
other	82.1	85.8	85.8
total	290.0	298.8	298.4

TABLE XIII

DAMAGE ENERGY PRODUCTION (keV·barns)
FOR 14- TO 15-MeV NEUTRONS ON NICKEL

Reaction	DISCS	Old NJOY	New NJOY
(n,p)+(n,d)+(n,t)	41.6	51.9	52.0
(n,α)	47.9	45.2	43.9
elastic	62.3	63.4	63.4
inelastic	64.7	58.3	58.3
other	83.5	48.5	48.4
total	300.0	267.3	266.0

The differences in inelastic scattering arise because DISCS uses isotropic CM scattering for everything, but NJOY uses anisotropic CM scattering for the levels and isotropic LAB scattering for the continuum.

To summarize, the NJOY system provides a convenient way to compute damage cross sections or DPA that are consistent with the heating, transmutation, gas production, and transport cross sections used for a particular analysis. The results compare well with those of other codes and provide improved results for high-energy capture reactions.

Remaining shortcomings include the neglect of recoil effects from charged particles in three- and four-body reactions such as (n,n'p) and the neglect of preequilibrium effects on the angular distributions of emitted particles. These effects are being attacked with a completely new approach for adding evaluated recoil spectra to the ENDF/B files.[81]

D. Radiation Damage Calculations with the RECOIL Code (R. E. MacFarlane and D. G. Foster, Jr.)

As pointed out in Sec. II-C, it is sometimes difficult to compute the detailed recoil spectrum needed to compute radiation damage production using the data avilable in the ENDF/B files. This problem becomes serious at energies from 10 MeV to 40 MeV, which will be used in the Fusion Materials Irradiation Test Facilty (FMIT). Fortunately, it is now becoming possible to compute the spectra of particles emitted from high-energy reactions using modern statistical model codes such as GNASH.[6] These spectra can be combined with angular distributions based on Kalbach-Mann systematics[82] to obtain distributions in energy and angle for the recoil nucleus using the RECOIL code.[81] In addition to the traditional damage cross section, RECOIL tabulates all the particle and recoil distributions directly in the new ENDF File 6 format. These tabulated spectra can then be used in subsequent codes to compute damage and nuclear heating.

RECOIL begins by reading and reorganizing the information available from a completed GNASH run. Preequilibrium ratios and photon level data are read from the printer output file. Global parameters, energy level schemes, and population increment data are read from an auxiliary binary output file. While this information is being gathered, the RECOIL code can optionally exclude neutron compound-elastic scattering, neutron discrete-inelastic scattering, and/or discrete-level particle production steps from the reaction data. These reactions and the "shape elastic" term can normally be computed more accurately using optical model codes.

Next, these reaction data are used to produce all possible "reaction stars." Each "star" consists of a series of steps characterized by a particular emitted particle of a particular energy. The probability of observing a particular star is just the product of the probabilities for each step as obtained from GNASH. Once a star has been formed, it is easy to determine that it belongs to a particular reaction, say (n,n'p). RECOIL ignores the order of the steps, and (n,n'p) will actually be the sum of (n,n'p) and (n,pn). Thus, a "reaction" in this sense is characterized by a particular recoil nucleus.

The center-of-mass (CM) momentum of this recoil nucleus is simply the negative of the vector sum of the momenta of all emitted particles. For two-particle final states, the calculation is easy and reliable. The CM energy of the recoil is scaled from the energy of the emitted particle using the appropriate mass ratio and accumulated into the appropriate bin of the recoil spectrum. The angular distribution for the recoil nucleus is just the complement of the distribution of the emitted particle as given by Kalbach-Mann systematics.

For complex reactions, a more approximate method is used. The full angular range for each emitted particle is sampled systematically (not randomly) using a Kalbach-Mann or uniform distribution. This divides each "star" into a large number of "substars," each with its own probability. The energy and emission angle of the recoil nucleus of each substar are then computed and used to increment the energy-angle distribution for that particular recoil nucleus.

When all stars have been processed, the result is a set of reaction cross sections and coupled energy-angle distributions for each emitted particle and each recoil nucleus.

As mentioned earlier, it is desirable to save these distributions in full detail for later use. For just this kind of application, a new ENDF/B format was recently adopted for use in ENDF/B-VI.

For the purposes of this file, any reaction is defined by giving the production cross section for each reaction product as a product of a reaction cross section, a product yield or multiplicity, and a normalized distribution for the product in energy and angle. As usual, the cross section is given in File 3; the other two factors are given in File 6. Correlations and sequences are ignored; that is, the distributions given are those that would be seen by an observer outside of a "black box" looking at one particle at a time. The process being described may be a combination of several different reactions, and the product distribution may be described using several different representations.

Because the new File 6 gives explicit yields for each particle and residual nucleus, it can be used easily to generate gas production and activation cross sections. Thus, all the information needed for heating, damage, gas production, activation, neutron transport, and particle transport is provided by File 3 and File 6 in a uniform and consistent way.

Existing GNASH calculations for iron[50,83] have been processed into File 6 format using RECOIL and an auxiliary code called MAKE6. At the same time, heat production and damage-energy production were computed from the calculated spectra. Sample results for the nonelastic damage and total heating are given in Table XIV together with corresponding results from previous methods. For this example, the differences in damage production are modest with the RECOIL results at 14 MeV lying about 7% lower than ENDF/B-V values. Improvement in the heating numbers is more dramatic. The difficulties in computing kerma from ENDF/B-V are well known;[84] for iron, the problems include neutron-photon energy-balance errors and the difficulty in working with a natural-element file. The new methods are expected to be even more important at higher energies.

Finally, Fig. 47 shows two typical recoil spectra as computed by these methods. Note the effects of discrete levels which show up in the elastic recoil spectrum at high energies.

TABLE XIV

COMPARISON OF DAMAGE-ENERGY PRODUCTION AND HEAT PRODUCTION FOR ^{56}Fe COMPUTED BY RECOIL WITH RESULTS FOR ENDF/B-V NATURAL IRON COMPUTED BY CONVENTIONAL METHODS

Energy (MeV)	RECOIL Damage[a] (keV·b)	ENDF/B-V Damage[a] (keV·b)	RECOIL Heat (MeV·b)	ENDF/B-V Heat (MeV·b)
10	174.3	192.4	0.972	-0.095
11	183.7	207.1	1.104	0.026
12	192.9	219.4	1.236	0.390
13	202.5	225.6	1.417	-0.863
14	212.7	231.9	1.613	-1.096
15	223.5	238.7	1.820	-2.451
16	235.0	252.1	2.059	-3.047
17	245.3	246.8	2.305	-0.310
18	255.7	262.3	2.576	1.482
19	263.7	261.0	2.826	2.006
20	270.8	259.5	3.054	2.602

---

[a] Nonelastic part only.

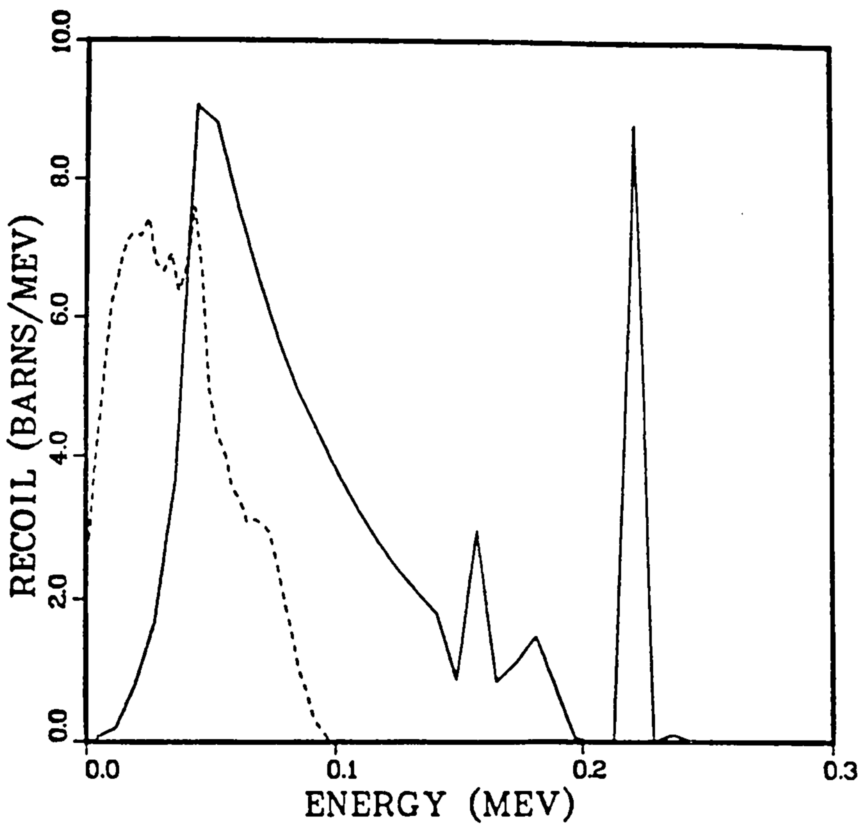

Fig. 47. Typical recoil spectra for ^{56}Fe at 14 MeV. Solid curve is inelastic and dashed curve is (n,2n).

E. Energy Balance of ENDF/B-V.2 (R. E. MacFarlane)

One of the shortcomings of many ENDF/B-V evaluations is that the energy contained in emitted neutrons and photons is not consistent with kinematic limits.[84] In practice, this leads to heat production cross sections (KERMA factors) that are either too small (often negative) or too large.

There are several sources for these problems; for example, photon and neutron sections produced by different evaluators, overly coarse models for inelastic scattering, inconsistent cross sections for photon interaction and neutron production, and uncritical use of histogram photon spectrum data. In addition, it is difficult to calculate the available energy for elemental evaluations because the files contain only average or limiting Q-values.

The ENDF evaluators have been aware of these problems for some time. Therefore, we decided to repeat and extend our original study[84] in order to see whether the new revision of ENDF/B-V has been improved. For this purpose, several useful improvements were made to the kinematic checks in the HEATR module[74] of NJOY. These included a better check of the energy balance of radiative capture (MF=12 and MT=102), and a calculation of kinematic limits for total photon production.

The results of the radiative capture tests at thermal energies are shown in Table XV. These errors reflect problems in either photon yields (MF=12) or photon spectra (MF=15). In addition, the tungsten isotopes show some errors in the resonance range. The elements Cl, K, and Ga seem to have energy-balance problems at thermal energies, and the elements W and Mo could be improved with new effective Q-values.

TABLE XV

PER CENT ERROR IN THERMAL-NEUTRON-INDUCED PHOTON ENERGY FOR ENDF/B-V REVISION 2

Isotope	Per Cent Error
^{55}Mn	+53.7
^{209}Bi	-10.5
^{59}Co	+8.0
^{181}Ta	-3.6
^{93}Nb	+1.4
^{138}Ba	-0.9
^{9}Be	-0.6

Figures 48 and 49 show examples of the total photon production test. This test is meaningful for isotopes at all energies--the dashed curve computed from ENDF should fall between the solid curves (kinematic limits). If the dashed curve is higher than the upper limit, negative kerma factors will usually be seen. For elements below the threshold, the test is only meaningful for multi-body reactions; that is, the results can be believed when the two kinematic limit curves are close together.

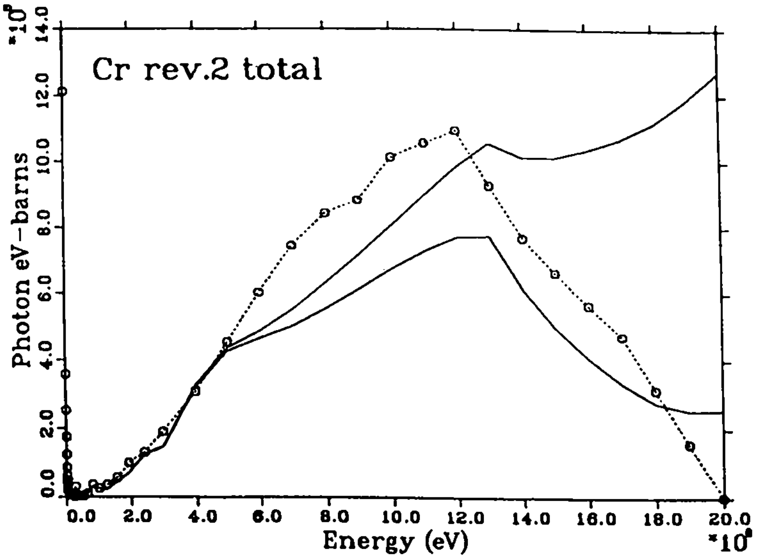

Fig. 48(a).

Fig. 48(b).

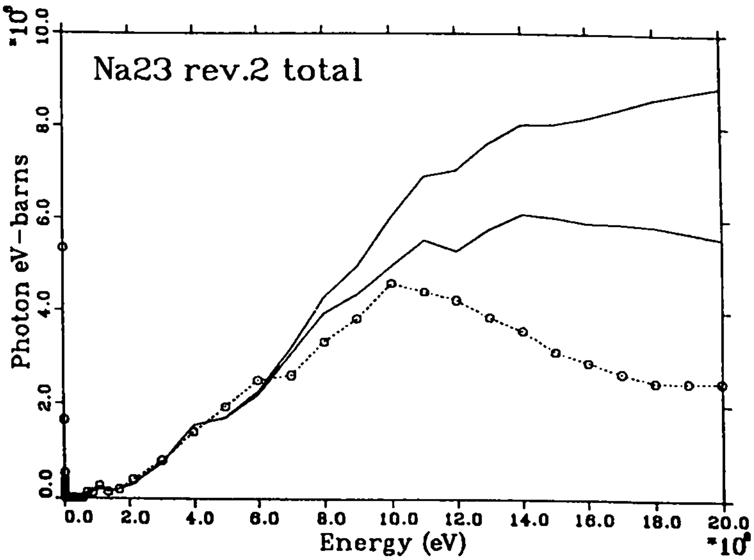

Fig. 48 (a and b). Examples of photon energy production tests for ENDF/B-V Revision 2. The dashed line shows the computed result and the two solid lines are kinematic limits.

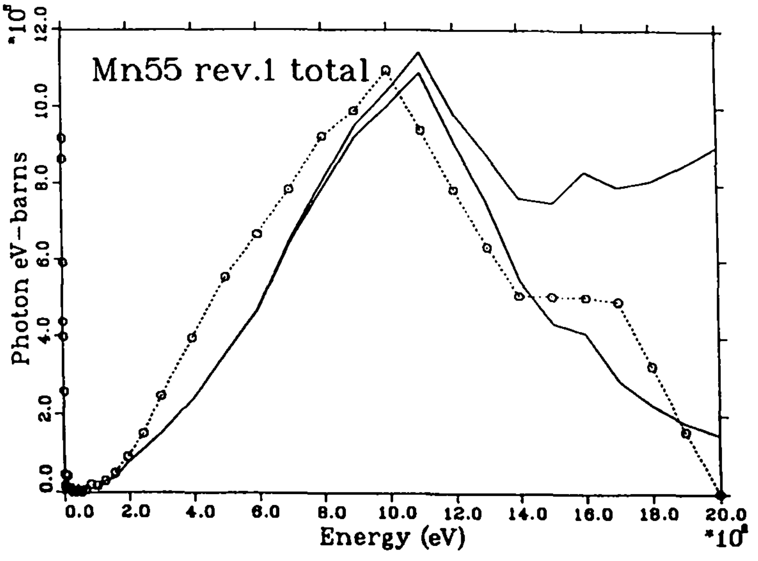

Fig. 49(a).

Fig. 49(b).

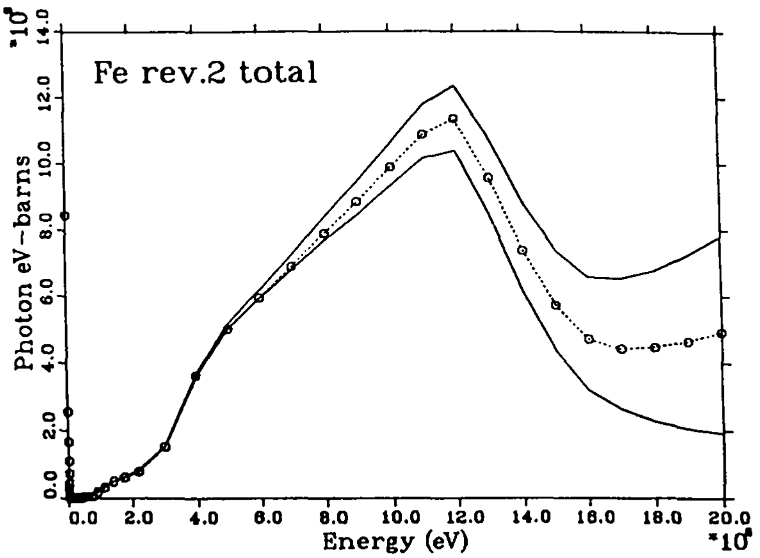

Fig. 49 (a and b). Examples of photon energy production tests for ENDF/B-V Revision 2. The dashed line shows the computed result and the two solid lines are kinematic limits.

A more detailed discussion of these results is being prepared for publication. They should be of some use in assigning priorities for the reevaluation of materials for applications where neutron and photon heating are important (for example, fusion reactors).

F. Fast-Reactor Doppler Coefficient (R. E. MacFarlane)

We participated in the Second Jackson Hole Colloquium on Fast-Reactor Physics, June 27-29, 1983, hosted by the Argonne National Laboratory. The subject was "The Doppler Effect in LMFBRs," and there were participants from the national laboratories, industry, and universities.

One of the basic benchmarks for Doppler calculations is the SEFOR experiment. This was a sodium-cooled, mixed-oxide, fast reactor designed for 20-MW steady-state power and transients peak power up to 10 000 MW. Many of its design features were chosen to allow separating the nuclear Doppler contribution from other sources (control rod expansion, core espansion, etc.). A full analysis of this reactor is difficult, but a simplified benchmark model has been prepared.[85] Our contribution to the meeting was calculations of this benchmark.

The calculations used our 80-group MATXS6 library that was generated by NJOY.[73,74] Self-shielded cross sections were prepared using TRANSX with both homogeneous and heterogeneous treatments of the fuel pin energy self-shielding. Spatial effects and the effects of the fuel bundle wrapper were ignored. One-dimensional calculations were made with ONEDA. This is a modified version of ONEDANT[86] that allows either diffusion or transport results to be obtained. Two-dimensional calculations were made with DIF3D.[87] The results are shown in Tables XVI and XVII.

TABLE XVI

SEFOR RESULTS WITH HETEROGENEOUS SELF-SHIELDING

Parameter	1-D Diff.	2-D Diff.	1-D Transp.
k_{eff} @ 677 K	1.00321	0.98679	1.01142
Corrections	-0.00396	-0.00396	-0.01082
C/E	0.9993	0.9828	1.0006
k_{eff} @ 1365 K	0.99654	0.98062	1.00470
Doppler Coefficient	-0.00952	-0.00881	-0.00959
Corrections	-0.00015	-0.00015	-0.00011
Calculated	-0.00967	-0.00896	-0.00970
C/E	1.21	1.12	1.21

TABLE XVII

SEFOR RESULTS WITH HOMOGENEOUS SELF-SHIELDING

Parameter	1-D Diff.	2-D Diff.	1-D Transp.
k_{eff} @ 677 K	0.99662	0.98184	1.00465
Corrections	-0.00149	-0.00149	-0.00835
C/E	0.99513	0.98035	0.99630
k_{eff} @ 1365 K	0.99121	0.97638	1.99921
Doppler Coefficient	-0.00772	-0.00779	-0.00776
Corrections	-0.00065	-0.00065	-0.00061
Calculated	-0.00837	-0.00844	-0.00837
C/E	1.05	1.06	1.05

These results are somewhat higher than previous results[88] or the results reported at the meeting by other contributors. The heterogeneity effect is especially strong using these methods. Future work will have to explore these differences and look into the effects of additional components of heterogeneity. One conclusion that can be drawn from an examination of these calculations: it is difficult to obtain accuracy for the Doppler efficient calculation better than 5%.

III. NEUTRON ACTIVATION, FISSION PRODUCTS, AND ACTINIDES

A. Neutron Activation of a Vanadium-Alloy Fusion-Reactor First Wall (D. W. Muir)

Vanadium alloys (such as V-20Ti and V-Cr-Ti) are attractive candidates for use as structural materials in fusion-reactor blankets both because of good mechanical properties at high temperatures and because of favorable activation characteristics.[89] The virtual absence[90] of long-lived neutron-activation products of vanadium, titanium, and chromium suggests the possibility of reprocessing and recycling vanadium-alloy blanket components after reasonably short cooling times (perhaps 30-50 years).

As described in Section I-J, the nuclear model code GNASH was used to calculate cross sections for several neutron-activation reactions in vanadium and titanium in order to allow an accurate assessment of induced radioactivity in the time scale of interest for recycling, namely, 1 to 100 years. As discussed below, we have also reviewed the available decay data for the radionuclides produced.

If one assumes that the noble-gas activation product ^{42}Ar ($t_{\frac{1}{2}}$ = 33 y) can be removed, for example, by heating, and if one further assumes that the activation of impurities can be neglected, then the gamma-ray dose near an irradiated blanket component manufactured from V-20Ti will be dominated, a few years after removal from the reactor, by x rays and internal bremsstrahlung photons from ^{49}V ($t_{\frac{1}{2}}$ = 0.90 y). After about 15 to 20 years, most of the dose will come from hard gamma rays from ^{44}Ti ($t_{\frac{1}{2}}$ = 47 y). A summary of the decay properties of these two nuclides is given in Table XVIII along with the relevant 14.1-MeV production cross sections obtained by interpolation from Table VI of Section I-J.

For radioactivity calculations, we have adopted an operating scenario in which a first wall of V-20Ti alloy is irradiated at a neutron wall loading of 10 MW/m^2 for a period, t, of two years (see Ref. 90). The neutron source is assumed to be uniformly distributed over a plasma region which extends from the center of a cylindrical vacuum vessel out to a plasma radius r_p, assumed to be equal to 0.7 times the first-wall radius r_w. For this value of r_p/r_w, and independent of the actual wall radius, the flux of unscattered 14.1-MeV neutrons arriving at the first wall will be 1.69 times the 14.1-MeV neutron current, which at 10 MW/m^2 is 4.44 x 10^{14} n/cm^2 sec. The first-wall uncollided flux, ϕ, is then 7.50 x 10^{14} n/cm^2 sec. As shown in Section I-J, all of the production reactions of interest here have high thresholds and steeply rising excitation functions. Because of this, it is a reasonable approximation here to calculate radionuclide production rates from ϕ alone, ignoring the contribution from lower energy scattered neutrons.

TABLE XVIII

ACTIVATION AND DECAY DATA FOR V AND Ti

Cross Section at 14.1 MeV	
^{51}V(n,2n)	0.524 b
^{50}V(n,2n)	0.692 b
^{46}Ti(n,2n)	0.0124 b
^{45}Ti(n,2n)	0.0926 b

	Half-Life	Photon Energy	Photons Per Decay
^{49}V	0.90 y	~ 250 keV[a]	~ 0.0003[b]
		4.5 keV[c]	0.196[c]
^{44}Ti	47 y	2.656 MeV	0.001
		1.499 MeV	0.009
		1.157 MeV	0.999

---

[a] Internal bremsstrahlung accompanying electron capture. The spectrum is a broad continuum extending from 0 up to 616 keV. (See Ref. 91.)

[b] Absolute intensity estimated from Eq. (8) of Ref. 92.

[c] Private communications from J. K. Tuli, Brookhaven National Laboratory, Upton, N. Y., and D. C. Kocher, Oak Ridge National Laboratory, Oak Ridge, Tenn., August 1983.

Both the ^{49}V production and the ^{44}Ti production can be calculated from equations of the following form:

$$\frac{dn_1}{dt} = -\lambda_1 n_1$$

$$\frac{dn_2}{dt} = -\lambda_2 n_2 + n_1 \sigma(1\rightarrow 2) \phi$$

$$\frac{dn_3}{dt} = -\lambda_3 n_3 + n_2 \sigma(2\rightarrow 3) \phi \quad .$$

Here λ_i denotes the total nuclide destruction rate, including both radioactive decay and neutron "burn-up" reactions. The transmutation cross sections $\sigma(i\rightarrow j)$ are just the relevant (n,2n) cross sections from Table XVIII. In all cases, the initial conditions are $n_1(0) = n_0$, $n_2(0) = 0$, and $n_3(0) = 0$. The solution for the nuclide concentrations after an irradiation time t is well known:

$$n_1 = n_0 \, e^{-\lambda_1 t} \quad ,$$

$$n_2 = n_0 \, \sigma(1\rightarrow 2) \, \phi \, t \, f(t) \quad ,$$

and

$$n_3 = n_0 \, \sigma(1\rightarrow 2) \, \sigma(2\rightarrow 3) \, \phi^2 \, t^2 \, g(t),$$

where

$$f(t) = \frac{e^{-\lambda_1 t} - e^{-\lambda_2 t}}{(\lambda_2 - \lambda_1)t}$$

and

$$g(t) = \frac{(\lambda_3-\lambda_2)e^{-\lambda_1 t} - (\lambda_3-\lambda_1)e^{-\lambda_2 t} + (\lambda_2-\lambda_1)e^{-\lambda_3 t}}{(\lambda_3-\lambda_2)(\lambda_3-\lambda_1)(\lambda_2-\lambda_1)t^2} \quad .$$

An exact evaluation of the factors f(t) and g(t) would be difficult because it would require energy-dependent cross sections for all target-destruction reactions, including (n,γ), and these data, for the most part, do not exist. Fortunately, the neutron spectrum at a typical reactor first wall is very hard, and this greatly reduces the data needs. For example, in the Culham Mark II design, the thermal neutron flux is seven orders of magnitude less than the 14-MeV flux.[90] In such a hard spectrum, the target-destruction reactions, like the production reactions, will occur mainly at 14 MeV. Adopting 0.7 barns as a typical target-destruction cross section, destruction rates in the neighborhood of 0.02 per year can be expected. Since we are interested in irradiadiation times in the neighborhood of t = 2 years, it is a good approximation to take

$$e^{-\lambda t} \cong 1 - \lambda t$$

for the stable and long-lived nuclides of interest (^{51}V, ^{50}V, ^{46}Ti, and ^{44}Ti).

For cases where $\lambda_1 t$ and $\lambda_2 t \ll 1$ and where $\lambda_3 \gg \lambda_1$ and λ_2, use of this approximation leads to the results $f(t) \cong 1$ and

$$g(t) \cong \frac{\lambda_3 t - 1 + e^{-\lambda_3 t}}{\lambda_3^2 \, t^2} \; . \tag{10}$$

Similarly, if $\lambda_1 t$ and $\lambda_3 t \ll 1$ and $\lambda_2 \gg \lambda_1$ and λ_3, then

$$f(t) \cong \frac{1 - e^{-\lambda_2 t}}{\lambda_2 \, t} \tag{11}$$

and

$$g(t) \cong \frac{\lambda_2 t - 1 + e^{-\lambda_2 t}}{\lambda_2^{\,2} \, t^2} \; .$$

If, in addition, $\lambda_2 t \gg 1$, the last result becomes simply

$$g(t) \cong \frac{1}{\lambda_2 \, t} \; . \tag{12}$$

After the irradiation of a V-20Ti first wall for a time t, the ratio of ^{49}V atoms to initial total vanadium atoms can be estimated using the approximations to g(t) and f(t) given in Eqs. (10) and (11) above:

$$\frac{n_{49}}{n_V} \cong 0.9975 \, \sigma_{51} \, \sigma_{50} \, \phi^2 \, \frac{\lambda_{49} t - 1 + e^{-\lambda_{49} t}}{\lambda_{49}^2}$$

$$+ \, 0.0025 \, \sigma_{50} \, \phi \, \frac{1 - e^{-\lambda_{49} t}}{\lambda_{49}} \; ,$$

where the first contribution results from the two-step process (^{51}V → ^{50}V → ^{49}V) and the second results from the direct production from the 0.25% abundant ^{50}V in natural vanadium. Here λ_{49} can be accurately approximated using the decay component alone, $\lambda_{49} \cong 0.77$ per year. Inserting cross-section values from Table XVIII and setting t = 2 years, we obtain

$$\frac{n_{49}}{n_V} = 3.02 \times 10^{-4} \ ,$$

with about 86% of the ^{49}V atoms resulting from the two-step process.

Similarly, the ratio of ^{44}Ti atoms to initial total titanium atoms is calculated using the simple result in Eq. (12),

$$\frac{n_{44}}{n_{Ti}} = 0.082 \ \sigma_{46} \ \sigma_{45} \ \phi^2 \ \frac{t}{\lambda_{45}} \ ,$$

where λ_{45} for highly radioactive ^{45}Ti is 1.97×10^3 per year. Again inserting numerical values, we obtain

$$\frac{n_{44}}{n_{Ti}} = 5.37 \times 10^{-11} \ .$$

In spite of the very low gamma-ray intensity from ^{49}V decays, it is clear from these results that, at early times, ^{49}V will dominate ^{44}Ti as a source of energetic gamma rays. It is also clear that eventually ^{44}Ti will dominate.

It is of interest to evaluate the gamma-ray exposure rate at the surface of a large, thick sheet of V-20Ti alloy. A useful formula for this is given in Ref. 90:

$$\text{Exposure (R/h)} = 6.57 \times 10^{-5} \sum_{\text{all } \gamma \text{ lines}} \bar{\mu}_a \ S_\gamma \ \frac{B}{2\mu_m} \ , \tag{13}$$

where $\bar{\mu}_a$ is the energy absorption coefficient of air (cm^2 g^{-1}), μ_m is the linear attenuation coefficient of the alloy (cm^2 g^{-1}), S_γ is the rate of gamma-ray energy emission per unit mass (MeV g^{-1} s^{-1}), and B is the gamma-ray dose build-up factor, a number around 2. Substituting the appropriate values in Eq. (13), we obtain the late-time exposure rate:

$$\begin{aligned}\text{Exposure} = {} & 2^{-T/0.90} \times 345 \text{ R/hour} \\ & + 2^{-T/47} \times 2.25 \text{ mR/hour} \ ,\end{aligned}$$

where the storage time T is measured in years.

After 20 years of storage, the exposure will have dropped to 1.75 mR/h. This level of radiation is comparable to the limit set by the US Government for radiation workers (1250 mrem in any 3-month period). While certainly not negligible, it probably would not present a serious obstacle to performing industrial operations, such as fabrication, with recycled V-20Ti.

In order to place our results for pure V-20Ti in perspective, it is helpful to consider very briefly the activation of possible impurities. From the materials-reprocessing viewpoint, the most troublesome impurities are those that can produce a long-lived gamma emitter such as ^{60}Co, ^{94}Nb, or ^{108}Ag. We have used data from Ref. 91 to estimate the concentrations of various impurities which result in surface exposure rates of 1 mR/h after 50 years of cooling, which is about the exposure level expected from ^{44}Ti at that time. To achieve this fairly low level, the initial concentration of Ag in the vanadium alloy would have to be less than 0.01 ppm, Co less than 0.1 ppm, Nb less than 1 ppm, and Ni, Cu, and Al less than 10 ppm. It is not clear whether or not such high purities will be economically attainable in the forseeable future.

B. Preliminary ENDF/B-VI Fission Yield Evaluations [T. R. England, B. F. Rider (General Electric Co., retired), D. C. George, R. J. LaBauve, and W. B. Wilson]

The results for 50 yield sets were reviewed at the NEA Specialists' Meeting on Yields and Decay Data of Fission Product Nuclides at Brookhaven National Laboratory, October 24-27, 1983.[93] While this was a general review, it was noted that the only effort comparable to that for ENDF/B-VI was that of E. A. C. Crouch in 1977.[94] Other evaluations are more limited in the effects treated, in the number of fissionable nuclides and incident neutron energies considered, and in the amount of measured data included. Many are simply compilations without evaluation. Each of the 50 yield sets in ENDF/B-VI include both independent and cumulative yields and their uncertainties, and each set and type contain 1100 to 1200 nuclides. Table XIX lists the 34 nuclides and type of energy included. Table XX lists some characteristics of the evaluations for ENDF/B-IV, -V, and -VI.

A number of integral tests have been made and compared to evaluations. Table XXI lists the total delayed neutron emission, and the total neutron emission is listed in Table XXII. Values in Table XXI require neutron emission probabilities (Pn values). Recent Pn evaluations, noted in the next section, were used.

Other tests are indicated in Ref. 93. Table XXIII lists the mass chain yields for 10 of the 50 sets, and Fig. 50 compares the values for ^{235}U, ^{238}U, and ^{239}Pu.

TABLE XIX

ENDF/B FISSION-PRODUCT YIELD SETS[a]

	Neutron Energy			
Nuclide	Thermal	Fast	14 MeV	Spon.
^{227}Th	6			
^{229}Th	6			
^{232}Th		456	56	
^{231}Pa		6		
^{232}U		6		
^{233}U	456	56	56	
^{234}U		6	6	
^{235}U	456	456	456	
^{236}U		56	6	
^{237}U		6		
^{238}U		456	456	6
^{237}Np		56	6	
^{238}Np		6		
^{238}Pu		6		
^{239}Pu	456	456	56	
^{240}Pu		56	6	
^{241}Pu	456	56		
^{242}Pu		56		
^{241}Am	6	6	6	
^{242M}Am	6			
^{243}Am		6		
^{242}Cm		6		
^{244}Cm				6
^{246}Cm	6			
^{248}Cm				6
^{249}Cf	6			
^{250}Cf				6
^{251}Cf	6			
^{252}Cf				56
^{253}Es				6
^{254}Es	6			
^{254}Fm				6
^{255}Fm	6			
^{256}Fm				6

---

[a] The numbers 4, 5, and 6 refer to ENDF/B Versions IV, V, and preliminary VI. ENDF/B-IV contains only independent yields and does not include uncertainties.

TABLE XX

SUMMARY OF ENDF EVALUATIONS[a]

QUANTITY	ENDF/B-IV	ENDF/B-V	PRELIM. ENDF/B-VI
YEAR	1974	1978	1983
FISSIONABLE NUCS.	6	11	34
NO. OF YIELD SETS	10	20	50
ISOMER RATIO EST.	50/50	YES	YES
PAIRING	NO	YES	YES
DELAYED NEUTRON	NO	YES	YES
CHARGE BALANCE	NO	YES	YES
TERNARY FISSION	NO	YES	YES
INDEP. YIELDS	YES	YES	YES
CUMULATIVE YIELDS	NO	YES	YES
UNCERTAINTIES	NO	YES	YES
NO. OF REFERENCES	956	1119	1274
NO. OF YIELDS	11000	44000	110000

---

[a] Beginning with ENDF/B-V, delayed neutron branching fractions have been incorporated into evaluations. Independent yields apply before delayed neutron emission and cumulative yields apply after emission.

TABLE XXI

DELAYED NEUTRON COMPARISONS (FROM VERSION E YIELDS)

FISSIONABLE NUCLIDE		CALCULATED VALUES PER 100 FISSIONS	ENDF/B-V EVAL.
^{235}U	(T)	1.77+/- 0.14	1.67
^{235}U	(F)	2.06+/- 0.27	1.67
^{235}U	(H)	1.08+/- 0.18	0.90
^{238}U	(F)	3.54+/- 0.36	4.40
^{238}U	(H)	2.71+/- 0.35	2.60
^{239}Pu	(T)	0.76+/- 0.05	0.65
^{239}Pu	(F)	0.68+/- 0.09	0.65
^{241}Pu	(T)	1.39+/- 0.12	1.62
^{233}U	(T)	0.96+/- 0.22	0.74
^{232}Th	(F)	5.69+/- 1.05	5.27
^{233}U	(F)	0.91+/- 0.15	0.74
^{233}U	(H)	0.70+/- 0.13	0.47
^{236}U	(F)	2.32+/- 0.31	----
^{239}Pu	(H)	0.38+/- 0.07	0.43
^{240}Pu	(F)	0.81+/- 0.11	0.90
^{241}Pu	(F)	1.39+/- 0.16	1.62
^{242}Pu	(F)	1.40+/- 0.16	1.50
^{232}Th	(H)	4.16+/- 1.05	3.00
^{237}Np	(F)	1.14+/- 0.15	----
^{252}Cf	(S)	0.61+/- 0.07	----
^{234}U	(F)	1.30+/- 0.21	----
^{237}U	(F)	3.50+/- 0.38	----
^{240}Pu	(H)	0.50+/- 0.09	0.62
^{234}U	(H)	0.76+/- 0.15	----
^{236}U	(H)	1.54+/- 0.23	----
^{238}Pu	(F)	0.79+/- 0.11	----
^{241}Am	(F)	0.50+/- 0.07	----
^{243}Am	(F)	0.79+/- 0.10	----
^{238}Np	(F)	2.15+/- 0.24	----
^{242}Cm	(F)	0.13+/- 0.03	----
^{227}Th	(T)	1.41+/- 0.41	----
^{229}Th	(T)	1.81+/- 0.58	----
^{231}Pa	(F)	1.60+/- 0.35	----
^{241}Am	(T)	0.53+/- 0.07	----
^{241}Am	(H)	0.25+/- 0.05	----
^{42M}Am	(T)	0.76+/- 0.11	----
^{245}Cm	(T)	0.60+/- 0.09	----
^{249}Cf	(T)	0.16+/- 0.03	----
^{251}Cf	(T)	0.73+/- 0.09	----
^{254}Es	(T)	0.39+/- 0.06	----
^{250}Cf	(S)	0.34+/- 0.05	----
^{244}Cm	(S)	0.44+/- 0.07	----
^{248}Cm	(S)	1.19+/- 0.14	----
^{253}Es	(S)	0.19+/- 0.04	----
^{254}Fm	(S)	0.06+/- 0.02	----
^{255}Fm	(T)	0.25+/- 0.04	----
^{256}Fm	(S)	0.16+/- 0.03	----
^{237}Np	(H)	0.96+/- 0.13	----
^{232}U	(T)	0.52+/- 0.09	----
^{238}U	(S)	5.67+/- 0.49	----

TABLE XXII

TOTAL NEUTRON COMPARISONS (VERSION E YIELDS)

NUCLIDE	CALCULATED	ENDF/B-V EVAL.
^{235}U (T)	2.66+/- 0.29	2.44
^{235}U (F)	2.45+/- 0.34	2.48
^{235}U (H)	4.37+/- 1.87	4.40
^{238}U (F)	2.99+/- 0.64	2.47
^{238}U (H)	4.48+/- 1.68	4.43
^{239}Pu (T)	2.91+/- 0.84	2.89
^{239}Pu (F)	2.90+/- 0.62	2.95
^{241}Pu (T)	2.95+/- 1.10	2.96
^{233}U (T)	2.52+/- 1.06	2.50
^{232}Th (F)	2.36+/- 1.60	2.02
^{233}U (F)	2.50+/- 0.64	2.51
^{233}U (H)	3.58+/- 3.31	4.27
^{236}U (F)	2.81+/- 3.35	2.38
^{239}Pu (H)	4.63+/- 2.57	4.92
^{240}Pu (F)	3.20+/- 2.49	2.88
^{241}Pu (F)	2.98+/- 1.31	2.96
^{242}Pu (F)	3.53+/- 3.68	2.89
^{232}Th (H)	3.91+/- 1.67	3.94
^{237}Np (F)	2.76+/- 0.95	2.77
^{252}Cf (S)	4.05+/- 2.04	----
^{234}U (F)	2.72+/- 4.30	2.42
^{237}U (F)	2.71+/- 5.64	2.50
^{240}Pu (H)	4.62+/- 4.05	4.93
^{234}U (H)	4.18+/- 4.86	4.24
^{236}U (H)	4.24+/- 4.64	4.15
^{238}Pu (F)	2.01+/- 5.99	2.97
^{241}Am (F)	2.98+/- 4.61	3.17
^{243}Am (F)	4.02+/- 6.07	3.36
^{238}Np (F)	2.29+/- 5.98	2.86
^{242}Cm (F)	3.60+/- 6.33	3.53
^{227}Th (T)	1.39+/- 5.22	----
^{229}Th (T)	2.45+/- 2.23	----
^{231}Pa (F)	2.47+/- 4.72	2.34
^{241}Am (T)	2.76+/- 3.36	3.09
^{241}Am (H)	4.46+/- 3.90	5.33
^{42M}Am (T)	2.92+/- 4.62	3.26
^{245}Cm (T)	3.37+/- 2.94	3.83
^{249}Cf (T)	4.17+/- 4.04	4.06
^{251}Cf (T)	3.64+/- 5.02	4.14
^{254}Es (T)	3.92+/- 4.72	----
^{250}Cf (S)	3.30+/- 4.15	----
^{244}Cm (S)	2.22+/- 3.60	----
^{248}Cm (S)	3.80+/- 4.38	----
^{253}Es (S)	4.38+/- 5.08	----
^{254}Fm (S)	4.23+/- 5.04	----
^{255}Fm (T)	3.15+/- 5.48	----
^{256}Fm (S)	4.43+/- 5.54	----
^{237}Np (H)	3.38+/- 4.85	4.74
^{232}U (T)	2.94+/- 4.84	3.13
^{238}U (S)	1.72+/- 2.57	----

TABLE XXIII

CHAIN YIELDS PER 100 FISSIONS AND UNCERTAINTIES (IN %)-VERSION E

MASS	U235T	U235F	U235H	U238F	U238H
66	6.608E-08 +/- 32.0	6.569E-07 +/- 23.0	2.930E-04 +/- 8.0	3.726E-06 +/- 32.0	8.449E-05 +/- 11.0
67	3.428E-07 +/- 32.0	2.110E-06 +/- 23.0	6.696E-04 +/- 8.0	2.155E-05 +/- 32.0	1.386E-04 +/- 16.0
68	5.658E-07 +/- 32.0	3.661E-06 +/- 23.0	9.088E-04 +/- 11.0	9.954E-06 +/- 16.0	2.985E-04 +/- 16.0
69	1.227E-06 +/- 32.0	7.901E-06 +/- 23.0	1.414E-03 +/- 32.0	1.290E-05 +/- 16.0	5.008E-04 +/- 16.0
70	2.841E-06 +/- 32.0	1.732E-05 +/- 23.0	2.418E-03 +/- 11.0	1.604E-05 +/- 16.0	9.002E-04 +/- 16.0
71	6.598E-06 +/- 32.0	4.220E-05 +/- 23.0	4.042E-03 +/- 11.0	2.009E-05 +/- 16.0	1.591E-03 +/- 16.0
72	2.524E-05 +/- 11.0	1.506E-04 +/- 23.0	6.066E-03 +/- 8.0	6.076E-05 +/- 32.0	2.994E-03 +/- 11.0
73	9.604E-05 +/- 32.0	4.910E-04 +/- 16.0	1.161E-02 +/- 11.0	2.080E-04 +/- 23.0	5.220E-03 +/- 11.0
74	3.209E-04 +/- 23.0	1.081E-03 +/- 23.0	1.743E-02 +/- 11.0	2.787E-04 +/- 32.0	8.001E-03 +/- 16.0
75	1.054E-03 +/- 23.0	6.936E-03 +/- 16.0	2.764E-02 +/- 11.0	4.645E-04 +/- 32.0	1.386E-02 +/- 16.0
76	3.300E-03 +/- 32.0	1.127E-02 +/- 23.0	4.097E-02 +/- 11.0	8.025E-04 +/- 23.0	2.197E-02 +/- 16.0
77	7.553E-03 +/- 8.0	2.925E-02 +/- 11.0	6.815E-02 +/- 11.0	3.310E-03 +/- 11.0	3.127E-02 +/- 8.0
78	2.070E-02 +/- 8.0	5.429E-02 +/- 11.0	1.022E-01 +/- 11.0	1.126E-02 +/- 23.0	4.084E-02 +/- 11.0
79	4.329E-02 +/- 6.0	8.505E-02 +/- 11.0	1.716E-01 +/- 8.0	3.278E-02 +/- 23.0	1.690E-01 +/- 11.0
80	1.270E-01 +/- 6.0	1.146E-01 +/- 23.0	2.596E-01 +/- 11.0	4.721E-02 +/- 32.0	2.127E-01 +/- 16.0
81	1.906E-01 +/- 4.0	2.091E-01 +/- 11.0	2.980E-01 +/- 11.0	1.083E-01 +/- 16.0	3.324E-01 +/- 11.0
82	3.224E-01 +/- 2.80	3.262E-01 +/- 11.0	6.077E-01 +/- 11.0	2.133E-01 +/- 16.0	4.526E-01 +/- 16.0
83	5.394E-01 +/- 0.50	5.734E-01 +/- 1.0	1.111E+00 +/- 6.0	3.952E-01 +/- 1.40	6.690E-01 +/- 2.80
84	1.003E+00 +/- 0.70	1.024E+00 +/- 1.40	1.544E+00 +/- 11.0	8.194E-01 +/- 1.40	1.124E+00 +/- 2.80
85	1.317E+00 +/- 0.35	1.350E+00 +/- 0.70	1.658E+00 +/- 2.80	7.398E-01 +/- 1.0	1.003E+00 +/- 1.40
86	1.968E+00 +/- 0.50	1.939E+00 +/- 1.0	2.626E+00 +/- 11.0	1.286E+00 +/- 1.0	1.571E+00 +/- 2.80
87	2.558E+00 +/- 0.50	2.482E+00 +/- 1.0	2.440E+00 +/- 4.0	1.604E+00 +/- 1.0	1.685E+00 +/- 2.0
88	3.565E+00 +/- 0.70	3.483E+00 +/- 0.70	3.374E+00 +/- 4.0	2.054E+00 +/- 1.40	2.215E+00 +/- 2.0
89	4.771E+00 +/- 1.0	4.412E+00 +/- 1.40	4.139E+00 +/- 2.80	2.784E+00 +/- 2.0	2.914E+00 +/- 2.0
90	5.755E+00 +/- 1.0	5.444E+00 +/- 0.70	4.594E+00 +/- 2.80	3.238E+00 +/- 1.40	3.166E+00 +/- 2.80
91	5.910E+00 +/- 1.0	5.721E+00 +/- 0.70	4.871E+00 +/- 4.0	3.979E+00 +/- 2.0	3.764E+00 +/- 2.80
92	5.977E+00 +/- 1.0	5.830E+00 +/- 1.0	5.164E+00 +/- 8.0	4.288E+00 +/- 2.80	3.926E+00 +/- 2.80
93	6.349E+00 +/- 0.70	6.244E+00 +/- 0.70	5.250E+00 +/- 6.0	4.882E+00 +/- 2.0	4.475E+00 +/- 2.80
94	6.417E+00 +/- 1.0	6.288E+00 +/- 0.70	5.221E+00 +/- 11.0	4.765E+00 +/- 4.0	4.894E+00 +/- 8.0
95	6.507E+00 +/- 1.0	6.414E+00 +/- 0.50	5.180E+00 +/- 4.0	5.106E+00 +/- 1.0	4.963E+00 +/- 2.0
96	6.274E+00 +/- 1.0	6.190E+00 +/- 0.70	5.299E+00 +/- 8.0	5.996E+00 +/- 4.0	5.578E+00 +/- 11.0
97	5.937E+00 +/- 0.70	5.984E+00 +/- 0.50	5.564E+00 +/- 6.0	5.546E+00 +/- 0.70	5.305E+00 +/- 2.0
98	5.747E+00 +/- 1.0	5.911E+00 +/- 0.50	4.215E+00 +/- 8.0	5.862E+00 +/- 1.0	5.457E+00 +/- 11.0
99	6.091E+00 +/- 1.0	5.765E+00 +/- 1.40	5.088E+00 +/- 2.80	6.163E+00 +/- 1.40	5.685E+00 +/- 1.40
100	6.232E+00 +/- 1.0	6.274E+00 +/- 1.0	4.042E+00 +/- 8.0	6.672E+00 +/- 1.0	4.996E+00 +/- 11.0
101	5.170E+00 +/- 1.0	5.199E+00 +/- 1.40	3.532E+00 +/- 8.0	6.202E+00 +/- 1.40	5.611E+00 +/- 2.80
102	4.308E+00 +/- 1.0	4.355E+00 +/- 1.0	3.333E+00 +/- 11.0	6.440E+00 +/- 1.0	4.609E+00 +/- 8.0
103	3.030E+00 +/- 1.0	3.241E+00 +/- 1.0	3.198E+00 +/- 2.80	6.299E+00 +/- 1.0	4.651E+00 +/- 2.0
104	1.909E+00 +/- 1.40	2.067E+00 +/- 2.0	2.187E+00 +/- 8.0	5.033E+00 +/- 1.0	3.587E+00 +/- 6.0
105	9.603E-01 +/- 1.40	1.169E+00 +/- 2.80	1.875E+00 +/- 4.0	4.075E+00 +/- 2.0	3.233E+00 +/- 2.0
106	3.999E-01 +/- 1.40	5.309E-01 +/- 1.0	1.577E+00 +/- 4.0	2.473E+00 +/- 1.40	2.434E+00 +/- 4.0
107	1.449E-01 +/- 2.80	2.763E-01 +/- 11.0	1.320E+00 +/- 11.0	1.234E+00 +/- 8.0	1.728E+00 +/- 6.0
108	5.091E-02 +/- 4.0	1.144E-01 +/- 16.0	1.210E+00 +/- 11.0	6.010E-01 +/- 16.0	1.222E+00 +/- 16.0
109	2.993E-02 +/- 8.0	8.254E-02 +/- 11.0	1.263E+00 +/- 4.0	2.423E-01 +/- 11.0	1.217E+00 +/- 8.0
110	2.514E-02 +/- 4.0	6.055E-02 +/- 16.0	1.113E+00 +/- 11.0	1.347E-01 +/- 16.0	1.026E+00 +/- 11.0
111	1.849E-02 +/- 4.0	4.266E-02 +/- 2.0	1.127E+00 +/- 2.80	7.478E-02 +/- 2.0	1.040E+00 +/- 2.80
112	1.279E-02 +/- 4.0	3.705E-02 +/- 2.0	1.104E+00 +/- 8.0	5.527E-02 +/- 4.0	1.006E+00 +/- 6.0
113	1.444E-02 +/- 6.0	3.219E-02 +/- 2.80	1.111E+00 +/- 8.0	5.146E-02 +/- 8.0	9.289E-01 +/- 6.0
114	1.251E-02 +/- 6.0	3.193E-02 +/- 2.80	1.086E+00 +/- 11.0	3.828E-02 +/- 16.0	7.184E-01 +/- 11.0
115	1.044E-02 +/- 8.0	2.831E-02 +/- 6.0	9.867E-01 +/- 4.0	3.294E-02 +/- 6.0	8.392E-01 +/- 4.0
116	1.521E-02 +/- 6.0	3.369E-02 +/- 2.0	1.085E+00 +/- 11.0	3.940E-02 +/- 11.0	6.753E-01 +/- 11.0
117	9.834E-03 +/- 8.0	2.946E-02 +/- 11.0	1.082E+00 +/- 8.0	3.658E-02 +/- 11.0	7.090E-01 +/- 8.0
118	7.034E-03 +/- 16.0	2.875E-02 +/- 11.0	1.104E+00 +/- 11.0	3.984E-02 +/- 11.0	8.344E-01 +/- 11.0
119	7.283E-03 +/- 11.0	2.804E-02 +/- 8.0	1.108E+00 +/- 11.0	3.439E-02 +/- 16.0	7.353E-01 +/- 11.0

TABLE XXIII (Cont.)

MASS	U235T			U235F			U235H			U238F			U238H		
120	7.514E-03	+/-	11.0	2.857E-02	+/-	8.0	1.113E+00	+/-	8.0	3.443E-02	+/-	16.0	7.898E-01	+/-	11.0
121	1.152E-02	+/-	6.0	3.299E-02	+/-	8.0	9.804E-01	+/-	6.0	3.773E-02	+/-	11.0	7.651E-01	+/-	4.0
122	8.785E-03	+/-	11.0	2.726E-02	+/-	11.0	1.170E+00	+/-	11.0	3.619E-02	+/-	16.0	8.627E-01	+/-	11.0
123	1.443E-02	+/-	4.0	3.890E-02	+/-	11.0	1.217E+00	+/-	11.0	3.891E-02	+/-	16.0	9.357E-01	+/-	11.0
124	1.737E-02	+/-	11.0	4.684E-02	+/-	11.0	1.316E+00	+/-	11.0	4.269E-02	+/-	16.0	1.050E+00	+/-	11.0
125	2.683E-02	+/-	4.0	5.411E-02	+/-	8.0	1.488E+00	+/-	8.0	4.565E-02	+/-	8.0	1.193E+00	+/-	6.0
126	4.454E-02	+/-	8.0	8.572E-02	+/-	11.0	1.503E+00	+/-	4.0	5.109E-02	+/-	8.0	1.365E+00	+/-	16.0
127	1.161E-01	+/-	4.0	3.024E-01	+/-	4.0	2.040E+00	+/-	4.0	1.331E-01	+/-	4.0	1.505E+00	+/-	6.0
128	3.315E-01	+/-	2.80	3.953E-01	+/-	11.0	2.490E+00	+/-	11.0	4.179E-01	+/-	6.0	1.675E+00	+/-	8.0
129	6.607E-01	+/-	6.0	8.443E-01	+/-	4.0	3.567E+00	+/-	8.0	9.441E-01	+/-	4.0	2.076E+00	+/-	8.0
130	1.733E+00	+/-	2.0	1.713E+00	+/-	6.0	3.648E+00	+/-	8.0	1.839E+00	+/-	6.0	3.202E+00	+/-	11.0
131	2.875E+00	+/-	0.50	3.209E+00	+/-	0.70	4.098E+00	+/-	2.80	3.232E+00	+/-	1.40	4.050E+00	+/-	2.0
132	4.282E+00	+/-	0.35	4.651E+00	+/-	0.70	4.883E+00	+/-	2.80	5.137E+00	+/-	1.40	4.846E+00	+/-	1.40
133	6.654E+00	+/-	0.35	6.716E+00	+/-	0.50	5.587E+00	+/-	6.0	6.748E+00	+/-	0.50	6.125E+00	+/-	2.0
134	7.780E+00	+/-	0.50	7.641E+00	+/-	0.50	5.729E+00	+/-	2.80	7.845E+00	+/-	2.0	6.547E+00	+/-	2.0
135	6.492E+00	+/-	0.35	6.565E+00	+/-	0.70	5.456E+00	+/-	4.0	6.950E+00	+/-	0.70	5.890E+00	+/-	2.0
136	6.267E+00	+/-	0.35	6.216E+00	+/-	0.50	5.334E+00	+/-	4.0	6.897E+00	+/-	2.80	5.744E+00	+/-	2.0
137	6.136E+00	+/-	0.50	6.210E+00	+/-	0.35	4.924E+00	+/-	2.80	5.999E+00	+/-	0.70	4.986E+00	+/-	2.0
138	6.627E+00	+/-	0.70	6.666E+00	+/-	0.70	4.584E+00	+/-	6.0	5.694E+00	+/-	1.40	4.859E+00	+/-	2.80
139	6.235E+00	+/-	1.0	6.327E+00	+/-	0.50	4.749E+00	+/-	4.0	5.630E+00	+/-	1.0	5.046E+00	+/-	2.80
140	6.134E+00	+/-	0.70	5.949E+00	+/-	0.70	4.493E+00	+/-	2.80	5.813E+00	+/-	0.70	4.619E+00	+/-	1.40
141	5.711E+00	+/-	1.0	5.891E+00	+/-	1.40	4.490E+00	+/-	4.0	5.404E+00	+/-	2.0	4.357E+00	+/-	2.80
142	5.733E+00	+/-	0.70	5.510E+00	+/-	1.0	4.248E+00	+/-	6.0	4.564E+00	+/-	1.0	4.100E+00	+/-	4.0
143	5.945E+00	+/-	0.35	5.715E+00	+/-	0.50	3.827E+00	+/-	2.80	4.584E+00	+/-	0.70	3.933E+00	+/-	2.80
144	5.443E+00	+/-	0.35	5.265E+00	+/-	0.70	3.147E+00	+/-	2.80	4.539E+00	+/-	0.70	3.655E+00	+/-	2.80
145	3.910E+00	+/-	0.35	3.765E+00	+/-	0.50	2.732E+00	+/-	6.0	3.776E+00	+/-	0.70	3.014E+00	+/-	4.0
146	2.977E+00	+/-	0.35	2.915E+00	+/-	0.50	2.235E+00	+/-	11.0	3.415E+00	+/-	0.70	2.094E+00	+/-	11.0
147	2.218E+00	+/-	0.50	2.120E+00	+/-	0.70	1.626E+00	+/-	4.0	2.542E+00	+/-	1.0	2.094E+00	+/-	2.0
148	1.657E+00	+/-	0.35	1.679E+00	+/-	0.35	1.218E+00	+/-	11.0	2.090E+00	+/-	0.70	1.759E+00	+/-	16.0
149	1.054E+00	+/-	1.0	1.031E+00	+/-	0.70	6.602E-01	+/-	8.0	1.613E+00	+/-	1.0	1.427E+00	+/-	6.0
150	6.434E-01	+/-	0.50	6.839E-01	+/-	0.50	5.183E-01	+/-	11.0	1.263E+00	+/-	1.0	1.099E+00	+/-	16.0
151	4.052E-01	+/-	0.70	4.110E-01	+/-	0.70	3.623E-01	+/-	8.0	8.017E-01	+/-	1.40	8.144E-01	+/-	6.0
152	2.587E-01	+/-	1.0	2.758E-01	+/-	2.0	2.621E-01	+/-	11.0	5.235E-01	+/-	1.0	5.888E-01	+/-	16.0
153	1.480E-01	+/-	2.80	1.602E-01	+/-	2.80	2.070E-01	+/-	11.0	3.818E-01	+/-	2.0	3.938E-01	+/-	6.0
154	7.225E-02	+/-	1.0	7.438E-02	+/-	4.0	8.137E-02	+/-	11.0	2.143E-01	+/-	1.0	2.564E-01	+/-	16.0
155	2.935E-02	+/-	4.0	4.043E-02	+/-	11.0	6.480E-02	+/-	11.0	1.278E-01	+/-	16.0	1.579E-01	+/-	16.0
156	1.341E-02	+/-	2.80	2.027E-02	+/-	2.80	5.378E-02	+/-	2.80	6.728E-02	+/-	2.0	1.093E-01	+/-	2.80
157	5.162E-03	+/-	8.0	6.766E-03	+/-	16.0	3.837E-02	+/-	11.0	3.714E-02	+/-	16.0	8.379E-02	+/-	16.0
158	1.989E-03	+/-	16.0	6.208E-03	+/-	16.0	2.389E-02	+/-	11.0	1.660E-02	+/-	16.0	4.334E-02	+/-	16.0
159	8.893E-04	+/-	6.0	2.756E-03	+/-	11.0	1.225E-02	+/-	8.0	7.158E-03	+/-	16.0	2.635E-02	+/-	11.0
160	1.146E-04	+/-	32.0	1.083E-03	+/-	16.0	7.301E-03	+/-	11.0	3.047E-03	+/-	23.0	1.594E-02	+/-	16.0
161	7.845E-05	+/-	4.0	3.241E-04	+/-	8.0	5.167E-03	+/-	8.0	1.154E-03	+/-	8.0	8.340E-03	+/-	4.0
162	6.909E-06	+/-	32.0	5.392E-05	+/-	23.0	2.832E-03	+/-	11.0	2.751E-04	+/-	32.0	6.040E-03	+/-	16.0
163	2.778E-06	+/-	32.0	8.991E-06	+/-	23.0	1.613E-03	+/-	11.0	1.649E-04	+/-	32.0	3.453E-03	+/-	16.0
164	8.708E-07	+/-	32.0	5.401E-06	+/-	23.0	9.931E-04	+/-	11.0	1.007E-04	+/-	32.0	2.027E-03	+/-	16.0
165	6.578E-07	+/-	23.0	2.158E-06	+/-	23.0	5.471E-04	+/-	11.0	6.574E-05	+/-	23.0	1.116E-03	+/-	16.0
166	2.920E-07	+/-	23.0	8.957E-07	+/-	23.0	2.780E-04	+/-	8.0	4.579E-05	+/-	32.0	6.349E-04	+/-	8.0
167	1.675E-07	+/-	23.0	3.590E-07	+/-	23.0	1.885E-04	+/-	11.0	3.904E-05	+/-	16.0	3.753E-04	+/-	16.0
168	3.825E-08	+/-	23.0	8.991E-08	+/-	23.0	1.084E-04	+/-	11.0	2.292E-05	+/-	32.0	2.035E-04	+/-	16.0
169	1.565E-08	+/-	23.0	5.394E-08	+/-	23.0	7.901E-05	+/-	8.0	1.375E-05	+/-	32.0	1.305E-04	+/-	8.0
170	3.281E-09	+/-	23.0	1.805E-08	+/-	23.0	3.299E-05	+/-	11.0	8.235E-06	+/-	32.0	6.058E-05	+/-	16.0
171	1.565E-09	+/-	23.0	6.269E-09	+/-	23.0	1.794E-05	+/-	11.0	4.611E-06	+/-	32.0	3.358E-05	+/-	16.0
172	5.397E-10	+/-	23.0	1.792E-09	+/-	23.0	1.662E-05	+/-	8.0	8.606E-06	+/-	32.0	2.161E-05	+/-	16.0

TABLE XXIII (Cont.)

MASS	PU239T	PU239F	PU241T	U233T	TH232F
66	1.877E-07 +/- 23.0	8.183E-07 +/- 16.0	1.370E-07 +/- 23.0	2.602E-07 +/- 23.0	1.184E-06 +/- 32.0
67	3.754E-07 +/- 23.0	2.699E-06 +/- 16.0	2.545E-07 +/- 23.0	1.179E-06 +/- 23.0	4.077E-06 +/- 32.0
68	1.313E-06 +/- 23.0	7.929E-06 +/- 16.0	5.874E-07 +/- 23.0	3.629E-06 +/- 23.0	1.494E-05 +/- 32.0
69	4.690E-06 +/- 23.0	2.941E-05 +/- 16.0	1.273E-06 +/- 23.0	9.980E-06 +/- 23.0	3.450E-05 +/- 32.0
70	1.591E-05 +/- 23.0	8.133E-05 +/- 16.0	4.604E-06 +/- 23.0	3.913E-05 +/- 23.0	6.752E-05 +/- 23.0
71	2.899E-05 +/- 23.0	1.770E-04 +/- 32.0	6.853E-06 +/- 23.0	1.724E-04 +/- 23.0	1.715E-04 +/- 23.0
72	9.726E-05 +/- 45.0	4.529E-04 +/- 32.0	2.545E-05 +/- 23.0	4.986E-04 +/- 23.0	4.247E-04 +/- 16.0
73	2.365E-04 +/- 23.0	7.006E-04 +/- 23.0	5.909E-05 +/- 16.0	1.086E-03 +/- 23.0	6.519E-04 +/- 16.0
74	5.477E-04 +/- 32.0	1.633E-03 +/- 16.0	9.790E-05 +/- 23.0	2.722E-03 +/- 23.0	1.179E-03 +/- 16.0
75	1.277E-03 +/- 32.0	2.332E-03 +/- 23.0	2.937E-04 +/- 23.0	8.159E-03 +/- 23.0	2.898E-03 +/- 16.0
76	2.828E-03 +/- 32.0	5.453E-03 +/- 16.0	9.791E-04 +/- 23.0	1.452E-02 +/- 23.0	6.890E-03 +/- 16.0
77	6.686E-03 +/- 11.0	1.207E-02 +/- 8.0	1.958E-03 +/- 23.0	2.601E-02 +/- 23.0	1.159E-02 +/- 8.0
78	2.752E-02 +/- 11.0	2.808E-02 +/- 16.0	8.973E-03 +/- 6.0	5.444E-02 +/- 23.0	4.559E-02 +/- 8.0
79	4.667E-02 +/- 23.0	5.929E-02 +/- 8.0	1.536E-02 +/- 16.0	1.502E-01 +/- 11.0	7.818E-02 +/- 11.0
80	1.147E-01 +/- 16.0	9.745E-02 +/- 16.0	2.991E-02 +/- 16.0	2.359E-01 +/- 23.0	1.985E-01 +/- 16.0
81	1.713E-01 +/- 16.0	1.346E-01 +/- 11.0	6.355E-02 +/- 16.0	3.670E-01 +/- 4.0	4.773E-01 +/- 11.0
82	2.061E-01 +/- 23.0	2.103E-01 +/- 8.0	1.380E-01 +/- 8.0	5.855E-01 +/- 2.80	1.100E+00 +/- 16.0
83	2.967E-01 +/- 0.70	3.108E-01 +/- 2.0	2.016E-01 +/- 2.0	1.014E+00 +/- 1.0	2.175E+00 +/- 2.0
84	4.724E-01 +/- 2.0	4.923E-01 +/- 1.40	3.526E-01 +/- 2.0	1.688E+00 +/- 1.0	3.992E+00 +/- 2.0
85	5.753E-01 +/- 0.50	6.016E-01 +/- 1.0	4.068E-01 +/- 1.40	2.227E+00 +/- 1.0	4.158E+00 +/- 1.40
86	7.647E-01 +/- 0.70	7.805E-01 +/- 1.40	5.960E-01 +/- 2.0	2.848E+00 +/- 1.40	6.553E+00 +/- 2.0
87	9.990E-01 +/- 0.70	1.023E+00 +/- 1.40	7.575E-01 +/- 2.0	4.034E+00 +/- 1.40	6.934E+00 +/- 2.80
88	1.342E+00 +/- 1.40	1.323E+00 +/- 1.40	9.788E-01 +/- 2.0	5.459E+00 +/- 1.40	7.291E+00 +/- 2.0
89	1.691E+00 +/- 2.80	1.727E+00 +/- 2.0	1.221E+00 +/- 4.0	6.335E+00 +/- 2.0	7.559E+00 +/- 4.0
90	2.082E+00 +/- 2.0	2.032E+00 +/- 1.0	1.539E+00 +/- 2.0	6.838E+00 +/- 1.40	7.968E+00 +/- 4.0
91	2.488E+00 +/- 1.0	2.499E+00 +/- 1.40	1.871E+00 +/- 2.0	6.551E+00 +/- 1.0	7.385E+00 +/- 2.0
92	3.003E+00 +/- 1.40	3.014E+00 +/- 1.0	2.333E+00 +/- 2.0	6.542E+00 +/- 1.40	6.852E+00 +/- 2.80
93	3.840E+00 +/- 1.40	3.811E+00 +/- 1.0	2.986E+00 +/- 2.0	6.953E+00 +/- 1.40	6.786E+00 +/- 4.0
94	4.340E+00 +/- 2.0	4.199E+00 +/- 1.0	3.430E+00 +/- 2.0	6.797E+00 +/- 1.40	5.713E+00 +/- 6.0
95	4.878E+00 +/- 2.0	4.670E+00 +/- 1.0	3.963E+00 +/- 2.0	6.347E+00 +/- 1.40	5.665E+00 +/- 2.80
96	4.956E+00 +/- 2.80	4.811E+00 +/- 1.0	4.431E+00 +/- 2.0	5.635E+00 +/- 1.0	4.444E+00 +/- 6.0
97	5.340E+00 +/- 2.0	5.318E+00 +/- 0.70	4.698E+00 +/- 2.0	5.498E+00 +/- 1.40	4.465E+00 +/- 1.40
98	5.894E+00 +/- 2.0	5.653E+00 +/- 1.0	4.977E+00 +/- 2.0	5.175E+00 +/- 1.40	3.709E+00 +/- 6.0
99	6.169E+00 +/- 2.0	5.956E+00 +/- 2.0	6.077E+00 +/- 2.0	4.877E+00 +/- 2.0	2.961E+00 +/- 2.0
100	6.819E+00 +/- 4.0	6.556E+00 +/- 0.70	6.272E+00 +/- 2.0	4.379E+00 +/- 1.40	1.382E+00 +/- 6.0
101	5.997E+00 +/- 1.40	6.653E+00 +/- 1.0	6.286E+00 +/- 2.0	3.168E+00 +/- 1.40	7.249E-01 +/- 11.0
102	6.075E+00 +/- 2.0	6.706E+00 +/- 1.0	6.658E+00 +/- 2.0	2.404E+00 +/- 1.40	3.737E-01 +/- 11.0
103	6.947E+00 +/- 2.0	6.846E+00 +/- 1.0	6.739E+00 +/- 4.0	1.593E+00 +/- 2.0	1.565E-01 +/- 4.0
104	6.017E+00 +/- 2.0	6.535E+00 +/- 1.0	7.099E+00 +/- 2.0	9.755E-01 +/- 2.80	9.175E-02 +/- 11.0
105	5.586E+00 +/- 2.0	5.344E+00 +/- 2.80	6.254E+00 +/- 2.80	4.939E-01 +/- 2.80	5.180E-02 +/- 2.80
106	4.328E+00 +/- 2.80	4.362E+00 +/- 1.40	6.127E+00 +/- 2.0	2.453E-01 +/- 2.0	5.320E-02 +/- 8.0
107	3.265E+00 +/- 6.0	2.957E+00 +/- 8.0	5.145E+00 +/- 11.0	1.131E-01 +/- 4.0	5.189E-02 +/- 11.0
108	2.115E+00 +/- 6.0	1.927E+00 +/- 8.0	3.599E+00 +/- 11.0	7.287E-02 +/- 6.0	6.272E-02 +/- 16.0
109	1.699E+00 +/- 8.0	1.590E+00 +/- 6.0	2.259E+00 +/- 6.0	4.326E-02 +/- 8.0	5.252E-02 +/- 6.0
110	6.279E-01 +/- 6.0	6.213E-01 +/- 8.0	1.340E+00 +/- 8.0	3.713E-02 +/- 4.0	7.259E-02 +/- 16.0
111	2.935E-01 +/- 2.80	3.547E-01 +/- 2.0	5.704E-01 +/- 4.0	1.944E-02 +/- 8.0	7.451E-02 +/- 6.0
112	1.229E-01 +/- 2.80	1.903E-01 +/- 2.80	2.366E-01 +/- 4.0	1.381E-02 +/- 8.0	8.004E-02 +/- 6.0
113	7.979E-02 +/- 4.0	1.268E-01 +/- 2.0	1.545E-01 +/- 6.0	1.312E-02 +/- 8.0	8.034E-02 +/- 4.0
114	5.877E-02 +/- 4.0	9.366E-02 +/- 2.0	7.342E-02 +/- 23.0	1.251E-02 +/- 8.0	7.507E-02 +/- 16.0
115	3.687E-02 +/- 4.0	7.017E-02 +/- 6.0	4.481E-02 +/- 16.0	1.258E-02 +/- 6.0	5.781E-02 +/- 4.0
116	4.840E-02 +/- 8.0	5.896E-02 +/- 6.0	2.913E-02 +/- 32.0	1.313E-02 +/- 11.0	7.362E-02 +/- 16.0
117	4.825E-02 +/- 8.0	6.859E-02 +/- 11.0	2.547E-02 +/- 23.0	1.204E-02 +/- 8.0	5.916E-02 +/- 2.80
118	3.933E-02 +/- 11.0	6.159E-02 +/- 11.0	2.428E-02 +/- 32.0	1.261E-02 +/- 8.0	6.298E-02 +/- 11.0
119	4.028E-02 +/- 11.0	5.966E-02 +/- 11.0	2.428E-02 +/- 32.0	1.293E-02 +/- 8.0	5.703E-02 +/- 16.0

TABLE XXIII (Cont.)

MASS	PU239T	PU239F	PU241T	U233T	TH232F
120	3.613E-02 +/- 11.0	5.657E-02 +/- 11.0	2.618E-02 +/- 23.0	1.425E-02 +/- 8.0	5.416E-02 +/- 16.0
121	3.730E-02 +/- 8.0	6.161E-02 +/- 11.0	2.667E-02 +/- 32.0	1.554E-02 +/- 11.0	4.728E-02 +/- 6.0
122	5.472E-02 +/- 11.0	7.256E-02 +/- 11.0	2.668E-02 +/- 32.0	1.528E-02 +/- 11.0	3.642E-02 +/- 16.0
123	4.011E-02 +/- 23.0	7.310E-02 +/- 16.0	2.773E-02 +/- 32.0	1.905E-02 +/- 32.0	2.926E-02 +/- 16.0
124	1.003E-01 +/- 11.0	1.235E-01 +/- 11.0	3.308E-02 +/- 32.0	2.520E-02 +/- 11.0	2.639E-02 +/- 16.0
125	1.131E-01 +/- 8.0	1.345E-01 +/- 8.0	4.905E-02 +/- 8.0	1.103E-01 +/- 11.0	3.360E-02 +/- 11.0
126	2.549E-01 +/- 8.0	2.863E-01 +/- 8.0	8.294E-02 +/- 16.0	2.518E-01 +/- 16.0	4.795E-02 +/- 16.0
127	4.981E-01 +/- 6.0	5.107E-01 +/- 8.0	2.333E-01 +/- 4.0	5.585E-01 +/- 11.0	7.551E-02 +/- 6.0
128	6.939E-01 +/- 11.0	8.923E-01 +/- 6.0	3.876E-01 +/- 23.0	8.098E-01 +/- 11.0	1.821E-01 +/- 16.0
129	1.387E+00 +/- 4.0	1.495E+00 +/- 6.0	8.381E-01 +/- 23.0	1.616E+00 +/- 16.0	2.824E-01 +/- 4.0
130	2.049E+00 +/- 16.0	2.372E+00 +/- 8.0	1.839E+00 +/- 11.0	2.165E+00 +/- 23.0	8.084E-01 +/- 16.0
131	3.874E+00 +/- 0.50	3.885E+00 +/- 0.70	3.091E+00 +/- 1.40	3.495E+00 +/- 1.0	1.615E+00 +/- 2.0
132	5.420E+00 +/- 0.70	5.323E+00 +/- 1.0	4.563E+00 +/- 1.40	4.799E+00 +/- 1.40	2.898E+00 +/- 1.40
133	7.019E+00 +/- 0.70	6.951E+00 +/- 0.70	6.736E+00 +/- 1.0	6.043E+00 +/- 1.0	3.944E+00 +/- 2.0
134	7.666E+00 +/- 0.70	7.389E+00 +/- 0.70	7.921E+00 +/- 1.40	6.133E+00 +/- 1.0	5.351E+00 +/- 2.0
135	7.610E+00 +/- 0.70	7.561E+00 +/- 0.70	7.243E+00 +/- 1.40	6.163E+00 +/- 2.0	5.491E+00 +/- 2.0
136	7.182E+00 +/- 1.0	7.040E+00 +/- 1.40	7.117E+00 +/- 1.40	6.865E+00 +/- 4.0	5.623E+00 +/- 2.0
137	6.685E+00 +/- 0.50	6.581E+00 +/- 0.70	6.720E+00 +/- 1.40	6.818E+00 +/- 0.70	5.800E+00 +/- 4.0
138	6.102E+00 +/- 1.40	6.129E+00 +/- 1.0	6.599E+00 +/- 2.0	5.906E+00 +/- 2.0	7.021E+00 +/- 11.0
139	5.534E+00 +/- 4.0	5.602E+00 +/- 1.40	6.231E+00 +/- 2.0	6.292E+00 +/- 4.0	7.146E+00 +/- 2.0
140	5.378E+00 +/- 1.0	5.293E+00 +/- 0.70	5.732E+00 +/- 2.0	6.515E+00 +/- 1.40	7.815E+00 +/- 2.0
141	5.299E+00 +/- 2.0	5.091E+00 +/- 2.80	4.892E+00 +/- 1.40	6.525E+00 +/- 2.80	7.320E+00 +/- 2.80
142	4.894E+00 +/- 1.0	4.803E+00 +/- 0.70	4.784E+00 +/- 1.40	6.694E+00 +/- 1.40	6.495E+00 +/- 4.0
143	4.442E+00 +/- 0.50	4.349E+00 +/- 0.50	4.590E+00 +/- 1.40	5.942E+00 +/- 1.0	6.588E+00 +/- 2.0
144	3.744E+00 +/- 0.50	3.692E+00 +/- 1.0	4.209E+00 +/- 1.0	4.671E+00 +/- 1.0	7.893E+00 +/- 2.80
145	2.997E+00 +/- 0.50	3.007E+00 +/- 0.50	3.269E+00 +/- 1.40	3.428E+00 +/- 1.0	5.287E+00 +/- 2.80
146	2.466E+00 +/- 0.50	2.457E+00 +/- 0.70	2.789E+00 +/- 1.40	2.569E+00 +/- 0.70	4.539E+00 +/- 2.80
147	2.027E+00 +/- 1.40	1.986E+00 +/- 1.0	2.285E+00 +/- 1.40	1.746E+00 +/- 2.80	2.926E+00 +/- 4.0
148	1.639E+00 +/- 0.50	1.654E+00 +/- 0.35	1.938E+00 +/- 1.0	1.289E+00 +/- 1.0	1.992E+00 +/- 2.80
149	1.226E+00 +/- 1.0	1.240E+00 +/- 0.70	1.476E+00 +/- 1.40	7.731E-01 +/- 2.80	1.059E+00 +/- 6.0
150	9.677E-01 +/- 0.50	9.922E-01 +/- 0.70	1.216E+00 +/- 1.40	5.066E-01 +/- 1.40	3.471E-01 +/- 16.0
151	7.545E-01 +/- 2.0	7.644E-01 +/- 1.40	9.134E-01 +/- 1.40	3.138E-01 +/- 2.0	3.551E-01 +/- 6.0
152	5.795E-01 +/- 1.40	5.977E-01 +/- 2.80	7.192E-01 +/- 1.40	2.124E-01 +/- 2.80	7.527E-02 +/- 16.0
153	3.502E-01 +/- 6.0	4.191E-01 +/- 4.0	5.411E-01 +/- 4.0	9.735E-02 +/- 6.0	6.443E-02 +/- 8.0
154	2.657E-01 +/- 1.40	2.619E-01 +/- 2.0	3.802E-01 +/- 2.0	4.641E-02 +/- 2.80	6.842E-03 +/- 23.0
155	1.593E-01 +/- 11.0	2.023E-01 +/- 11.0	2.422E-01 +/- 8.0	2.141E-02 +/- 23.0	3.598E-03 +/- 23.0
156	1.188E-01 +/- 2.80	1.434E-01 +/- 4.0	1.719E-01 +/- 2.80	1.153E-02 +/- 6.0	2.541E-03 +/- 11.0
157	7.258E-02 +/- 6.0	1.039E-01 +/- 8.0	1.353E-01 +/- 4.0	5.313E-03 +/- 8.0	9.271E-04 +/- 23.0
158	3.737E-02 +/- 23.0	6.232E-02 +/- 16.0	9.426E-02 +/- 23.0	2.260E-03 +/- 32.0	4.611E-04 +/- 32.0
159	1.974E-02 +/- 6.0	3.691E-02 +/- 11.0	4.800E-02 +/- 4.0	7.773E-04 +/- 6.0	9.699E-05 +/- 32.0
160	8.549E-03 +/- 32.0	2.228E-02 +/- 16.0	2.095E-02 +/- 23.0	3.175E-04 +/- 32.0	6.868E-05 +/- 32.0
161	4.681E-03 +/- 6.0	7.984E-03 +/- 4.0	8.464E-03 +/- 4.0	1.113E-04 +/- 6.0	1.440E-05 +/- 23.0
162	2.126E-03 +/- 32.0	5.602E-03 +/- 23.0	2.723E-03 +/- 23.0	1.527E-05 +/- 32.0	7.929E-06 +/- 32.0
163	8.594E-04 +/- 32.0	2.539E-03 +/- 45.0	9.824E-04 +/- 23.0	7.142E-06 +/- 32.0	4.611E-06 +/- 32.0
164	3.243E-04 +/- 32.0	1.566E-03 +/- 45.0	3.152E-04 +/- 23.0	2.351E-06 +/- 32.0	2.021E-06 +/- 32.0
165	1.284E-04 +/- 23.0	8.150E-04 +/- 32.0	9.845E-05 +/- 23.0	7.450E-07 +/- 23.0	3.512E-07 +/- 23.0
166	6.387E-05 +/- 16.0	5.899E-04 +/- 32.0	6.598E-05 +/- 23.0	4.524E-07 +/- 32.0	1.372E-07 +/- 32.0
167	1.758E-05 +/- 32.0	2.574E-04 +/- 32.0	2.985E-05 +/- 23.0	6.323E-08 +/- 32.0	9.701E-08 +/- 32.0
168	4.915E-06 +/- 32.0	7.365E-05 +/- 32.0	1.361E-05 +/- 23.0	1.627E-08 +/- 32.0	5.262E-08 +/- 32.0
169	1.666E-06 +/- 32.0	2.481E-05 +/- 32.0	5.760E-06 +/- 23.0	5.515E-09 +/- 32.0	2.672E-08 +/- 32.0
170	3.499E-07 +/- 64.0	7.271E-06 +/- 32.0	1.676E-06 +/- 23.0	1.638E-09 +/- 32.0	1.061E-08 +/- 32.0
171	1.672E-07 +/- 32.0	2.478E-06 +/- 32.0	3.142E-07 +/- 23.0	5.429E-10 +/- 32.0	4.611E-09 +/- 32.0
172	4.934E-08 +/- 32.0	7.367E-07 +/- 32.0	1.047E-07 +/- 23.0	1.808E-10 +/- 32.0	2.371E-09 +/- 32.0

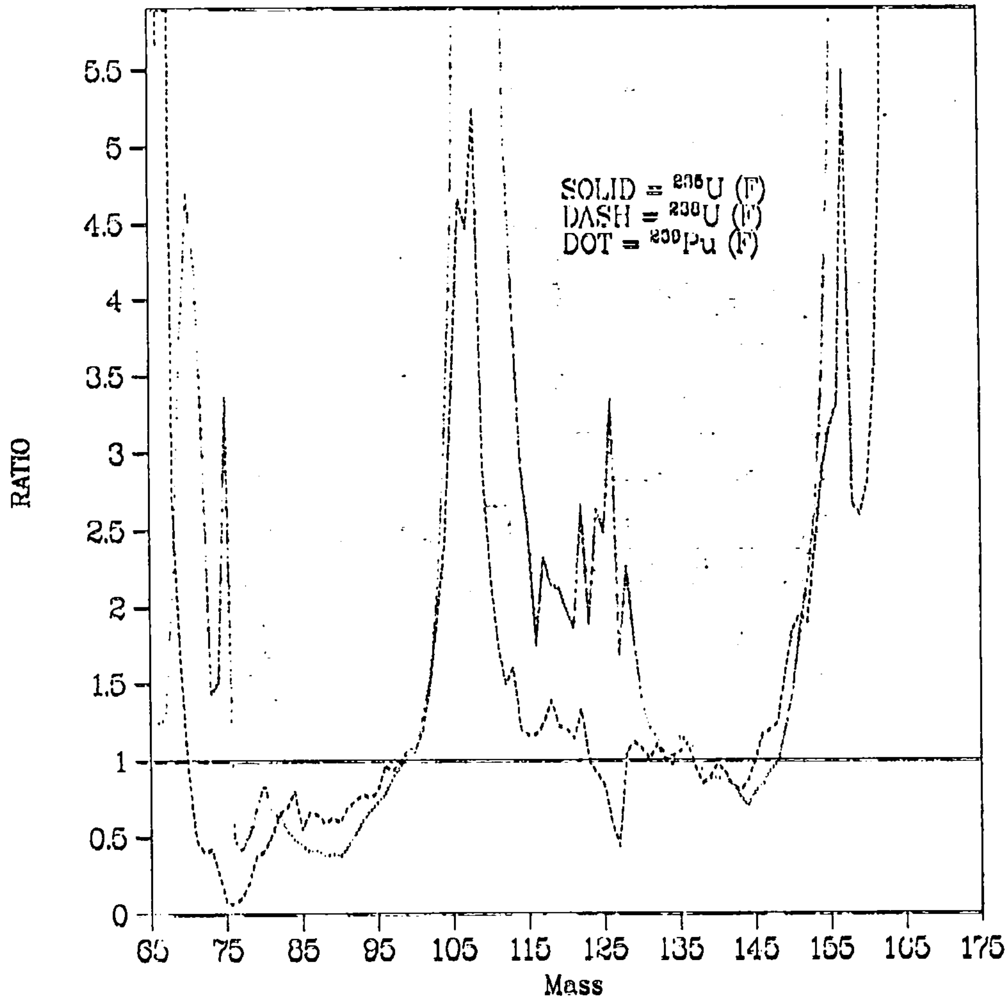

Fig. 50. Ratio of ^{238}U(F) and ^{239}Pu(F) chain yields to ^{235}U(F) (Ver. E).

C. Delayed Neutron Spectra and Pn Values [T. R. England, W. B. Wilson, (F. M. Mann, and R. E. Schenter, Hanford Engineering Development Laboratory)]

1. Spectra.

Delayed neutron spectra can now be calculated using fission-product yields, precursor emission probabilities, and individual nuclide emission spectra. Some results presented in the last progress report have been revised and are now published.[95] These results are based on ENDF/B-V fission yield data and the Pn values in Ref. 96. These spectra, subject to some minor changes, are expected to replace the integral evaluations now in ENDF/B-V.

2. Pn Values.

Since the publication of Ref. 2, the Pn values have been reevaluated[97] and recently submitted for <u>Nuclear Science and Engineering</u> publication. Preliminary $\bar{\nu}_d$ values using the revised Pn values and revised fission yields are listed in the previous section. The reader should note the small value calculated for ^{238}U fast fission. This is apparently due to an excessively large even-odd Z-pairing (~ 32%) used in the evaluation of fission yields. All pairing values used in the yield evaluations are listed in Table XXIV. Recent measured data suggest the pairing effect should have been the same as for ^{235}U fast fission (15%). In fact, this pairing does increase the calculated $\bar{\nu}_d$ to 4.04 ± 0.4 per 100 fissions in agreement within the uncertainty with the ENDF/B-V integral evaluation. Figure 51 shows the effect of pairing on mass chain yields for three incident neutron energies.

It should be understood that accurate calculations of $\bar{\nu}_d$ require extremely accurate values of precursor yields and Pn values, whereas the ENDF/B spectra, being normalized, do not require the same accuracy. Therefore we use the calculated $\bar{\nu}_d$ values primarily as a rough test of the quality of the yields and Pn values. The normalized spectra, however, are clearly better than the limited measured values for reasons described in Ref. 95.

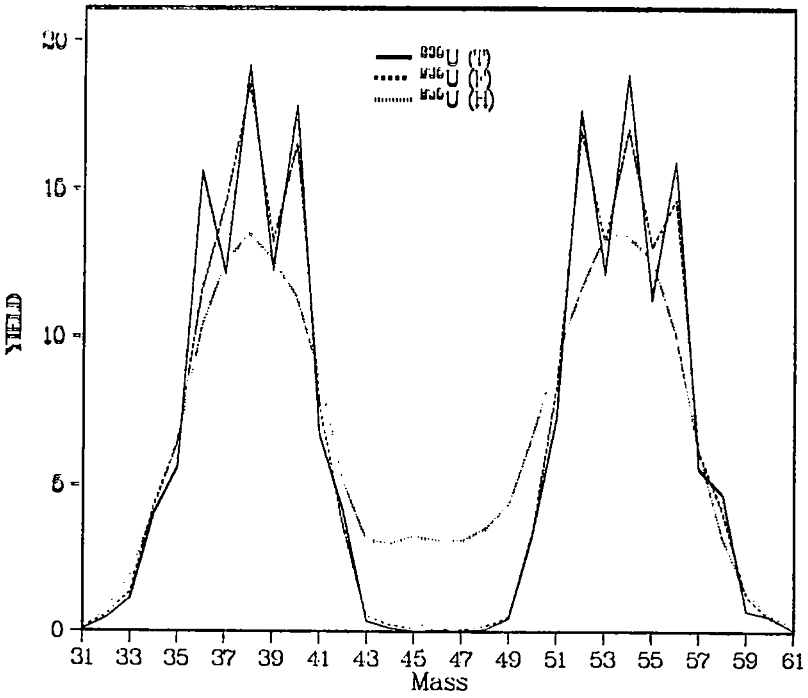

Fig. 51. Sum of direct yields by charge.

TABLE XXIV

PAIRING EFFECTS USED IN EVALUATION[a]

NUCLIDE	PROTON EFFECT,X	NEUTRON EFFECT,Y
U235T	0.228 +/- 0.034	0.044 +/- 0.034
U235F	0.151 +/- 0.179	0.029 +/- 0.039
U235HE	0.015 +/- 0.016	0.003 +/- 0.004
U238F	0.329 +/- 0.479	0.063 +/- 0.100
U238HE	0.018 +/- 0.019	0.003 +/- 0.004
PU239T	0.171 +/- 0.206	0.033 +/- 0.044
PU239F	0.124 +/- 0.143	0.024 +/- 0.031
PU241T	0.206 +/- 0.256	0.040 +/- 0.055
U233T	0.210 +/- 0.264	0.041 +/- 0.056
TH232F	0.327 +/- 0.469	0.063 +/- 0.098
U233F	0.143 +/- 0.168	0.028 +/- 0.037
U233HE	0.015 +/- 0.016	0.003 +/- 0.004
U236F	0.166 +/- 0.200	0.032 +/- 0.043
PU239H	0.015 +/- 0.016	0.003 +/- 0.004
PU240F	0.244 +/- 0.321	0.047 +/- 0.021
PU241F	0.141 +/- 0.166	0.027 +/- 0.036
PU242F	0.364 +/- 0.554	0.070 +/- 0.114
TH232H	0.018 +/- 0.019	0.003 +/- 0.004
NP237F	0	0
CF252S	0.050 +/- 0.040	0.010 +/- 0.040
U234F	0.079 +/- 0.089	0.015 +/- 0.020
U237F	0.102 +/- 0.116	0.020 +/- 0.024
PU240H	0.117 +/- 0.132	0.023 +/- 0.030
U234HE	0.016 +/- 0.018	0.003 +/- 0.005
U236HE	0.017 +/- 0.019	0.003 +/- 0.004
PU238F	0	0
AM241F	0	0
AM243F	0	0
NP238F	0	0
CM242F	0.067 +/- 0.074	0.013 +/- 0.016
TH227T	0	0
TH229T	0.274 +/- 0.301	0.053 +/- 0.058
PA231F	0	0
AM241T	0	0
AM241H	0	0
A242MT	0	0
CM245T	0	0
CM249T	0.109 +/- 0.120	0.021 +/- 0.023
CF251T	0	0
ES254T	0	0
CF250S	0	0
CM244S	0	0
CM248S	0	0
ES253S	0	0
FM254S	0	0
FM255T	0	0
FM256S	0	0
NP237H	0	0
U232T	0	0
U238S	0	0

[a] X = fractional change in model estimated yields based on the product charge. Y = fractional change due to neutron pairing. The effect is positive for even pairing and negative for odd pairing.

D. Development of CINDER-3 Depletion Package [W. B. Wilson, T. R. England, R. J. LaBauve, R. E. Schenter (HEDL)]

Our recent activities in local utilization of 2- and 3-dimensional diffusion and transport codes in fast-reactor physics calculations have resulted in the formation of the versatile fuel depletion package CINDER-3. This code may be coupled to any reactor physics code that provides initial nuclide atom densities, energy group fluxes, and resonance self-shielded group cross sections for abundant nuclides in each spatial region. The package returns end-of-time step atom densities of explicit nuclides and lumped nonexplicit fission-product and actinide quantities for use in a subsequent reactor physics calculation. These lumped quantities, accumulated separately for nonexplicit fission products and actinides, include atom densities and group cross sections for (n,n), (n,n'), (n,2n), (n,γ), and total neutron absorption in an arbitrary user's group structure.

The code package, shown schematically in Fig. 52, combines the functions of the CINDER-2[98] nuclide inventory code and its ENDF/B-V-based data library[99] with the TOAFEW-V[100] collapsing code and library of processed ENDF/B-V 154-group cross sections augmented with (n,2n) cross sections from model calculations at HEDL. All calculations use the chain library, giving the basic nuclear data describing the various nuclide couplings by fission yield, radioactive decay, and neutron absorption. Inventories within each region at the end of a time step (EOS) are calculated using the energy group fluxes, nuclide atom densities, and group cross sections associated with the region at the beginning of the time step (BOS). Cumulative calculated EOS results (exposure, burnup, atom densities, cross sections, etc.) are sequentially recorded for each region. Region atom densities are initialized with values supplied in the initial call for the region; thereafter, region BOS atom densities are taken from the previously recorded EOS region data. Region cross sections are supplied in the following heirarchy: (a) previous EOS cross-section values, if other than the first call for this region; (b) collapse of 154-group data with user-supplied multigroup weighting flux, if requested, by AFEW--a modified version of TOAFEW-V; and (c) explicit nuclide self-shielded values provided in the call.

CINDER-3 follows fission products yielded by the neutron-induced and/or spontaneous fission of 31 actinides initially present and/or produced within the fuel. Fission rates are calculated with the average of BOS and EOS actinide atom densities. Thermal, fast, or high-energy neutron-induced fission yields may be selected by the user. These yields were taken from ENDF/B-V yield sets using surrogate yield sets where necessary.

Cray 1S region inventory calculations with the package, using 8 energy groups and 80-group weighting spectra, have required 1-5 s per call. Ancillary calculations of decay power, decay spectra, or other grouped nuclide properties may be performed with other codes using summarized regional outputs.

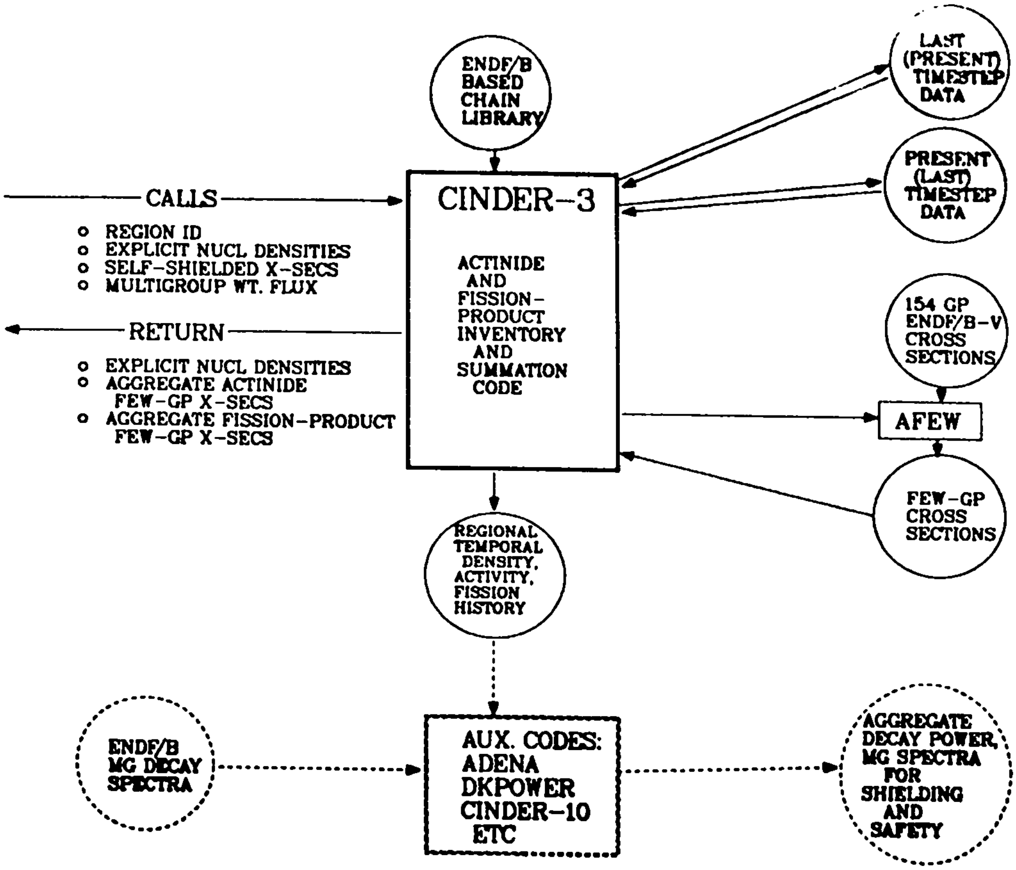

Fig. 52. Schematic of CINDER-3 depletion.

E. DKPOWR Code Development (W. B. Wilson, T. R. England, R. J. LaBauve, and D. C. George)

The DKPOWR code was first developed to combine exponential pulse-function expressions for fission-product decay power with calculated fission histories to determine total fission-product decay power following fuel irradiation.[101] The code used decay power pulse functions fit to CINDER-10 ENDF/B-IV summation calculations[102] or fits to combinations of calculated and measured decay power data for ^{235}U and ^{239}Pu as incorporated in the ANSI/ANS-5.1-1979 Standard for Decay Heat Power in Light Water Reactors.[103] These functions were restricted to ^{235}U thermal fission, ^{238}U fast fission, and ^{239}Pu thermal fission; the decay power from all other fissions are represented by the ^{235}U thermal fission pulse function.

DKPOWR now retains the capability of decay power calculations with the 1979 Standard, including the interpolation or extrapolation of tabular values of the upper limit neutron absorption correction G_{max}. Fission-product decay power uncertainties are calculated with pulse functions fit to tabular data of the Standard.[103] The limited actinide decay power due to ^{239}U and ^{239}Np are also calculated using an improved algorithm. Integrated fission-product and actinide decay energy from shutdown are calculated with algorithms resulting from the integration of the decay power algorithm of the Standard.

Pulse-function fits to CINDER-10 summation calculations with ENDF/B-V data of fission-product decay power, fission-product decay activity (curies), 18-group fission-product β spectra, and 19-group fission-product γ spectra have been completed. These are now included in a DKPOWR library for ^{232}Th fast fission, ^{233}U thermal fission, ^{235}U thermal fission, ^{238}U fast fission, ^{239}Pu thermal fission, and ^{241}Pu thermal fission. All other fissions, as before, are represented by the ^{235}U thermal fission pulse function unless otherwise specified.

Output of DKPOWR now includes results calculated with the ANSI/ANS-5.1-1979 Standard functions and with functions fit to CINDER-10 ENDF/B-V summation calculations. These results are tabulated as follows:*

Results of Calculations with the ANSI Standard

Table I:	Summary of input fission history, as assigned to the associated and surrogate fission pulse functions of the ANS/ANSI Standard and of the ENDF/B-V calculations.
Table II:	Fission-product decay power, uncertainties, absorption correction; limited actinide decay power.
Table III:	Fission-product and actinide decay energy.

---

*Examples of these tables may be seen in Los Alamos informal document LA-UR-84-146, W. B. Wilson, T. R. England, R. J. LaBauve, and D. C. George, "DKPOWR: A Code for the Calculation of Decay Power, Energy, Curies, and Multigroup β and γ Spectra Using Pulse Functions," to be presented at the American Nuclear Society's Annual Meeting, New Orleans, Louisiana, June 3-8, 1984.

Results of Calculations with Pulse Functions Fit to CINDER-10 Summation Calculations with ENDF/B-V Data

Table IV:	Fission-product decay power.
Table V:	Fission-product decay energy.
Table VI:	Fission-product decay activity, curies.
Table VII:	Multigroup fission-product beta decay spectra.
Table VIII:	Multigroup fission-product gamma decay spectra.

F. (α,n) Neutron Production in Boron-Containing Systems [R. T. Perry (Texas A&M University) and W. B. Wilson]

Boron is often used as a thermal reactor poison because of its large thermal neutron absorption cross section, which is due largely to the 3.8-kb (n,α) thermal cross section of ^{10}B (~ 20 at.%). Alphas produced in the (n,α) reactions, having an average energy in the range of 1.75-2 MeV, have some probability of experiencing ^{10,11}B(α,n) reactions and thus reintroducing neutrons into the system. We have performed SOURCES code[7] calculations of (α,n) neutron production probabilities P(E) for 2-MeV alphas emitted in three boron-containing systems, as summarized in Table XXV. These calculations employed alpha-particle-stopping cross-section data of Ziegler[104] and ^{NAT}B(α,n) cross-section data of Walker.[105] The P(E) value of 6.01 x 10^{-7} calculated for ^{NAT}B is lower than the 2-MeV thick-target yield of 7.6 x 10^{-7} calculated by Lisken and Paulsen,[106] probably because of the different stopping cross-section data sources used.

The (α,n) neutron production in water containing 500 ppm B is due to reactions with ^{17,18}O as well as ^{10,11}B. We have used the ^{17}O and ^{18}O cross sections from a previous evaluation,[107] which combined data of Bair and Willard,[108] Bair and Haas,[109] Bair and del Campo,[110] and Hansen et al.,[111] following the suggestions of Ombrellaro and Johnson.[112]

The alphas produced in B_4C may react with ^{13}C as well as ^{10,11}B. The ^{13}C(α,n) cross section used was taken from Bair and Haas.[109]

Of these boron-containing systems, the highest probability of a ^{10}B(n,α)-produced alpha experiencing an (α,n) reaction is calculated to be 6.1 x 10^{-7}. Thus, we conclude that the neutrons reintroduced by (α,n) reactions would have a neglibible effect on reactor physics calculations.

TABLE XXV

(α,n NEUTRON PRODUCTION BY 2-MeV ALPHAS)

	Target Component	Atom Fraction	P(E) Neutron/Alpha
Case 1			
Natural Boron	B	1	6.0147×10^{-7}
Case 2	B	2.7784×10^{-4}	2.8469×10^{-10}
Natural Boron in Water	^{17}O	1.2663×10^{-4}	6.0846×10^{-12}
(500 ppm by weight)	^{18}O	6.7981×10^{-4}	1.2429×10^{-11}
			3.0320×10^{-10}
Case 3	B	.8	4.7405×10^{-7}
B_4C	^{13}C	.00222	4.6726×10^{-10}
			4.7452×10^{-7}

IV. CORE NEUTRONICS CODE DEVELOPMENT IN SUPPORT OF LMFBR CARBIDE CORE ASSESSMENT (R. J. LaBauve, T. R. England, D. C. George, R. E. MacFarlane, and W. B. Wilson)

Los Alamos is currently involved in the assessment of carbide fuels as applied to cost-optimized and inherently safe LMFBR designs. In support of this effort, the Applied Nuclear Science Group (T-2) has been participating in the evaluation and testing of basic nuclear data, providing processed data for use in methods comparisons, and in developing a code system to be used for the neutronic calculations in the Los Alamos National Laboratory advanced core design and assessment effort. This report concerns progress made in the last of these areas, namely, the code system development.

A general layout of the code system for neutronics calculations is shown in Fig. 53. Starting with the basic nuclear data file (currently ENDF/B-V), the code system consists of a data-processing module, a core calculation module, and a depletion module. Our approach in establishing this code system in a timely manner is to use existing, proven codes in the three modules and to link them via the standard interface system.[113] The nuclear data codes and interface systems we are using have all been supported under the physics program of the Office of Breeder Reactor Technology of the Department of Energy over the past 15 years or so.

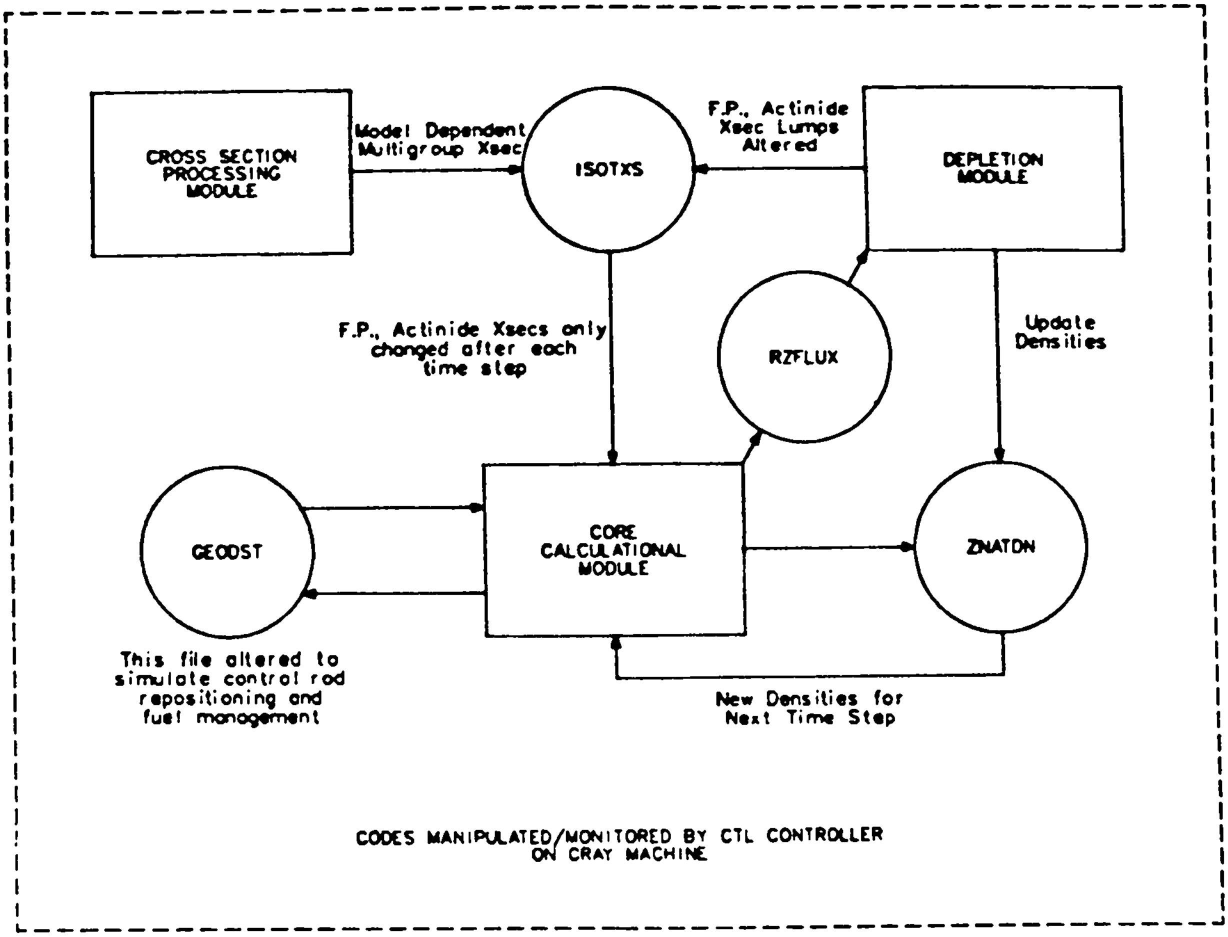

Xsec Processing - NJOY + TRANSX and Related Codes
Core Calculation - DIF3D, TWODANT, TWOHEX
Depletion - CINDER III

Fig. 53. Code system for neutronics calculations.

Non-nodal and nodal versions of the Argonne National Laboratory three-dimensional diffusion code DIF3D[87] were brought up on the Los Alamos Cray computer. These were validated by running LCCEWG benchmark problems and comparing results with those from other laboratories. The ANL depletion code REBUS-3[114] was also brought up on the Cray, but indications are that this code will have to be restructured ("overlayed") in order to run efficiently on the Cray.

The NJOY code system[73,115] was used to prepare a preliminary set of carbide LMFBR cross sections based on the CDS homogeneous carbide core.[116] The processing path used is shown in Fig. 54, and note in the figure that data were generated both in the standard interface ISOTXS format and the DTF format. The data in the DTF format were supplied to the Los Alamos Core Design Group (Q-12) for use in 2DB[117] calculations.

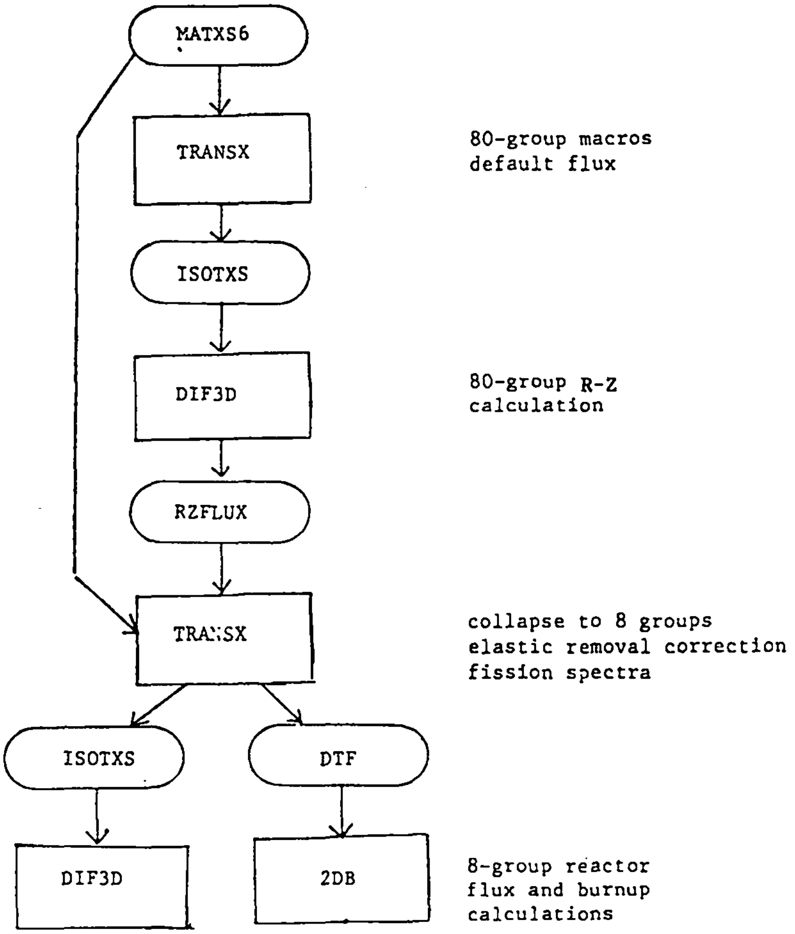

Fig. 54. Processing path for preliminary carbide reactor cross sections.

A modification of the CINDER code package [98,100] was selected for the depletion module of the neutronics code system shown in Fig. 53. The module was linked to the DIF3D code by means of standard interface files, and this preliminary version of the neutronics code system was validated by making test problem comparisons with the 2DB code. The linking was achieved by making use of CTL--a local controller. CTL is much like the COSMOS controller and is designed for interactive as well as batch use. It provides for sequential control of tasks such as retrieval from and storage to the Central File System, execution of programs, and file handling. The calculational model used in the comparison with 2DB was a carbide version of the G.E. modular reactor concept; the core mid-plane layout is shown in Fig. 55 and the R-Z layout is shown in Fig. 56. Group-averaged nuclear cross-section data used in the calculations were those generated by the NJOY code system from the ENDF/B-VI data base for previous studies of the carbide version of the CDS.

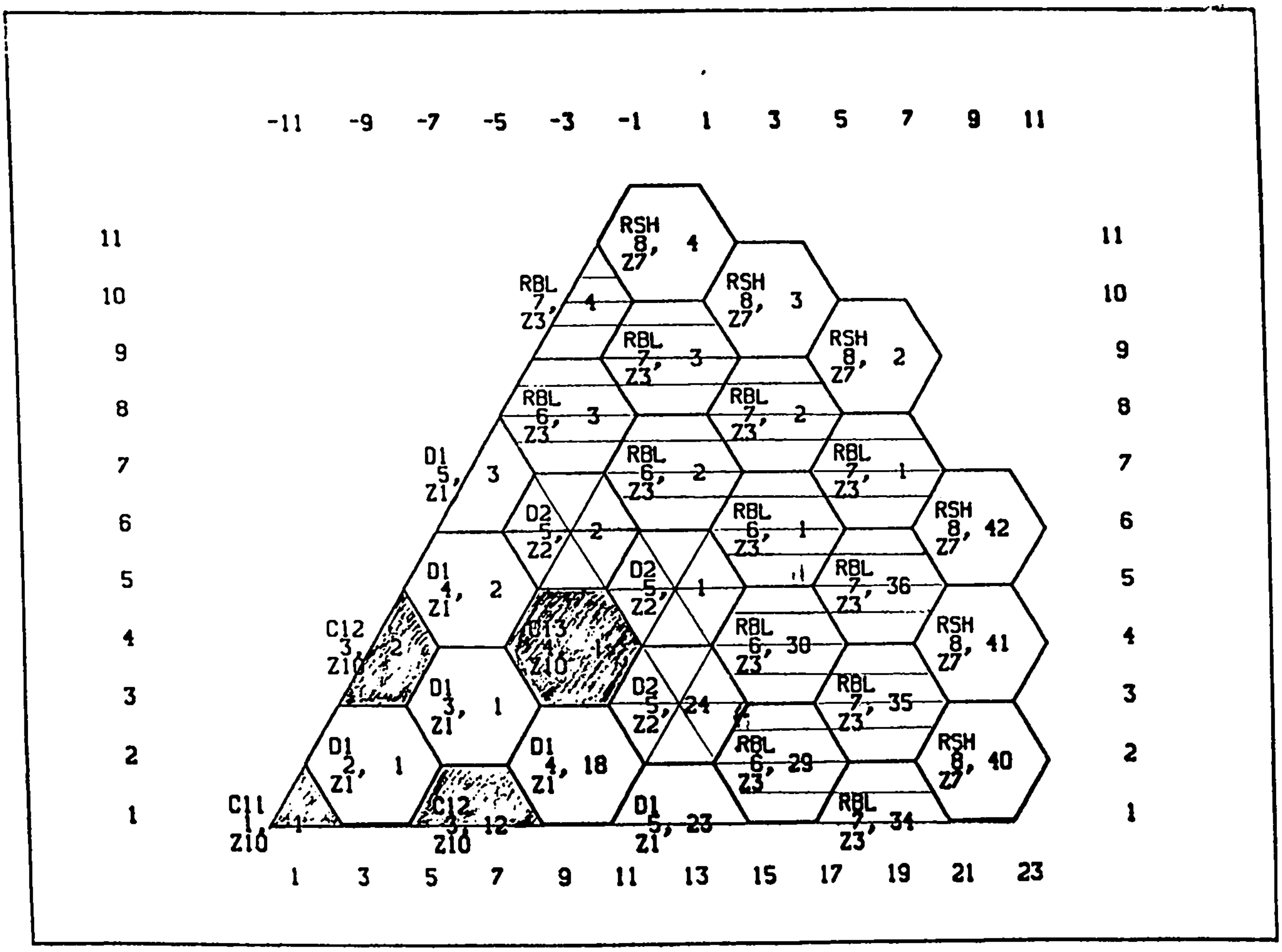

Fig. 55. Carbide modular reactor model - core mid-plane layout.

In the first comparison, parallel DIF3D-CINDER and 2DB R-Z model runs were made. These were at 70% full power (0.7 x 345 MW) in increments of 100 days for 500 days continuous operation time. Results are shown in Table XXVI and in Figs. 57-61. The difference seen in the beginning-of-life (BOL) values for k-effective for the two calculations in Fig. 57 are mainly due to the fact that 2DB uses a single fission spectrum for all regions, whereas DIF3D uses a composition-dependent spectrum in each region. Also note that the loss in k-effective as calculated by DIF3D-CINDER is greater than calculated by 2DB. The reasons for this are evident from Figs. 58-61. Note that the CINDER module shows a faster buildup of fission products in the driver and blanket regions than does the 2DB depletion module (Figs. 58 and 59), whereas the depletion of the ^{239}Pu in the driver regions and buildup of ^{239}Pu in the blankets are essentially the same for both codes (Figs. 60 and 61). Other differences, seen in Table XXVI, are insignificant.

The R-Z model was also used in a BOL calculation using the TWODANT[118] discrete-ordinates transport codes. A value of k-effective = 1.1854 was obtained for this run. This is to be compared with the value of 1.1791 obtained with 2DB and the value of 1.1768 obtained with DIF3D. Note that the same single table (P_0-transport corrected) set of multigroup nuclear data was used in calculations with all three codes, so that the differences seen in these eigenvalues are due to transport vs diffusion theory.

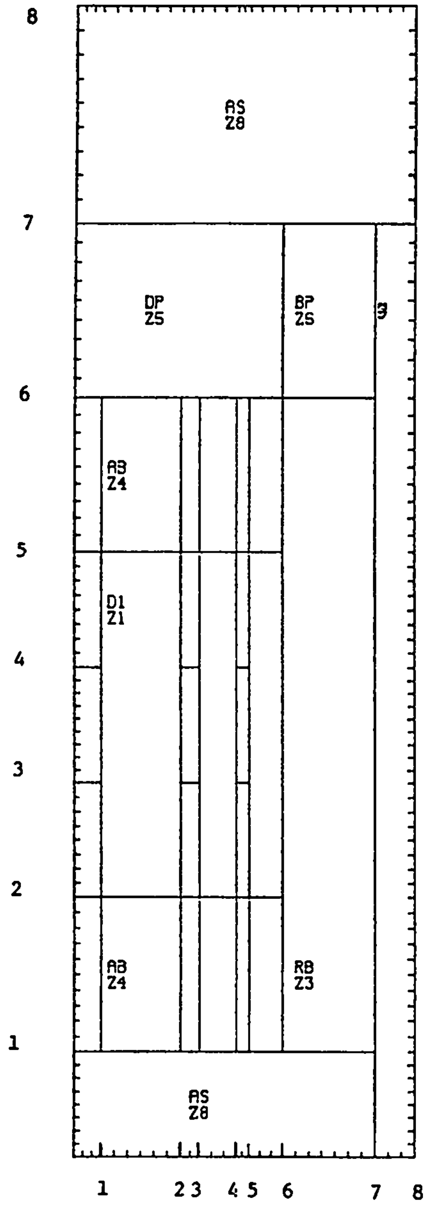

No.	R(cm)	Z(cm)
1	7.72	31.11
2	30.97	76.84
3	36.28	110.71
4	46.93	144.57
5	50.59	178.44
6	60.26	224.16
7	86.94	274.96
8	98.50	339.09

Fig. 56. R-Z model of G. E. carbide.

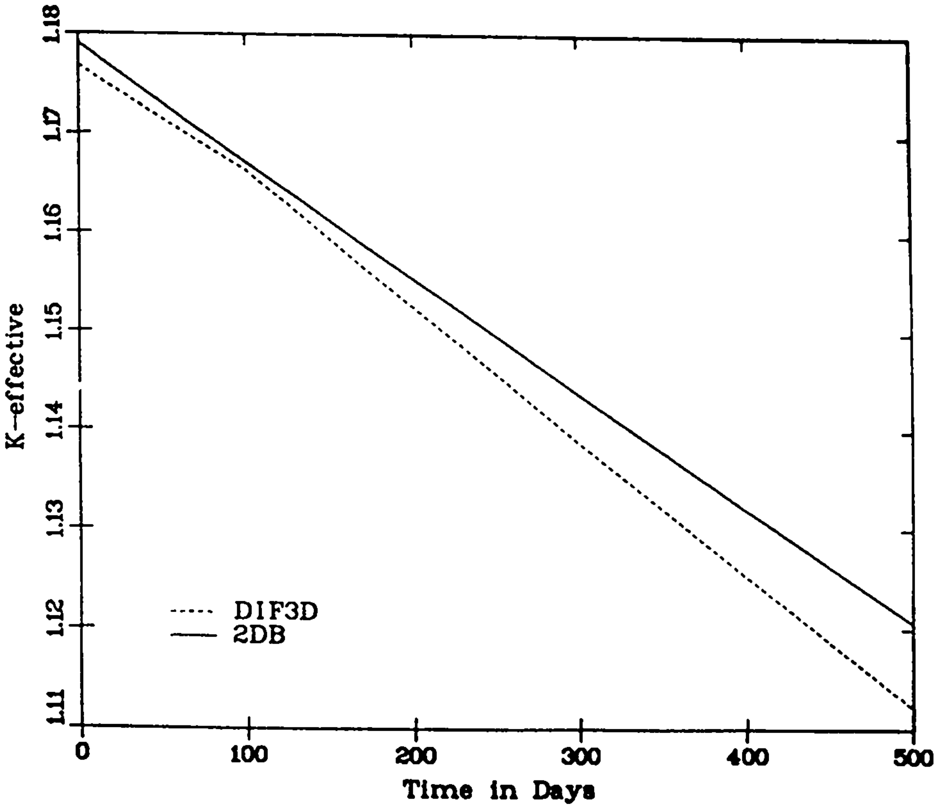

Fig. 57. Comparison of eigenvalue behavior during depletion.

Fig. 58. Comparison of build-up of fission products in driver regions.

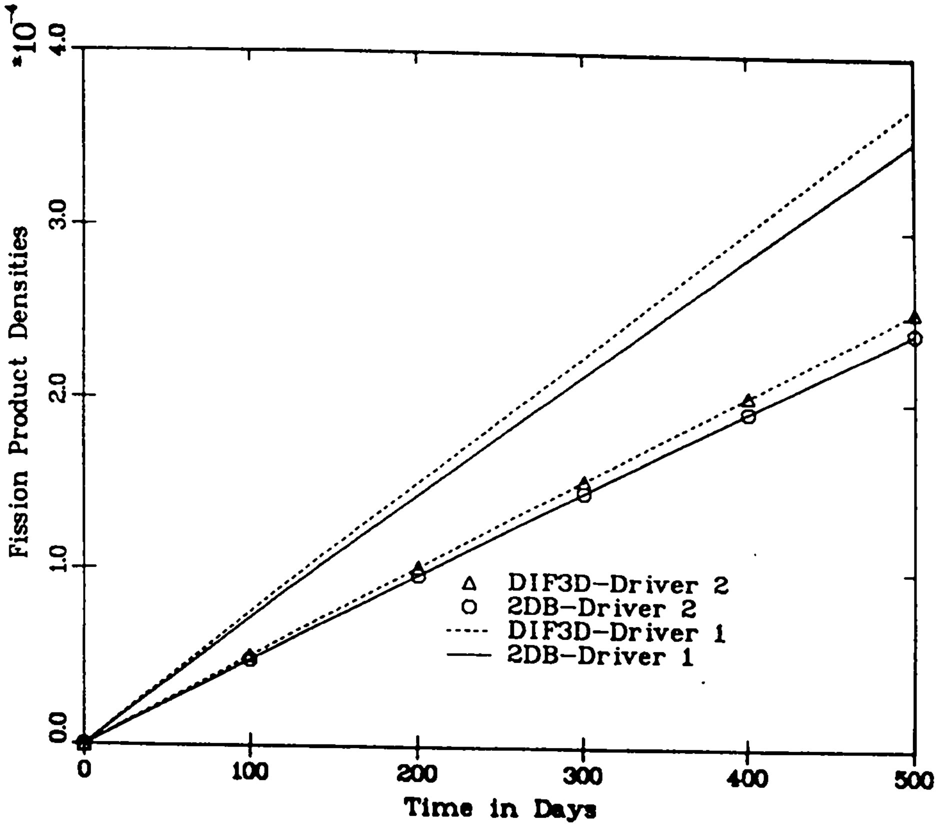

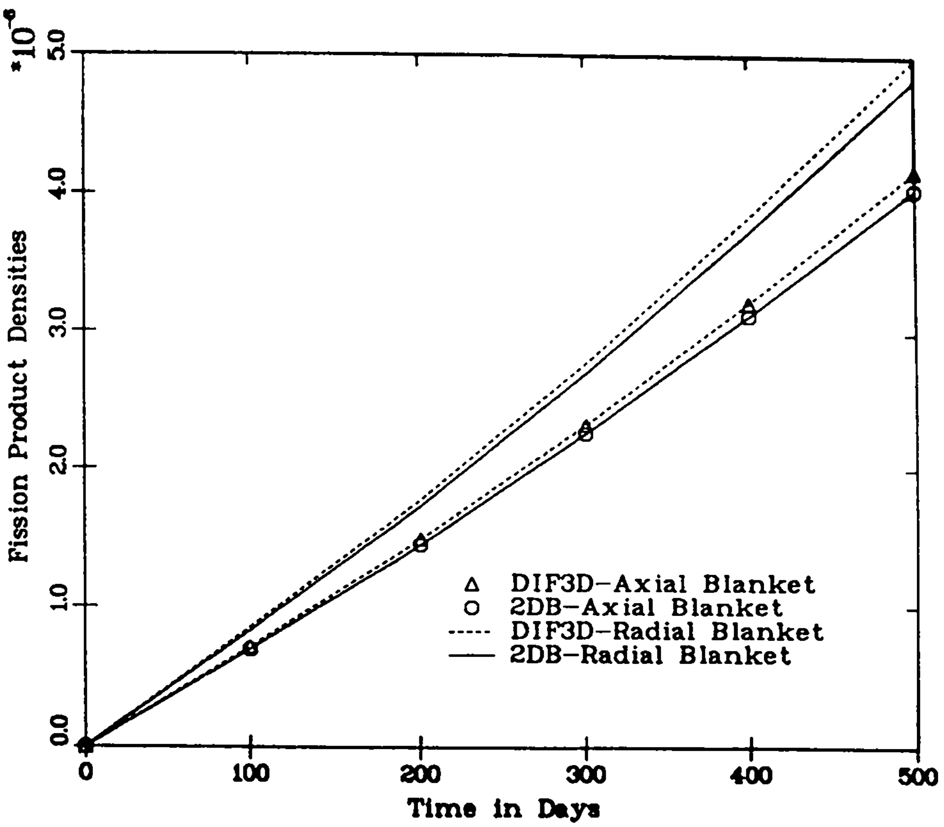

Fig. 59. Comparison of build-up of fission products in blanket regions.

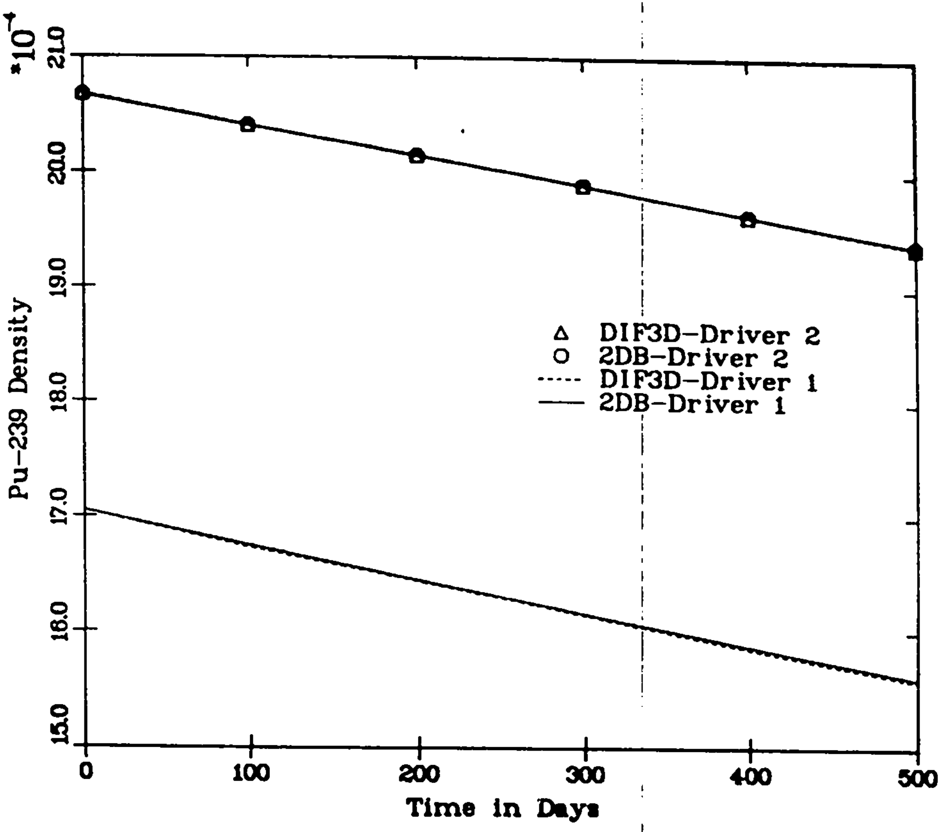

Fig. 60. Comparison of ^{239}Pu depletion in driver regions.

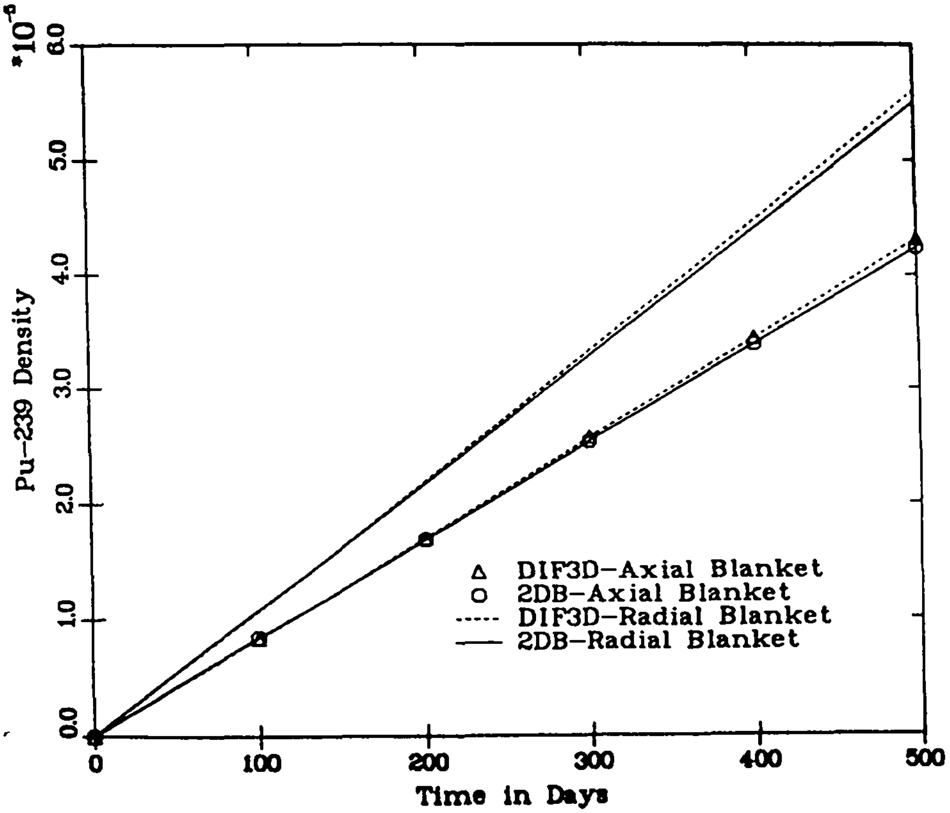

Fig. 61. Comparisons of ^{239}Pu build-up in blanket regions.

TABLE XXVI

COMPARISON OF 2DB AND DIF3D RESULTS

Sample Problem: "G.E.-Modular" Core With Carbide Fuel

	2DB	DIF3D
Avg. Inner Driver Flux:	1.9595	2.0155 x 10^{15}nv
Avg. Outer Driver Flux:	1.1044	1.1363 x 10^{15} nv
Avg. Radial Blkt. Flux:	2.2643	2.3333 x 10^{14} nv
Flux Ratios:		
$\frac{\text{(Outer Driver)}}{\text{(Inner Driver)}}$	0.5636	0.5639
$\frac{\text{(Radial Blkt.)}}{\text{(Inner Driver)}}$	0.1156	0.1158
K_{eff}	1.1791	1.1768

REFERENCES

1. G. M. Hale and D. C. Dodder, "A=4 Level Structure from an R-Matrix Analysis of the Four-Nucleon System," B. Zeitnitz, Ed., Proc. 10th Int. Conf. Few Body Problems in Physics, Karlsruhe, W. Germany, August 1983, p. 207 (1983).

2. S. Fiarman and W. E. Meyerhof, "Energy Levels of Light Nuclei A=4," Nucl. Phys. A 206, 1 (1973).

3. W. Grüebler, V. König, P. Schmelzbach, B. Jenny, and J. Vybiral, "New Highly Excited ^{4}He Levels Found by the ^{2}H(d,p)^{3}H Reaction," Nucl. Phys. A 369, 381 (1981).

4. J. C. Legg, W. D. Simpson, and S. T. Emerson, "Study of Excited States of ^{4}He, Using the ^{6}Li(d,α)α^* Reaction," Bull. Am. Phys. Soc. 11, 724 (1966).

5. A. D. Bacher and T. A. Tombrello, "Search for States of ^{4}He Using ^{2}H(d,d) and ^{2}H(d,p)^{3}H," Nucl. Phys. A 113, 557 (1968).

6. P. G. Young and E. D. Arthur, "GNASH: A Preequilibrium-Statistical Nuclear Model Code for Calculations of Cross Sections and Emission Spectra," Los Alamos Scientific Laboratory report LA-6947 (November 1977).

7. E. D. Arthur, Comp., "Applied Nuclear Data Research and Development: Oct. 1, 1982-March 31, 1983," Los Alamos National Laboratory report LA-9841-PR (August 1983).

8. F. Ajzenberg-Selove, "Energy Levels of Light Nuclei A=5-10," Nucl. Phys. A 320, 1 (1979).

9. F. Ajzenberg-Selove and C. L. Busch, "Energy Levels of Light Nuclei A=11-12," Nucl. Phys. A 336, 1 (1980).

10. C. Cowan, ENDF/B-V Data File for ^{11}B (MAT 1160), described in "ENDF-B Summary Documentation," Brookhaven National Laboratory report BNL-NCS-17541 (ENDF-201), R. Kinsey, Ed., National Nuclear Data Center, Brookhaven National Laboratory, Upton, N. Y. (July 1979).

11. H. Gruppelaar, H. A. J. van der Kamp, and P. Nagel, "International Nuclear Model and Code Comparison on Pre-Equilibrium Effects," Nuclear Energy Agency Nuclear Data Committee report NEANDC-177U (April 1983).

12. D. Hermsdorf, A. Meister, S. Sassonoff, D. Seelinger, K. Seidel, and F. Shahin, "Differentielle Neutronenemissionsquerschnitte $\sigma_{nM}(E_0;E,\theta)$ bei 14.6 MeV Einschaussenergie für die Elemente Be, C, Na, Mg, Al, Si, P, Sn, Ca, Ti, V, Cr, Mn, Fe, Co, Ni, Cu, An, Ga, Se, Br, Zr, Nb, Cd, In, Sn, I, Ta, W, Au, Hg, Pb, und Bi," Zentralinstitut für Kernforschung report ZfK-277 (1974).

13. A. Marcincowski, R. W. Finlay, G. Randers-Pehrson, C. E. Brient, R. Kurup, S. Mellema, A. Meigooni, and R. Tailor, "Neutron Emission Cross Sections at 25.7 MeV: ^{51}V, ^{56}Fe, ^{65}Cu, ^{93}Nb, and ^{209}Bi," Nucl. Sci. Eng. 83, 13 (1983).

14. J. Frehaut, A. Bertin, R. Bois, and J. Jary, "Status of (n,2n) Cross Section Measurements at Bruyères-le-Châtel, " M. R. Bhat and S. Pearlstein, Eds., Proc. Symp. Neutron Cross-Sections from 10 to 50 MeV, Brookhaven, New York, May 12-14, 1980 (Brookhaven National Laboratory report BNL-NCS-51245, 1980), p. 399.

15. L. R. Veeser, E. D. Arthur, and P. G. Young, "Cross Sections for (n,2n) and (n,3n) Reactions above 14 MeV," Phys. Rev. C 16, 1792 (1977).

16. S. M. Grimes, R. C. Haight, and J. D. Anderson, "Charged-Particle-Producing Reactions of 15-MeV Neutrons on ^{51}V and ^{93}Nb," Phys. Rev. C 17, 508 (1978).

17. F. G. Perey, "Optical-Model Analysis of Proton Elastic Scattering in the Range of 9 to 22 MeV," Phys. Rev. 131, 745 (1963).

18. J. R. Huizenga and G. Igo, "Theoretical Reaction Cross Sections for Alpha Particles with an Optical Model," Nucl. Phys. 29, 462 (1962).

19. A. Gilbert and A. G. W. Cameron, "A Composite Nuclear-Level Density Formula with Shell Corrections," Can. J. Phys. 43, 1446 (1965).

20. O. Bersillon, "SCAT2 - A Spherical Optical Model Code," in Centre d'Études de Bruyères-le-Châtel report, pub. by the Commissariat a l'Energie Atomique, CEA-R-4712 (1978), p. 111.

21. G. L. Morgan and E. Newman, "The Au(n,xγ) Reaction Cross Section for Incident Neutron Energies between 0.2 and 20.0 MeV," Oak Ridge National Laboratory report ORNL-TM-4973 (1975).

22. J. P. Delaroche, "Potential Optique Nucleon-^{197} Au Entre 10 keV et 57 MeV," Int. Conf. Neutron Physics and Nuclear Data for Reactors and Other Applied Purposes, Harwell, England (1978), p. 366.

23. J. Raynal, "Optical Model and Coupled-Channel Calculations in Nuclear Physics," International Atomic Energy Agency report IAEA SMR-9/8 (1970).

24. C. L. Dunford, "A Unified Model for Analysis of Compound Nuclear Reactions," Atomics International report AI-AEC-12931 (1970).

25. J. L. Cook, H. Ferguson, and A. R. Musgrove, "Nuclear Level Densities in Intermediate and Heavy Nuclei," Aust. J. Phys. 20, 477 (1967).

26. P. Axel, "Electric Dipole Ground State Transition Width Strength Function," Phys. Rev. 125, 671 (1962).

27. D. M. Brink, thesis, Oxford University (1955).

28. M. A. Lone, "Photon Strength Functions," Proc. Third Int. Symp. Neutron Capture Gamma-Ray Spectroscopy and Related Topics, Brookhaven, New York, September 18-22, 1978 (Plenum Press, New York, 1979), p. 161.

29. S. F. Mughabghab and D. I. Garber, "Neutron Cross Sections, Volume 1, Resonance Parameters," Brookhaven National Laboratory report BNL-325, 3rd Ed., Vol. 1 (1973).

30. S. Joly, D. M. Drake, and L. Nilsson, "Gamma-Ray Strength Functions *for* ^{104}Rh, ^{170}Tm, and ^{198}Au," Phys. Rev. C 20, 2072 (1979).

31. G. D. Loper, L. M. Bollinger, and G. E. Thomas, "Search for the Pygmy Resonance in ^{197}Au(n,γ)^{198}Au," in Argonne National Laboratory report ANL-7971, "Physics Division Annual Review, 1 April 1971-1 March 1972" (1972), p. 7.

32. A. Veyssiere, H. Beil, R. Bergere, P. Carlos, and A. Leprêtre, "Photoneutron Cross Sections of ^{208}Pb and ^{197}Au," Nucl. Phys. A 159, 561 (1970).

33. H. Kitazawa, Y. Harima, H. Yamakoshi, Y. Sano, T. Kobayashi, and M. Kawai, "Gamma-Ray Production Cross Sections for MeV Neutrons," Proc. Int. Conf. on Nucl. Cross Sections for Technol., Oct. 22-26, 1979, Knoxville, Tenn. (NBS Special Publication 594, 1980), p. 775.

34. S. F. Mughabghab, ENDF/B-V Data File for ^{197}Au (MAT 1379), described in "ENDF-B Summary Documentation," BNL-NCS-17541 (ENDF-201), R. Kinsey, Ed., National Nuclear Data Center, Brookhaven National Laboratory, Upton, N.Y. (July 1979).

35. E. D. Arthur, "Calculation of Neutron Cross Sections on Isotopes of Yttrium and Zirconium," Los Alamos Scientific Laboratory report LA-7789-MS (April 1979), p. 24.

36. H. Vonach, A. Chalupka, F. Wenninger, and G. Staffel, "Measurement of the Angle-Integrated Secondary Neutrons Spectra from Interaction of 14-MeV Neutrons with Medium and Heavy Nuclei," M. R. Bhat and S. Pearlstein, Eds., Proc. Symp. on Neutron Cross Sections from 10 to 50 MeV, Brookhaven, N.Y., May 12-14, 1980 (Brookhaven National Laboratory report BNL-NCS-51245, 1980), p. 343.

37. J. G. Hayes and T. B. Ryves, "Simultaneous Evaluation of Some Important Cross Sections at 14.70 MeV," Ann. Nucl. Eng. 8, 469 (1981).

38. B. P. Bayhurst, J. S. Gilmore, R. J. Prestwood, J. B. Wilhelmy, N. Jarmie, B. H. Erkkila, and R. A. Hardekopf, "Cross Sections for (n,xn) Reactions between 7.5 and 28 MeV," Phys. Rev. C 12, 451 (1975).

39. D. W. Barr, S. A. Beatty, M. M. Fowler, J. S. Gilmore, R. J. Prestwood, E. N. Treher, and J. B. Wilhelmy, "(p,xn) Measurements on Strontium Isotopes" in "Nuclear Chemistry Division Annual Report FY1982," Los Alamos National Laboratory report LA-9797-PR (June 1983).

40. J. C. Dousse, D. M. Drake, J. Gursky, J. D. Moses, N. Stein, and J. W. Sunier, "Coincident Neutron-Proton Emission from Proton Bombardment of ^{87}Sr and ^{91}Zr," Los Alamos National Laboratory report LA-9924.

41. P. G. Young, Comp., "Applied Nuclear Data Research and Development: April 1-June 30, 1981," Los Alamos National Laboratory report LA-9060-PR (December 1981).

42. S. M. Grimes, J. D. Anderson, A. K. Kerman, and C. Wong, "Role of Isospin in Statistical Processes," Phys. Rev. C 5, 85 (1972).

43. P. G. Young, Comp., "Applied Nuclear Data Research and Development, October 1, 1981-March 31, 1982," Los Alamos National Laboratory report LA-9468-PR (March 1982).

44. E. D. Arthur, Comp., "Applied Nuclear Data Research and Development, April 1, 1982-September 30, 1982," Los Alamos National Laboratory report LA-6947-PR (April 1983).

45. S. F. Mughabghab, M. Divadeenam, and N. E. Holden, Neutron Resonance Parameters and Thermal Cross Sections-Part A (Academic Press, New York, 1981).

46. C. H. Johnson, R. L. Kernell, and S. Ramavataram, "The ^{89}Y(p,n)^{89}Zr Cross Section Near the First Two Analogue Resonances," Nucl. Phys. A 107, 21 (1968).

47. P. S. Miller and G. T. Garvey, "Charge Exchange in Medium Mass Nuclei as Observed by the (p,np) Reaction," Nucl. Phys A 163, p. 65 (1971).

48. L. J. B. Goldfarb, J. A. Gonzalez, M. Posner, and K. W. Jones, "The ^{40}Ca(t,d_0)^{41}Ca Reaction Near the Coulomb Barrier," Nucl. Phys. A 185, 337 (1972).

49. F. D. Becchetti and G. W. Greenlees, "A General Set of ^{3}He and Triton Optical-Model Potentials for A>40, E<40 MeV," Proc. Int. Symp. Polarization Phenomena in Nuclear Reactions, Madison, Wisconsin, 1970 (1971), p. 682.

50. E. D. Arthur and P. G. Young, "Evaluated Neutron-Induced Cross Sections for ^{54,56}Fe to 40 MeV," Los Alamos Scientific Laboratory report LA-8626-MS (ENDF-304) (December 1980).

51. C. Michael Lederer and Viginia S. Shirley, Table of Isotopes, Seventh Ed. (John Wiley and Sons, Inc., New York, 1978).

52. R. L. Kiefer and M. Hillman, "Relative Yields of ^{58g}Co,^{58m}Co, and ^{56}Co Produced by Low Energy Tritons," J. Inorg. Nucl. Chem. 31, 915 (1969).

53. D. W. Muir and E. D. Arthur, "Improved Activation Cross Sections for Vanadium and Titanium," Proc. Third Topical Meet. on Fusion Reactor Materials, Albuquerque, New Mexico, September 1983 (to be published), Los Alamos National Laboratory document LA-UR-83-2567.

54. F. G. Perey, "Optical Model Analysis of Proton Elastic Scattering in the Range of 9 to 22 MeV," Phys. Rev. 131, 745 (1962).

55. O. F. Lemos, "Diffusion Elastique de Particules Alpha," Orsay: Centre de Spectrométrie de Masse report A136 (1972).

56. R. J. Peterson, "Inelastic Scattering of 17.5-MeV Protons from ^{51}V, ^{52}Cr, ^{55}Mn, anc ^{56}Fe," Ann. of Phys. 53, 40 (1969).

57. H. F. Lutz, W. Bartolini, T. H. Curtis, and G. M. Klody, "Inelastic Scattering of 14.4-MeV Protons by the Even Isotopes of Titanium," Phys. Rev. 187 (1969), 1479.

58. Experimental data provided from the CSISRS compilation by the National Nuclear Data Center, Brookhaven National Laboratory, Upton, New York.

59. S. Grimes, R. C. Haight, and J. D. Anderson, "Measurement of Sub-Coulomb Barrier Charged Particles Emitted from Aluminum and Titanium Bombarded by 15-MeV Neutrons," Nucl. Sci. Eng. 62, 187 (1977).

60. L. R. Veeser, "Prompt Neutrons from Neutron-Induced Fission of ^{237}Np," Phys. Rev. C 17, 385 (1978).

61. V. G. Vorobeva, B. D. Kuzinov, V. V. Malinovsky, N. N. Semenova, and V. I. Volodin, "Measurements of Average Number of Prompt Neutrons from Neutron-Induced Fission of ^{237}Np," Nuclear Constants 3(38), 44 (1980).

62. J. Frehaut, A. Bertin, and R. Bois, "Measurement of $\bar{\nu}_p$ and $\bar{E}_\gamma$ for the Fission of ^{232}Th, ^{235}U, and ^{237}Np Induced by Neutrons with Energies Between 1 and 15 MeV," K. H. Böckhoff, Ed., Proc. Int. Conf. Nucl. Data Sci. Technol., Antwerp, Belgium, September 6-10, 1982 (D. Reidel Publ. Co, Dordrecht), p. 78 (1983).

63. J. P. Unik, J. E. Gindler, L. E. Glendenin, K. F. Flynn, A. Gorski, and R. J. Sjoblom, "Fragment Mass and Kinetic Energy Distributions for Fissioning Systems Ranging from Mass 230 to 256," Proc. Third I.A.E.A. Symp. Phys. and Chem. of Fission, Rochester, New York, August 13-17, 1973 (International Atomic Energy Agency, Vienna, 1974, Vol. II, p. 19.

64. M. J. Bennett and W. E. Stein, "Kinetic Energies of Fragments from Seven Fission Reactions at Low Excitation Energies," Phys. Rev. 156, 1277 (1967).

65. D. G. Madland and J. R. Nix, "Calculation of the Prompt Neutron Spectrum and Average Prompt Neutron Multiplicity for the Spontaneous Fission of ^{252}Cf," K. H. Böckhoff, Ed., Proc. Int. Conf. Nucl. Data Sci. Technol., Antwerp, Belgium, September 6-10, 1982 (D. Reidel Pub. Co., Dordrecht), p. 473 (1983).

66. Data available on magnetic tape from the National Nuclear Data Center, Brookhaven National Laboratory under A. H. Wapstra and K. Bos (1982), to be published.

67. P. Möller and J. R. Nix, "Atomic Masses and Nuclear Ground-State Deformations Calculated with a New Macroscopic-Microscopic Model," At. Data Nucl. Data Tables 26, 165 (1981).

68. J. W. Boldeman, D. Culley, and R. J. Cawley, "The Fission Neutron Spectrum from the Spontaneous Fission of ^{252}Cf," Trans. Am. Nucl. Soc. 32, 733 (1979).

69. W. P. Poenitz and T. Tamura, "Investigation of the Prompt-Neutron Spectrum for Spontaneously-Fissioning ^{252}Cf," K. H. Böckhoff, Ed., Proc. Int. Conf. Nucl. Data Sci. Technol., Antwerp, Belgium, September 6-10, 1982 (D. Reidel Pub. Co., Dordrecht), p. 465 (1983).

70. S. Amiel, "Delayed Neutrons in Fission," Proc. Second I.A.E.A. Symp. on Phys. and Chem. of Fission, Vienna, Austria, 1969 (Int. Atomic Energy Agency, Vienna), p. 569 (1969).

71. J. R. Smith, "Status of ^{252}Cf $\bar{\nu}$ and its Impact on Thermal Reactor Parameters," Proc. Symp. Nucl. Data Problems for Thermal Reactor Applications, Brookhaven National Laboratory, 1978 (Electric Power Research Institute report EPRI-NP-1093), p. 5-1 (1979).

72. R. R. Spencer, R. Gwin, and R. Ingle, "A Measurement of the Average Number of Prompt Neutrons from Spontaneous Fission of Californium-252," Nucl. Sci. Eng. 80, 603 (1982).

73. R. E. MacFarlane, D. W. Muir, and R. M. Boicourt, "The NJOY Nuclear Data Processing System, Volume I: User's Manual," Los Alamos National Laboratory report LA-9303-M (ENDF-324) (May 1982).

74. R. E. MacFarlane, D. W. Muir, and R. M. Boicourt, "The NJOY Nuclear Data Processing System, Volume II: The NJOY, RECONR, BROADR, HEATR, and THERMR Modules," Los Alamos National Laboratory report LA-9303-M (ENDF 324) (May 1982).

75. R. Kinsey, "ENDF-102 Data Formats and Procedures for the Evaluated Nuclear Data Files, ENDF," Brookhaven National Laboratory report BNL-NCS-50496 (ENDF-102), 2nd Ed. (ENDF/B-V) (1979).

76. T. A. Gabriel, J. D. Amburgey, and N. M. Greene, "Radiation-Damage Calculations: Primary Knock-On Atom Spectra, Displacement Rates, and Gas Production Rates," Nucl. Sci. Eng. 61, 21 (1976).

77. D. G. Doran, "Neutron Displacement Cross Sections for Stainless Steel and Tantalum Based on a Lindhard Model," Nucl. Sci. Eng. 49, 130 (1972).

78. R. K. Smither and L. R. Greenwood, "Displacement Damage Calculations Using ENDF/B-V Cross Sections Including Thermal Neutron Capture and Beta Decay Effects," Proc. 4th ASTM-Euratom Symp. on Reactor Dosimetry, EUREG/CP-0029, p. 793.

79. K. Kikuchi and M. Kawaii, Nuclear Matter and Nuclear Reactions (John Wiley & Sons, Inc., New York, 1968), p. 135.

80. F. M. Mann, "HAUSER*5, A Computer Code to Calculate Nuclear Cross Sections," Hanford Engineering Development Laboratory report HEDL-TME-78-83 (July 1979).

81. R. E. MacFarlane and D. G. Foster, Jr., "Advanced Nuclear Data for Radiation Damage Calculations," Proc. Third Topical Meet. on Fusion Reactor Materials, Albuquerque, New Mexico, September 12-22, 1983 (to be published), Los Alamos document LA-UR-83-2628.

82. C. Kalbach and F. M. Mann, "Phenomenology of Continuum Angular Distributions I-Systematics and Parameterization," Phys. Rev. C 21, 112 (1981).

83. E. D. Arthur and P. G. Young, "Evaluation of Neutron Cross Sections to 40 MeV for ^{54,56}Fe," in "Symposium on Neutron Cross Sections from 10 to 50 MeV, Vol. II," Brookhaven National Laboratory report BNL-NCS-51245 (July 1980).

84. R. E. MacFarlane, "Energy Balance of ENDF/B-V," Trans. Am. Nucl. Soc. 33, 681 (1979).

85. "ENDF-202, Cross Section Evaluation Working Group Benchmark Specifications," Brookhaven National Laboratory report BNL-19302 (ENDF 202) (November 1974 with corrections).

86. R. Douglas O'Dell, F. W. Brinkley, Jr., and D. R. Marr, "User Manual for ONEDANT: A Code Package for One-Dimensional, Diffusion-Accelerated, Neutral-Particle Transport," Los Alamos National Laboratory report LA-9184-M (February 1982).

87. R. D. Lawrence, "The DIF3D Neutronics Option for Two- and Three-Dimensional Theory Calculations in Hexagonal Geometry," Argonne National Laboratory report ANL-83-1 (March 1983).

88. R. B. Kidman, "ENDF/B-IV, LIB-IV, and the CSEWG Benchmarks," Los Alamos National Laboratory report LA-7355-MS (June 1978).

89. D. Steiner, "Nuclear Performance of Vanadium as a Structural Material in Fusion-Reactor Blankets," Nuclear Fusion 14, 33 (1974).

90. O. N. Jarvis, "Selection of Low-Activity Elements for Inclusion in Structural Materials for Fusion Reactors," UKAEA Harwell report AERE-R 10496 (1982).

91. R. W. Hayward and D. D. Hoppes, "Radiative Orbital Electron Capture in Vanadium-49," Phys. Rev. 104, 183 (1956).

92. B. G. Petterson, "Internal Bremsstrahlung," Chap. XXV (D) of "Alpha-, Beta-, and Gamma-Ray Spectroscopy, Vol. 2," K. Siegbahn, Ed., North-Holland Publishing Company, Amsterdam (1965).

93. T. R. England and B. F. Rider, "Status of Fission Yield Evaluations," invited paper for the NEA Specialists' Meeting on Yields and Decay Data of Fission Product Nuclides, Brookhaven National Laboratory, October 24-27, 1983 (Proceedings to be published), Los Alamos National Laboratory document LA-UR-83-3531.

94. E. A. C. Crouch, "Fission-Product Yields from Neutron-Induced Fission," Atomic and Nuclear Data Tables, Vol. 19, No. 5 (May 1977).

95. T. R. England, W. B. Wilson, R. E. Schenter, and F. M. Mann, "Aggregate Delayed Neutron Intensities and Spectra Using Augmented ENDF/B-V Precursor Data," Nucl. Sci. Eng. 85, 139-155 (1983). [Note: Los Alamos National Laboratory report LA-UR-83-1270 (April 1983), the supporting document, contains spectra for 20 yield sets.]

96. T. R. England, R. E. Schenter, and F. Schmittroth, "Delayed Neutron Calculations Using ENDF/B-V Data," Proc. ANS/APS Int. Conf. Nucl. Cross Sections for Technology, Knoxville, Tenn., October 11-26, 1979, NBS Special Publication 594, US National Bureau of Standards (1980).

97. F. M. Mann, M. Schreiber, R. E. Schenter, and T. R. England, "Compilation of Neutron Precursor Data," K. H. Böckhoff, Ed., "Proc. Int. Conf. Nucl. Data Sci. Technol., Antwerp, Belgium, September 6-10, 1982, (D. Reidel Pub. Co, Boston), p. 272, (1983).

98. W. B. Wilson, T. R. England, R. J. LaBauve, M. E. Battat, D. E. Wessol, and R. T. Perry, "Status of CINDER and ENDF/B-V Based Libraries for Transmutation Calculations," in Proc. Int. Conf. on Nuclear Waste Transmutation, July 22-24, 1980; The University of Texas at Austin, March 1, 1981, p. 673.

99. W. B. Wilson, T. R. England, and R. J. LaBauve, "Formation and Testing of ENDF/B-V Based Fission-Product and Actinide Data Libraries for CINDER-2," in "Applied Nuclear Data Research and Development July 1-September 20, 1981," Los Alamos National Laboratory report LA-9262-PR, pp. 51-57 (March 1982).

100. W. B. Wilson, T. R. England, R. J. LaBauve, and R. M. Boicourt, "TOAFEW-V Multigroup Cross-Section Collapsing Code and Library of 154-Group-Processed ENDF/B-V Fission-Product and Actinide Cross Sections," Electric Power Research Institute report NP-2345 (April 1982).

101. C. I. Baxman and P. G. Young, Comps., "Applied Nuclear Data Research and Development January 1-March 31, 1979," Los Alamos Scientific Laboratory report LA-7843-PR (May 1979).

102. T. R. England and W. B. Wilson, "TMI-2 Decay Power: LASL Fission-Product and Actinide Decay Power Calculations for the President's Commission on the Accident at Three Mile Island," Los Alamos Scientific Laboratory report LA-8041-MS, Revised (March 1980), p. 34.

103. "American National Standards Institute/American Nuclear Society Standard for Decay Heat Power in Light Water Reactors," ANSI/ANS-5.1-1979 (August 1979).

104. L. F. Ziegler, Helium Stopping Powers and Ranges in All Elemental Matter, Vol. 4 of The Stopping and Ranges of Ions in Matter series (Pergamon Press, New York, 1977).

105. R. L. Walker, "The (α,n) Cross Section of Boron," Phys. Rev. 76, 244 (1949).

106. H. Lisken and A. Paulsen, "Neutron Yields of Light Elements Under α-Bombardment," Atom. Kernenergie 30, 59 (1977).

107. R. T. Perry and W. B. Wilson, "Neutron Production from (α,n) Reactions and Spontaneous Fission in the ThO_2, UO_2, and $(U,Pu)O_2$ Fuels," Los Alamos National Laboratory report LA-8869-MS (1981).

108. J. K. Bair and H. B. Willard, "Level Structure in Ne^{22} and Si^{30} from the Reactions $O^{18}(\alpha,n)Ne^{21}$ and $Mg^{26}(\alpha,n)Si^{29}$," Phys. Rev. 128, 299 (1962).

109. J. K. Bair and F. X. Haas, "Total Neutron Yield from the Reactions $^{13}C(\alpha,n)^{16}O$ and ^{17} $^{18}O(\alpha,n)^{20}$ ^{21}Ne," Phys. Rev. C 7, 1356 (1973).

110. J. K. Bair and J. Gomez del Campo, "Neutron Yields from Alpha-Particle Bombardment," Nucl. Sci. Eng. 71, 18 (1979).

111. L. F. Hansen, J. D. Anderson, J. W. McClure, B. A. Pohl, M. L. Stelts, J. J. Wesolowski, and C. Wong, "The (α,n) Cross Sections on ^{17}O and ^{18}O Between 5 and 12.5 MeV," Nucl. Phys. A 98, 25 (1967).

112. P. A. Ombrellaro and D. L. Johnson, "Subcritical Reactivity Monitoring: Neutron Yields from Spontaneous (α,n) Reactions in FFTF Fuel," Hanford Engineering Development Laboratory report HEDL-TME-78-39 (June 1978). Information in this document was supplemented and updated.

113. R. D. O'Dell, "Standard Interface Files and Procedures for Reactor Physics Codes, Version II," Los Alamos National Laboratory report LA-6941-MS (September 1977).

114. B. J. Toppel, "A User's Guide for the REBUS-3 Fuel Cycle Analysis Capability," Argonne National Laboratory report ANL-83-3 (March 1983).

115. R. J. Barrett and R. E. MacFarlane, "The MATXS-TRANSX System and the CLAW-IV Nuclear Data Library," Proc. Int. Conf. Nucl. Cross Sections for Technol., October 22-26, 1979, Knoxville, Tenn. (NBS Special Publication 594, 1980), p. 213.

116. L. D. Felten and L. B. Levitt, Eds., "Liquid Metal Fast Breeder Reactor Conceptual Design Study, Phase I," Atomics International report FBR-79-3 (September 1979).

117. W. W. Little, Jr., and R. W. Hardy, "2DB User's Manual-Revision 1," Battelle-Pacific Northwest Laboratories report BNWL-831, Rev. 1 (August 1969).

118. R. Alcouffe, R. D. O'Dell, F. W. Brinkley, Jr., D. W. Marr, W. Walters, "User's Guide for TWODANT Two-Dimensional Diffusion Accelerated Neutral Particle Discrete Ordinates Transport Code," computer accessible from R. Alcouffe, Group X-6, Los Alamos National Laboratory (to be published as LA-MS report). See also R. D. O'Dell, F. W. Brinkley, Jr., and D. R. Marr, "User's Manual for ONEDANT: A Code Package for One-Dimensional, Diffusion-Accelerated, Neutral-Particle Transport," Los Alamos National Laboratory report LA-9184-M (February 1982).

☆U.S. GOVERNMENT PRINTING OFFICE:1984—776-026 / 4100

Printed in the United States of America
Available from
National Technical Information Service
US Department of Commerce
5285 Port Royal Road
Springfield, VA 22161

Microfiche (A01)

Page Range	NTIS Price Code	Page Range	NTIS Price Code	Page Range	NTIS Price Code	Page Range	NTIS Price Code
001 025	A02	151-175	A08	301-325	A14	451-475	A20
026 050	A03	176 200	A09	326-350	A15	476 500	A21
051 075	A04	201-225	A10	351 375	A16	501 525	A22
076 100	A05	226-250	A11	376-400	A17	526-550	A23
101 125	A06	251-275	A12	401-425	A18	551 575	A24
126 150	A07	276 300	A13	426 450	A19	576 600	A25
						601-up*	A99

*Contact NTIS for a price quote.

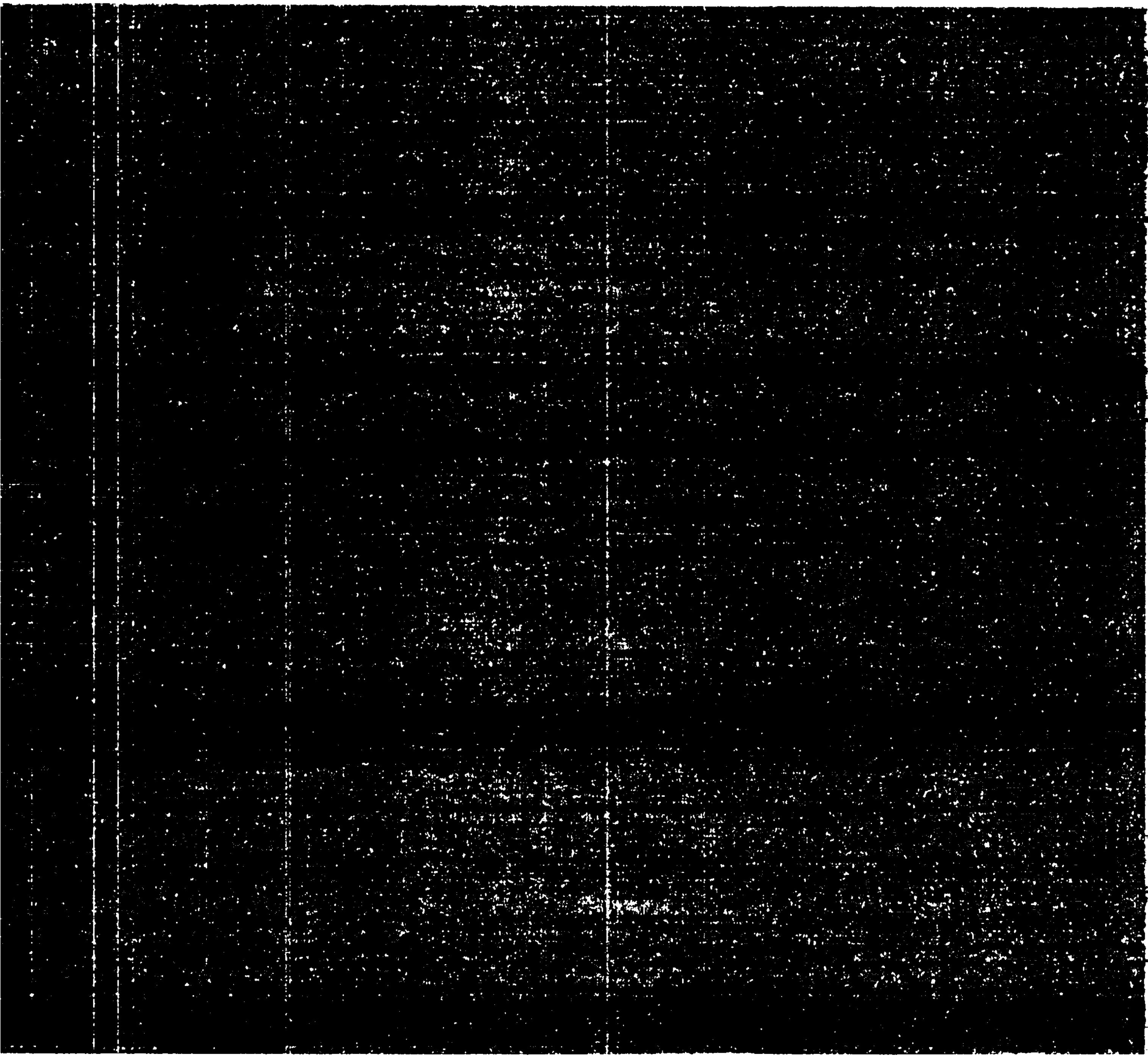

Los Alamos